STOCHASTIC ANALYSIS OF FUNCTIONAL BEHAVIOUR

OF SURFACES IN CONTACT

by

M.K.R. Rao

Department of Mechanical Engineering

McGill University, Montreal, Canada

A thesis submitted to the faculty of Graduate Studies and Research in partial fulfillment of the requirements for the degree of Master of Engineering.

ABSTRACT

An experimental technique called Optical Grating Topography (OGT) has been developed to provide measurements of relatively rough anisotropic surfaces. Using the principle of Schmaltz microscopy, this technique employs multiple scanning to obtain data for subsequent computation of surface parameters. The computational procedure is based on Quantitative Stereology, and permits one to determine not only the conventional surface roughness parameters, but also the mean 'individual bearing area' (IBA). The latter is obtained from the IBA distribution determined from the joint exponential density distribution of the intercept ("cut") length for the X-Y directions. The knowledge of the mean IBA which is a new concept introduced in the present work, is essential for the analysis of the functional behaviour of the interface in contact problems.

Applying the Gaussian Random Process theory, the IBA density distribution is also determined analytically. The comparison with values determined from measurements reveals close agreement for heights of asperities at Ra level and above it. It is shown that this IBA can be directly obtained from spectral analysis of the given surface. It is found that the initial portion of the Auto-covariance function for the CI machined ground surface is of Gaussian form. Using this result along with the density of IBA, the possible determination of cut-off relevant to contact theory is discussed.

RESUME

Une technique expérimentale appelée OGT ('Optical Grating Topography') a été développée afin d'obtenir des mesures sur des surfaces relativement rugeuses et anistropiques. Utilisant le principe de la microscopie de Schmaltz, cette technique consiste en des balayages multiples fournissant des données d'ôu sont extraits les paramètres de surface. La méthode de calcul est basée sur la Stéréologie Quantitative et permet de déterminer non seulement les paramètres de rugosité conventionnels, mais aussi le IBA moyen ('Individual Bearing Area'). Ce dernier s'obtient de la distribution IBA à partir de la densité de distribution jointe exponentielle dans les directions X, Y. Une connaissance du IBA moyen, qui est nouveau concept introduit dans le présent ouvrage, est essentielle pour l'analyse du comportement fonctionnel de l'interface dans les problémes de contact.

En appliquant la théorie GRP ('Gaussian Random Process'), la distribution de densité IBA est également déterminée analytiquement. Comparant cette dernière aux valeurs mesurées, on obtinent un bon accord pour la hauteur des aspérités au niveau Ra et au-dessus. Il est montré que ce IBA peut être obtenu directement par l'analyse spectrale de la surface en question.

On trouve que la portion initiale de la fonction d'autocovariance pour la surface polie a la meule de la fonte est de
forme Gaussienne. Utilisant ce résultat combiné à la densité
IBA, la détermination possible du 'cut-off' dans le câdre de la
théorie de contact est discutée.

STATEMENT OF ORIGINALITY AND CONTRIBUTION TO THE KNOWLEDGE

The author of this these claims originality for the following contributions to the characterization of surfaces for the description of their functional behaviour of surfaces in contact:

- 1. The development of an experimental technique called Optical Grating Topography (OGT) based on the principle of Schmaltz Microscopy with the purpose of obtaining the profile measurements free from the error caused by stylus profilometer. The machined ground surface of $R_{\rm m} \geq 0.76\,\mu{\rm m}$ for which this technique was developed are too rough for the application of laser based interferometric technique.
- 2. The development of the computational procedure for 3-D surface characterization leading to the individual bearing areas and their distribution. The procedure is based on the principles of Quantitative Stereology and Digital Signal Processing. It involves the determination of the joint exponential density distribution of intercept length which is obtained from OGT.
- 3. The analytical determination of the 3-D density distribution of IBA based on Gaussian Random Process. It is found that this density distribution is of the form a*

 K₀ (a*) where a* is the normalized IBA and K₀ the modified Bessel function. This density function will allow, in conjunction with the local stress, the formulation of the stochastic theory of deformation.

ACKNOWLEDGEMENTS

I would like to extend my sincere gratitude to Professor D.R. Axelrad who patiently guided me through the course of this research work, and who was a constant source of inspiration and knowledge. Thanks to him for the use of the highly sophisticated micro-mechanics laboratory where the OGT was developed and also for financing it. I wish to express my gratitude and appreciation to my research supervisor, Professor L. Kops for his helpful comments and suggestions throughout the course of this study.

I am also obliged to the NSERC of Canada for supporting this work financially through a research grant to Professor L. Kops.

In the course of this study, I had several interactions with other students of this department, especially Mr. Eduardo Turcott whose help and skill in the laboratory is immensely appreciated. My thanks to Dr. K. Rezai, Senior Engineer in Pratt and Whitney, for initiating me into the interesting field of optics by giving me the idea of using the principle of grating line shadow for the measurement of surface roughness. Thanks also to Mr. Ralph Wieland, Branch Manager of Zeiss Optics for supplying the optical equipment and giving useful tips in photomicrography.

I am grateful to Dr. K. Mitsui of MITI, Japan, and Professor S. Kaneko of University of Tokyo, Japan, for the fruitful discussion on image processing techniques. My thanks

also go to the participants of the NAMRC XIV Conference at the University of Minnesota for their helpful comments on what was later incorporated in this thesis.

Lastly, I would like to extend my sincere thanks to Ms. Dorothy Harriss for the typing of this thesis.

TABLE OF CONTENTS

ABSTRACT	******		™ -		1
RESUME				1	ii
STATEMENT OF OR	IGINALITY AN	D CONTRIBU	TION TO K	NOWLEDGE	111
ACKNOWLEDGEMENT	S			. "	iv
TABLE OF CONTEN	TS		•		vi
LIST OF NOTATIO	N		•		ix
LIST OF FIGURES		•			xiv
GLOSSARY		•		•	xvii
CHAPTER 1. INT	RODUCTION				
CHAPTER 1. INT	RODUCTION			,	
1.1 Important	ce of surfac	e characte	rizatioņ.		. 1
1.2 Review of	methods used	d in the m	easuremen	t	
of surface	e topography	· · ·			3
1.2.1 Cor	ntact method	S		•	4.
1.2.2 Nor	-contact me	thods		•	4
1.3 Evaluation	on of availa	ble method	s.	•	13
1.4 Offtline	of the thesi	s.			14
			•		
CHAPTER 2. OPT	ICAL GRATING	TOPOGRAPH	Y .		
2.1 Introduc	tion.		1		16
2.2 Descripti	on of the 0	GT system∉	•		18
2.3 Operation	of the OGT	system.			° 20
2.3.1 Es	tablishing t	he optical	l geometr	У	20
₩ 2.3.2 Me	easurement p	rocedures			21

2.4 Specifications of OGT.	
2.5 Computational procedure.	23
2.5.1 Statistical analysis	² 24
2.5.2 Spectral analysis	· 28
2.5.3 Practical computations	31
2.6 Determination of mean intercept length and	• • ,
its distribution.	33
2.6.1 Application of quantitative stereology	34
2.6.2 Density distribution of intercept	
length and bearing area	36
2.7 Error analysis of OGT.	42
2.7.1 Effect of diffraction at the straight	
edge of the shadow	42
2.7.2 Effect of digitization using 0.1 mm	
resolution stylus	43
2.7.3 Effect of calibration	> 44
2.7.4 Results of error analysis	44
2.8 Discussion of results obtained from OGT.	45
2.9 Summary.	46
700 PERE 3 - PRINTER OF GUIDE GEORGE GUIDE	
CHAPTER 3. REVIEW OF SURFACE CHARACTERIZATION MODELS	
3.1 Introduction.	48
3.1.1 Profile descriptors	48
3.1.2 Surface descriptors	53
3.2 Surface and profile characterization based on	
power spectral density function.	-57
3.3 Summary.	60

۵

CHAPTER 4. 3-D CHARACTERIZATION OF SURFACES BASED ON INDIVIDUAL BEARING AREA.

BASED ON INDIVIDUAL BEARING AREA.	1
4.1 Introduction.	•
4.2 Auto covariance function (ACF) of the surface	62 [°]
4.3 Power spectral density function (amplitude	
spectrum) of the surface.	66
4.4 Determination of intercept lengths and their	
distribution.	67
4.5 Determination of individual bearing areas	
and their distribution.	71
4.6 Determination of mean intercept length	
and density distribution of bearing areas	
for different loads	73
4.7 Determination of cut-offs:	73
4.7.1 Low pass cut-off	. 75
4.8 Discussion of results:	79
4.9 Summary.	84
CHAPTER 5. CONCLUSION AND RECOMMENDATIONS	4
5.1 Conclusions.	86
5.2 Recommendations.	90
LIST OF REFERENCES	92
APPENDIX A	A.1
APPENDIX B	A.iv

LIST OF NOTATIONS

ROMAN LETTER SYMBOLS

A Nominal cross-sectional area.

A(f) Amplitude spectrum or Power Spectral Density

Function (PSDF)

A_A Areal fraction.

A_C Tostal area of contact.

Ae Coefficient of an exponential Auto-Covariance

Function.

 $A_{D}(\omega)$ Profile amplitude spectrum.

 $A_{S}(\omega)$ Surface amplitude spectrum of PSDF.

A_T Measurement area

a_b, a Individual Bearing Area (IBA).

a* Normalized IBA.

c Shape factor.

D Standard deviation.

d Distançe between two elements being observed

through system of lenses.

D(i) Standard deviation of intercept length.

ds Diameter of specimen.

E Expected frequency of occurrence.

f Frequency.

G(x),G(r) Auto covariance function (ACF).

 $G_{\mathbf{x}}(0), G_{\mathbf{Y}}(0)$ Variance of the surface for scanning along 'X'

and 'Y' directions respectively.

G'(x),G'(y) The first derivative of ACF along 'X' and 'Y'

directions respectively.

G(x,y) The cross-correlation function.

H Hardness of material in BHN (kg/mm²).

1x Intercept length along 'X' direction.

Intercept length along 'Y' direction.

K Bessel function.

L Sampling length.

L_m Limit of useful magnification (L.U.M.).

M Number of points correlated.

mn 'n'th moment of the PSDF.

 m_0, m_2, m_4 . $0_{th}, 2_{nd}$ and 4_{th} moment of the PSDF respectively.

m_{Oy}, m_{2y}, m_{4y} Oth, 2nd and 4th moment of the PSDF respectively along 'Y' direction.

N Number of digitized points.

Na Numerical Aperture (NA).

N_{1X} Number of intercept lengths along 'X' direction.

Number of intercept lengths along 'Y' direction.

N₁ Total number of intercept lengths in a given area.

n Number of contact spots or bearing area.

O Observed frequency of occurrence.

P(a_b) Probability distribution of IBA.

 $p_{X}(z),p_{Y}(z)$ -Probability density distribution of heights along 'X' and 'Y' directions respectively.

pxy(1x,iy) Joint Probability density distribution of
intercepts length along 'X' and 'Y' directions.

R_X,R_y Curvature along 'X' and 'Y' directions respectively.

R _m	Maximum height of the profile ($R_{ extsf{max}}$)
W	Load in Kg.
77 (X)	Lag window.
w(f)	Spectral window.
1.4.1	Direction of grinding.
171	Across the direction of grinding.
2	Profile heights from the mean line.
2 *	Normalized profile heights.
Z'(x)	First derivative of the profile heights along 'x
	direction.
2"(x)	Second derivative of the profile heights along 'x'
	direction.
z	Profile heights from datum.

GREEK LETTER SYMBOLS

α	Bandwidth parameter.
$\alpha_{\mathbf{W}}$	The first parameter of Weibull distribution (i.e.,
	equation 4.9)
B W	Autocovariance length.
β	The third parameter in the Weibull distribution
	(1.e., equation 4.59).
Υ	The second parameter of Weibull distribution (i.e.,
	equation 4.9).
η	Number of degrees of freedom in Poisson
	distribution.
θ	Variable used in equation 4.13.
λ, Α ₁ , λ ₂	Correlating lengths
$\lambda_{\mathbf{x}}, \lambda_{\mathbf{y}}$	Lineal fraction along 'X' and 'Y' directions
	respectively.
$^{\lambda}$ L	Wavelength of light.
μ	Generalized Inverse Gaussian Distribution.
σ	Variable used in equation 4.54.
Υ	One of the parameters of the Inverse Gaussian
	Distribution.
τ	Imaginary number.
ф	One of the parameters of the Inverse Gaussian
	Distribution.
X	Chi of chi-squared goodness of fit.
Ψ	One of the parameters of the Inverse Gaussian

Distribution.

 ω Radial frequency. ω_{H} High pass cut-off ω_{L} Low pass cut-off.

LIST OF FIGURES

Ü

Chapter 1

- Fig. 1.1 Distortion of profile reading due to finite dimension of stylus tip (exaggerated) [17].
- Fig. 1.2 Effect of stylus tip radius on measured roughness of various surfaces [17].
 - 1. Planed 2. Electo-eroded 3. Milled 4. Ground
 - 5. Electochemically sunk 6. Honed.
- Fig. 1.3 Simulated profile with RMS = 10 μ m, L = 100 μ m and radius of stylus tip = 25 μ m, illustrating:
 - measured profile 2. compensated profile 3. Using further compensation [17].

CHAPTER 2

- Fig. 2.1 Principle of Schmaltz microscopy
- Fig. 2.2 Optical system used by Schmaltz [19].
- Fig. 2.3 Schematic of optical Grating Topography, OGT.
- Fig. 2.4 General arrangement of OGT set-up
- Fib. 2.5 Flow chart for the operation of OGT system.
- Fig. 2.6 Grating lines on optically flat mirror.
- Fig. 2.7 Grating lines on machined ground surface
- Fig. 2.8 Examples of application of OGT
 - a) OGT photograph of 0.001" step
 - b) OGT photograph of the belt ground surface
 - c) OGT photograph of the surface, obtained on the surface grinder
- Fig. 2.9 Computational flow chart.

- Fig. 2.10 1000x magnified photograph of the delineated grating profile.
- Fig. 2.11 Density distribution of heights of the profile obtained along the direction of grinding.
- Fig. 2.12 Density distribution of heights of the profile obtained across the direction of grinding.
- Fig. 2.13 Concept of auto-correlation function.
- Fig. 2.14 Auto-correlation function for the surface profile along the direction of grinding
 - b) across the direction of grinding.
- Fig. 2.15 Principle of auto covariance computations by means of Discreet Fourier-Transform
- Fig. 2.16 Amplitude spectrum of the surface profile
 - a) along the profile
 - b) across the profile

Ç.

- Fig. 2.17 3-D surface representation by means of parallel scanning lines.
- Fig. 2.18 Concept of lineal fraction and its relationship to the area fraction.
- Fig. 2.19 Definition of intercept length: $_{\omega}$ i_{χ} and i_{γ} for along and across the direction of grinding.
- Fig. 2.20 Distribution of intercept length along 'X' and 'Y' direction.
- Fig. 2.21 Distribution of intercept length at various scan levels.
- Fig. 2.22 Distribution of individual bearing area.
- Fig. 2.23 Effect of diffraction at straight edge [19].

Chapter 3.

- Fig. 3.1 Average wavelength for different surfaces [17].
- Fig. 3.2 The bearing length curve or Abbott curve [22].

Chapter 4.

- Fig. 4.1 Definition of ACF to determine the intercept length.
- Fig. 4.2 The ACF of the surface.
- Fig. 4.3 Amplitude spectrum at various loads.
- Fig. 4.4 Comparison of mean intercept length determined from measurement as compared to that obtained by equation 4.23.
- obtained from measurement as compared to that obtained using density destribution given equation 4.30.
- Fig. 4.6 The distribution of intercept length at various levels.
- Fig. 4.7 The normalised density distribution of IBA.
- Fig. 4.8 Growth of number of intercept lengths compared to that obtained by equation (4.22).
- Fig. 4.9 Density distribution of heights: a) unloaded b)

 10.5MPa c) 44 MPa d) 77.3 MPa
- Fig. 4.10 Variation of mean intercept length with various scan levels and hence load.
- Fig. 4.11 Density distribution of bearing areas at various scan levels
- Fig. 4.12 Variation in the IBA of various scan levels and hence load.

Glossary

1. Abbott curve [17]:

Bearing area fractions plotted as a function of height.

2. Baire function [20]:

The set Iy of all real numbers 'x' such that $g(x) \le y$ should be a countable union or intersection of intervals for any y; only then $\{Y \le y\}$ is an event. If g(x) has this property, it is called a Baire function.

3. Functional filtering:

It is the confinement of the measurement of the profile to the portion of the spectrum that takes part in the functional behaviour of surface. It involves the determination of low pass and high pass cut-off.

 High-pass cut-off: The cut-off which rejects the long wavelengths.

Low-pass cut-off: The cut-off which rejects the short wavelengths.

- 5. Lay: The direction of the predominant surface pattern, originarily determined by the production method used.
- 6. Cut-off or meter cut-off [17]:
 In a profile meter instrument, the conventionally defined wavelength separating the transmitted from the attenuating components of the effective profile.
- 7. Pass band: The frequency of the surface considered between the high and low pass cut-off.

8. Point spread function: Consider an object with an irradiance distribution $I_0(y,z)$ followed by an optical system which creates an image $I_i(y,z)$. The object information is transformed into the image by a process which can be represented mathematically as

$$I_{i}(Y,Z) = \int_{-\infty}^{\infty} I_{0}(Y,Z) S(Y-Y,Z-z) dy dz$$

where S(Y-y,Z-z) is called point spread functions.

In the case of perfect lens system, for example, S would be any pattern (similar to Newton's ring).

9. Roughness [17]:

The irregularities in the surface texture which are inherent in the production process, but excluding waviness and errors of form.

10. Waviness [17]:

The component of surface texture upon which roughness is super imposed. Waviness may result from such factors as machine or workpiece deflections, vibration, chatter, heat treatment or warping strains.

CHAPTER 1

INTRODUCTION

1.1 Importance of surface characterization

Topography can be considered as a narrow bandwidth irregularities covering the form or shape of the surface. Due to these irregularities which is the characteristic of the basic machining process, the surface is random in nature. Therefore, the surface irregularities may be considered to exist in the form of roughness or waviness. Moreover, depending on the presence of the preferred orientation of these irregularities (direction of lay), the surface becomes either anisotropic or isotropic. From this it is evident that the characteristics of the surface are so complex that their precise definition with a single parameter is not possible. becomes necessary, therefore, to characterize the surface in terms of parameters relevant to the problem so as to permit its use as indices to performance under actual operating conditions.

It is known from the experimental work of Abrams and Kops [1] that the surface texture (roughness and work waviness, isotropic or anisotropic) influences the manner in which two metallic rough surfaces in contact interact. In addition to this, it is clear that the tribological qualities (wear, friction, lubrication, fatigue, strength, etc.) are also

directly related to the surface texture [2]. Hence, the need arises to characterize the surface texture in such a way that it can be used to describe the functional behaviour of surface.

Many studies have been done to characterize the surface in terms of the center line average (CLA), root mean square (RMS), height density curves, correlation function and spectral densities [3]. This random process analysis, however, rests on two assumptions which are unnecessary: (1) the statistics of the surface are the same as the statistics of the profile of the surface, and (2) the asperities have spherical (regular geometrical) caps [4]. Osman and Sankar [5] realized the inadequacy of these parameters and, using the concept of stochastic excursion obtained parameters in the form of the mean intercept length at the mean level. This analysis was based on the assumption of an isotropic Gaussian process with the statistics of the surface being the same as that of the profile.

In many engineering applications involving contact it is sufficient to know the bearing area, its growth at different levels of irregularities, height and its distribution on the surface. This is due to the fact that it is through these discreet areas that the electric or thermal heat flux passes in problems related to electric or thermal contact resistance. Moreover, if this local bearing area and their corresponding probability density function together with the well defined local stress is employed, it is possible to formulate a stochastic theory of deformation for the solution of an elastic

contact problem. This suggests the necessity of extended surface characterization in terms of individual bearing areas and its distribution for the surface. It is proposed that such an approach of characterizing the surface in terms of individual bearing area and its distribution, and also in terms of the parameters like CLA, RMS, mean slope and curvature, should be sufficient to describe the functional behaviour of surface in contact problems.

1.2 Review of methods used in the measurement of surface topography:

There are various methods available to measure the surface irregularities. Each one of them possesses its own advantages and disadvantages inherent in the basic design and principles involved. The choice of any one of the methods depends on the following conditions:

- 1. Expected height variations in asperities.
- 2. Height sensitivity required.
- 3. Type of surface; i.e., specular or diffusive.
- 4. Cost and complexity involved in the analysis following the measurements made using this technique.
- 5. Resolution of-the-available method.

The available techniques can be broadly categorized into:

- 1. Contact methods.
- 2. Non-contact methods.

1.2.1 Contact methods:

Among the contact methods the main instrument still used extensively is the stylus profilometer. In this instrument a narrow diamond stylus of finite dimensions traces lightly across the surface contour to produce a time varying voltage output whose magnitude is directly proportional to the height of the surface contour. This voltage output is of a high pass frequency, filtered so as to include only surface spatial frequency components above a certain cut-off frequency. The period of the cut-off is defined as the 'roughness width' cut-off. The average absolute deviation of the filtered signal from its mean value is then used to define the roughness of surface.

The other contact methods described in [6] are mentioned mainly for their historical significance. They are no longer used as measurement techniques.

1.2.2 Non-contact methods.

As shown in Table 1, the first and foremost technique used falls into the category of light section microscopy. This method is essentially a non-destructive, non-contacting procedure that is quicker and easier to set up. This principle has also been employed in the Optical Grating Topography to be discussed subsequently.

Before discussing the interferometry method a few remarks as to the use of speckle in application of a laser light source to the measurement of surface topography should be made. The use of specular reflection measurements for the

Table 1

Techniques for Measuring the Roughness of Ground, Polished and Machined Surfaces; Roughness Greater Than 100 A rms [6]

Technique	Comments		
Light section microscopy	Light section microscope for heights 1-400 µm with a sensitivity of +0.5µm		
Fringe contrast ratio, Twyman- Green interferometer	Laser illuminations; end mirrors are reference and test surface respectively; roughness in range 10 A to $^{\lambda}_{\ell}/^{5}$ obtained from from fringe contrast ratio		
Single wavelength holographic interferometer	Interference between hologram and light reflected from test specimen; roughness in range 0.05 - 0.80 m obtained from contrast ratio		
Two wavelength holographic interferometry	Extension of above method for measurement of rougher surfaces using coherent light of two different wavelengths; theory only		
Two-beam and multiple-beam Frizeau fringes in inter-ference microscope	Interference microscopes of different designs; general roughness range $\lambda_{\ell}/20$ to $\lambda_{\ell}/2$ but can be rougher for surfaces with regular profiles or isolated scratches; lateral resolution depends on magnification and numerical aperture		
Stylus instrument	Surface profiles of bead blasted aluminium and machined steels; data digitized to yield height distribution function; roughness range 0.01 - 1.1 µm		

Stylus instrument

Surface profiles of ground and sand blasted metals; data digitized to yield height and slope distribution functions; roughness range 0.5 - 3.0 μm

Stylus instrument

Surface profile of ground steel surface; data digitized to yield height and slope distributions and other surface statistics; roughness 0.5µm

Light scattering

Specular reflectance of aluminized ground glass and ground steel; roughness range 0.16 - 1.3 µm

Light scattering

Specular reflectance at two angles of incidence; machined metals, ground glass, silicon in roughness range 0.1 - 10 mm

Light scattering

Specular reflectance of polished aluminium and steel; roughness range $0.09 - 0.08 \mu m$

Light scattering

Total integrated scatter to detect scratches, digs, and microroughness on mirrors and transparent domes

Optical profilometer

Small laser beam scanned over reflecting surface to detect isolated surface defects; height sensitivity 0.05 m

White light speckle

Moving rough surface; correlation between speckle contrast in broadband illumination and roughness when roughness is comparable to coherence length of light; ground, polished, sanded, and machined metal surfaces, in roughness range 0.1 - 6.4 µm

Laser speckle pattern

Mov,ing rough surface illuminated with diverging beam; roughness and correlation length determined from degree of coherence of transmitted beam; roughness range 0.4 - 0.9 μm for ground glass surfaces; upper limit of roughness related to magnitude of beam spread

Polychromatic laser

Speckle patterns of scattered light from ground glass correlated with roughness; roughness range 1 - 3 m; no correlation for 10 m roughness

Laser speckle pattern

Contrast in monochromatic speckle pattern from ground glass determined by scanning detector; roughness range 0.2 ~ 0.5 \text{Lm}; maximum roughness measurable 0.5 \text{Lm}

determination of surface roughness has been investigated earlier in reference [7]. The results show a significant correlation of the specular reflection measurement with the roughness measurements obtained by stylus profilometer. However, this correlation is constrained due to two assumptions:

- The roughness must be less than 15% of the wavelength of the employed illumination.
- 2. The height distribution should be a Gaussian distribution.

It should be noted that when any rough surface is illuminated with spatially coherent light and observed with a finite aperture optical system, speckle can be observed. Such speckles are produced because the light is received at each point in the image from several different points on the object, due to the limited resolution of the system. The path length of the light from each point on the surface depends on the height of the surface at that particular point. If the height varies significantly across the width of the point spread function, interference effects will occur known as speckles. The size of the speckles is known to be related to the Numerical Aperture (NA) of the observing system. speckles are the main reason for not using the coherent laser light source in the case of optical section microscopy. Furthermore, these speckles mix with the grating image and hence cause reduction in contrast which is not favourable for a faithful reproduction of profiles.

Most of the holographic interferometric techniques reported so far have been for measuring the depth contour of large surfaces, i.e., generation of contours of constant depth or for the measurement of the root mean square (RMS) roughness only. Even for polished specimens no good agreement could be reached [8]. Moreover, the requirement of parallel wavefronts in the holographic interferometry is the main draw-back, as this involves expensive devices not necessary for the range of measurements encountered in the rough ground surface. The other interferometry method like the Mirau interferometry [14] is a good means of measuring surface topography as it gives sharp lines with good contrast (unlike holography), but is limited in measuring surfaces having specular reflection characteristics.

The three beam interferometry [9] is perhaps the most sensitive for the case under consideration, since it depends upon the intensity changes in the interference bands, which is a measure of the irregularities on the surface. The principle in this technique is based on the common path three beam shearing interferometer in which the outer beams act as a reference while the middle beam scans the surface. Though one of the best ways when employed to measure film thicknesses, it has limitations as far as measurement of surface roughness is concerned. It requires two reference surfaces having the same intensity of reflection as that of the surface under study and using the same source of light. In spite of this it has a low NA.

Another method developed by Sato and Hori [10] aims at

determining the profile of the surface roughness by integrating the intensity of back scattered electronic signals. The disadvantages are:

- It requires Scanning Electron Microscope (SEM) for observation equipped with two or probably three integrators.
- The sample must be supplied with a conductive coating.
- It is very time-consuming.

Although light scattering methods represent simple and straight-forward implementation of surface characteristics, they do not measure the surface structure directly. The simplest instrument of this type is the glossmeter (ISO2812 or ASTM D523), which measures the specular reflectance of the surface [11]. Specular reflectance, however, increases with an increase in the refractive index and is also influenced by the smoothness of the test surface. Hence the gloss data obtained are not a sole function of the surface topography; at best they can give only an average surface topography.

Clarke and Thomson [11] have developed a laser scanning analyser [LSA] system, whereby a laser beam is reflected from a polygonal mirror rotating at high speed down onto the surface of a workpiece. It is then reflected into a fixed photoconductor receiver with a wide aperture that is used to measure defects. It also comes with a narrow slit for the measurement of surface roughness. Considering a minimum spot

reflectance or scattering from the test surface over an angular range of 30°. Unfortunately, this scanning technique measures a specific angular reflectance at different locations on the surface and thus represents only an average angular reflectance of the test surface over the scanning range. It is from this that the RMS roughness and other informations like CLA can be deduced.

It is seen that these techniques inherently average over a region of the test surface, and thus cannot directly obtain the actual surface profiles. The accurate measurement of scattered light over many orders of magnitude from the specular direction is quite difficult and time-consuming. Further, a surface preparation is important for the measurement of very smooth surfaces. For very rough surfaces, a more complicated vector diffraction theory must be used in order to predict the actual surface structure.

employing multiple beam fringes of equal chromatic order (FECO). FECO are formed when a collimated beam of white light undergoes multiple reflections between two partially silvered surfaces, one of which is the surface whose profile is being measured and the other is a super-smooth reference surface. Using a TV camera for the detection of the positional displacement of the fringes, this technique yielded accuracies of the order of 0.8 nm RMS for the measurement of surface profiles. Lateral resolution of this system has been reported

to be between 2 and 4µm over a 1mm profile length. Signal averaging in the system increases the measurement time, and therefore severe environmental precautions must be taken to ensure the accuracy of measurement. Also, the system requires that the surfaces being analysed have high reflectivity.

Both the "Differential Interference Contrast" (DIC) and the "Nomarksi polarization interferometer" techniques (12) are useful for qualitative assessments of surface topography; however, quantitative results may be difficult to obtain. While interferometers of this type are easy to operate, and essentially insensitive to vibration, they have the disadvantage that they measure the slope of the surface irregularities only, rather than the irregularities themselves. Furthermore, since they measure surface slope irregularities in one direction only, the sample orientation is important.

Recent advances in the field of electrical engineering have resulted in the development of a topografiner [3]. It consists of a servo controlled non-contacting field emission which maintains a constant current between a conducting specimen and itself. The motion of the probe is amplified and displayed forming an isometric picture as the surface is scanned in a series of parallel traverses. This instrument has a high resolution, but is restricted to very small specimens and has the added disadwantage of requiring conducting specimens in a high vacuum.

Another class of measurement technique belongs to the Category of focus error detection developed by Mitsui, Ozawa

and Kohno. Herein the change in focus of the optical system due to change in height of surface irregularities is detected by the principle of astigmatism [15]. While this method can give high resolution (0.01 μ m), it can be used only on specular surfaces like diamond machined surfaces. The other disadvantage is in the effect of diffraction figure which is inherent in any focus error detection technique.

1.3 Evaluation of available methods.

Various methods for the measurement of surface and the brief description of its advantages and disadvantages was discussed in the last section of this chapter. From this it is evident that not a single instrument can be universally accepted to measure all the types of surfaces encountered during machining. Stylus profilometers have very good sensitivity $(0.01\mu m)$, but have disadvantages due to the effect of stylus size and load. Distortion of the profile due to finite dimensions of the - stylus tip [16] is as shown in Figure 1.1. The effect of stylus tip radius on measured roughness [16] as shown in Figure 1.2 also shows how the stylus profilometer can give results deviating from the actual value. The other sources of error, like filtering due to skid and the effect of stylus geometry on its dynamic response, are discussed in reference [17]. Recently De Vries and Cheng-Lih Li [18] have tried to solve this problem due to stylus geometry by developing suitable algorithms covering the range of 12.5 - 2.5 µm stylus radius They developed kinematic and geometric algorithms to

compensate for stylus geometry so as to present a better picture of the true surface profile. The extent to which the compensation could be achieved is as shown in Figure 1.3.

The optical method employing the principle of Schmaltz microscopy is perhaps the simplest and most elegant [19]. Observable detail with the Schmaltz projection method depends on the resolving power of the microscope objective. The major source of error in this technique arises from the diffraction that takes place at the edge of the shadow. However, the height of shadow can be estimated to a very small error for irregularities of maximum depth greater than .76 µm [19]. Moreover, by using a concept similar to Biernawski's multiple shade topography [20], one can apply multiple scanning of the surface for 3-D surface characterization as discussed in the next chapter.

1.4 Outline of the thesis:

The main purpose of this thesis is to characterize the surface in terms of parameters necessary to describe the functional behaviour of surfaces in contact. In many engineering applications like the determination of electric and thermal contact resistance and the analysis of deformation of interface formed by two surfaces in contact, it is sufficient to determine the local bearing area and its distribution on the surface. For it is through these discreet areas that most of the electric or heat flux passes. The subsequent computation

of the digitized data obtained by using OGT leads to the determination of not only the conventional parameters like CLA, RMS, mean slope and curvature, but also the individual bearing area and its distribution. This procedure of 3-D characterization is described in three steps.

In order to statistically determine the individual bearing area and its distribution the OGT was developed. The first step, therefore, is the literature review of the measurement technique available for profile description of surfaces. This was already described in the last section of this chapter.

The second step is in the description of the Optical Grating Topography technique for measuring the surface. Having obtained the profiles of the surface, they have to be digitized and processed to obtain the parameters. The technique and computational procedure is described in Chapter 2.

Review of the existing models describing the surface characterization forms the main content of the Chapter 3. This chapter discusses the various models that have been developed in the past to obtain parameters. Finally, as a last step, the extended characterization of surfaces and the proposed application to contact problem is discussed in Chapter 4. The analytical determination of the parameters in terms of the moments of the statistical function forms the main part of this chapter. Its correlation with the experimental results obtained by using OGT is also discussed.

Finally, Chapter 5 states the conclusions and recommendations which arise from this study.

CHAPTER 2

OPTICAL GRATING TOPOGRAPY

2.1 Introduction

The characterization of surfaces for the description of their functional behaviour in contact problems, like those in machine tool joints, requires a measurement method which could be free from the error caused by the stylus of a profilometer. relatively high surface roughness of machined ground surfaces in the case under study precludes the application of profilometers which use a laser based optical interferometer Other optical techniques, which rely on the specular reflection of the surface or use special coatings to enhance the intensity of reflection, are also not suitable for the surface's which are the subject of the present investigation. To obtain a detailed description of the surface to be studied, perhaps the best way is to obtain a profile section or a contour section of the surface. Although this sounds logistically feasible, difficulties can be visualized in doing it. While the introduction of distortion in the profile when taking sections can in no way be ignored, the destruction of the surface in doing so discourages us in adopting methods underlying this principle. To circumvent this difficulty a German scientist, G. Schmaltz, cited in [19] developed a purely optical means of obtaining a profile curve based on the principle of optical cut. This is illustrated in Figure 2.1.

The optical system used is also shown in Figure 2.2. The illuminator projects an image of a straight edge, or a slit, on the surface in the field of view of the microscope. Both objectives in microscope for observation and illumination are alike. The 45° angle between the observation and illimination system results in:

- maximum intensity of light entering microscope objective.
- 2. correct focus over the entire illuminated band.
- 3. magnification in the direction of height and depth.

Since it is intended to multiple scan the surface, a concept similar to Biernawski's multiple shade topography, some modifications were made to the set-up originally used by Schmaltz. These modifications were in replacing:

- 1.0 a slit by a transparent grating of 330 lines/mm
- 2. fixed illuminating objective by a movable objective which permits adjustment for obtimum brightness and contrast of grating lines,
- and, 3. a fixed observation objective by an epiplan objective (with greater working distance than conventional objective) mounted on a focussing gear. This permits observation of other grating lines on the surface without moving the workpiece or set-up.

Subsequent profile computation both across and along machined lay direction leads to the determination of surface parameters for the surface. In particular, the OGT method was

used to define parameters of the bearing area, essential in the contact problem. Both the analysis and the computational procedure is presented in this chapter along with the description of the measuring technique.

2.2. Description of the OGT system

Referring to the diagrammatic sketch of the OGT given in Figure 2.3, it can be seen that the apparatus consists essentially of two optical arrangements: illumination and observation. The various components that makes the OGT system are:

- 1. Light source: Light used for this technique was ordinary white light. This type of light was necessary since, as discussed before, the coherent light source like 'Laser' causes speckle which distorts the grating line image and interfers with the edge of these lines.
- 2. Collecting lens: The system of lenses (convex) collects the light from the source and lets it pass through the microscope body for the illumination of the grating.
- 3. Transparent grating: The transparent grating plate consisting of 330 lines/mm was placed behind the movable objective. The lines from this grating were projected on the surface of the sample to obtain the profiles for measurement.
- 4. Traversing objective mount: This is a movable (x,y) mount which carries the illuminating objective on

one side and a grating plate on the other side.

- 5. Objective for illumination: This objective is flo,
- .25 NA used for projecting the grating lines on to the surface of the sample.
- 6. Specimen mount: This mount is an x,y positioner for holding the specimen or workpiece. The workpiece could be moved along x,y axis for measurements at different locations on the surface.
- 7. Objective for observation: This consisted of an epiplan objective fl6, 0.35 NA with greater working distance than the conventional objective of the same class. This objective is used for both transmission as well as reflecting microscopes.
- 8. Focus control: The entire microscope was mounted on a precision focussing gear to observe the grating line images.
- 9. Binocular phototube: This was meant for manual observation of the grating line image prior to using camera. This facilitated the control of the focus.
- 10. High eye point eyepiece 10%.
- 11. ACM microscope: The microscope body was used as it could carry all the above mentioned components and also the polaroid camera.
- 12. Camera with automatic exposure control.
- 13. Collecting lens tube: This tube was necessary for two reasons: (1) to carry the system of collecting lens, (2) to maintain alignment of the axis of

collecting lens and the objective forming the illuminating arrangement.

2.3 Operation of the OGT system.

The operation of the OGT is schematically shown in Fig. 2.5.

It is evident from this figure that it essentially consists of two main procedures:

- 1. Establishing the geometry of the optical system and observing the effect of the grating lines on an optically flat mirror.
- 2. Maintaining the same geometry and repeating the procedure on sample surfaces for measurements.

2.3.1 Establishing the optical geometry:

From Figure 2.1 it is clear that the parameters which influence the observation of the topography of surface are:

- 1. the angle of observation and,
- i1. the angle of incidence of lines on the surface of the sample.

Moreover, the amount of delineation of the grating line depends on:

- i. the above two parameters describing the geometry of OGT and,
- ii. the amount of variation in depth of surfaces.

 Therefore, by knowing the amount of delineation in the grating line image due to the known step height or depth which is obtained from the photograph, it is possible to get the two parameters describing the geometry of the OGT. Once this

geometry of OGT is established, it is now ready to measure the surface irregularities that might exist in the form of either roughness or waviness.

2.3.2 Measurement Procedures:

Without disturbing the projecting part of the system, the grating lines are now made to fall on the surface to be examined. It is possible that in the first attempt the grating lines on the surface of the sample may not be sharp. sharpness is obtained by adjusting the workpiece distance from the illuminating objective and observation objective. this adjustment for maximum brightness and contrast, the grating line image obtained on the surface of the sample is photographed for further processing. The effect of the optically flat mirror on the grating line image photograph obtained from OGT is shown in Figure 2.6. When compared with Figure 2.7, which is the grating line image photograph obtained by applying OGT on the machined ground surface, it is clear that the delineation of the grating line as seen in this figure is due to the effect of surface irregularities. Measurement of this delineation in the grating line with respect to that obtained from optically flat mirror gives the heights of the surface irregularities.

Some more examples of the application of the OGT are given in Figure 2.8. The measurement of the one thousandth of an inch step obtained on the sample by surface grinding is shown in Figure 2.8a. It can be seen that the measurement

accuracy is of the order of 0.1µm. Figures 2.8b and 2.8c show the surface irregularities obtained by applying OGT technique on belt grounded surface and the ground surface obtained by surface grinder respectively. The difference in heights of irregularities is clearly noticeable. Figure 2.8b not only shows surface irregularities in the form of roughness, but also the waviness which is not observable on the ground surface in Figure 2.8c.

2.4 Specification of OGT

The specifications of the OGT employed to measure the surface topography are:

- l. Resolution: The limit of resolution is the minimum distance, 'd', of two structural elements, e.g., two adjacent hairs if they are to be imaged as two separate elements instead of one. There are two types of resolution relevant to the present technique. The axial resolution is 1.6µm [21] and the lateral resolution for the objectives used is 0.65µm [14].
 - 2. Limit of useful magnification: When the smallest object detail of magnitude 'd', resolved in the image formed by an objective of given NA, has been magnified by the combined performance of the objective and the occular (eye piece) so that its image has the same magnitude as that of the smallest detail which the eye can resolve, the limit of useful magnification (L.U.M.) has been reached. The L.U.M. (Lm) for OGT is 2666.

2.5 Computational Procedure.

For the determination of the syrface characteristics required in the description of the surface irregularities which includes the concept of individual bearing areas (IBA), it may be instructive to discuss first the computational flow chart to be used in conjunction with the obtained observation by the OGT This flow chart is shown in Figure 2.9. observed delineated grating line obtained due to surface irregularities present on the surface is magnified 1000X. This is as shown in Figure 2.10. The magnified photograph is then digitized in 640 KB IBM-PC with HIPAD DT 114-S digitizer and a D7-11-1109 stylus with 0.1mm resolution. Digitization of the contour lines of the grating and the subsequent processing of the digitized data is achieved through the interface with AMDAHS 5850. The processing of the digitized data consisted of statistical and power spectral analysis. The latter leads to the determination of parameters like variance of height slope and curvature.

Since the surface under consideration is highly anisotropic, the concept of Quantitative Stereology is used to extract the socialled 'lineal fraction' of the profile in the direction of scanning, i.e., in the machining direction 'X' or transverse to it in the 'Y' direction. If not all scanning lines have been included, the program is sent back for the above outlined computation. If the digitizion and Quantitative

Stereological principles have been completed for all the scanning lines of the test sample the program is concluded by the calculation of the probability distribution function of the area (IBA). The detailed scanning and computational procedure is discussed below.

2.5.1 Statistical Analysis.

The statistical analysis involves the determination of the density distribution of heights of the irregularities of the surface. This analysis is necessary in order to check the type of distribution of surface heights. The density distribution was plotted for both along the direction of grinding and perpendicular to the direction of grinding. The density distribution as obtained from the measurements taken from OGT for a typical profile is as shown in Figures 2.11 and 2.12. - The density distribution looks slightly skewed because of the effect of the sampling [22]. It can be shown that even a random sample from Gaussian population when sampled and histograms plotted would give a statistical scatter and could give skewness. In order to check the type of distribution the chi-squared goodness of fit [23] was employed and the nullhypothesis was accepted as true. The difference between the observed and experted values was not the least significant, and could have occurred with a probability of greater than 10% by The Gaussian model was therefore accepted. chance alone. profiles were checked and almost all showed typically similar One of the tabluated results is shown below as an results. example.

A chi-squared test yields a quantitative measure in terms of the probability of the differences between observed and expected values being explained by chance. Chi-squared is found by using the equation:

$$\chi^2 = \frac{(0-E)^2}{E}$$
 (2.1)

where 0 - observed frequencies

Clearly, close agreement between observed and expected values result in small values of χ^2 . At the outset the null hypothesis was assumed that both observed and theoretical results come from the Gaussian distribution. In calculating the theoretical frequencies the mean and the total frequency of the observed results were employed, thus imposing two conditions or restrictions. The number of degrees of freedom was thus

$$\eta = 9 - 2 = 7$$

Referring to standard tables the value of χ^2 for 7 degrees of freedom was 12.02 at probability level of 0.1.

The tables shown below are self-explanatory. Here (z/D) is the standardized height of asperities and other symbols have the usual meaning as discussed earlier.

Table 2

ż

Determiniation of goodness of fit for measurements obtained perpendicular to the direction of grinding

·				
z/D .	0	E	0-E	(0-E) /E
	y.			
-1.06	36	30,	6	1.2
-0.83	15	12	3 ,	0.75
-0.606	17	12	5	2.0
-0.378	11	16	-5	1.56
-0.151	24	18	6	2.00
0.075	13 '~	12	1	very small
0.3	25	24	1	11
0.53	10	16	-6	2.2
0.757	49	50	-1	"

$$0 = 200$$
 and $\chi^2 = 9.61$

As calculated value of 9.61 is less than 12.03, the null hypothesis is accepted as true.

Applying similar procedure for data obtained from QGT for profiles along the direction of grinding we get,

Determination of goodness of fit for measurements obtained along the direction of grinding.

Table 3

z/D	o	E	0-E	(0-E) /E
-0.8	16	21	^{**} 25	1
-0.5	15	9	36	4
-0.2	12	12	0	o
0.175	16	14	4	0.3
0.4	13	12	1	very small
0.7	7	10	9	0.9
1.0 .	9	11	-n 4	0.3
1.9	6	11 -	25	2.3
2.2	6	3.4	6.76	2.0

$$0 = 100 \text{ and } \chi^2 = 10.86$$

Here again the value of χ^2 is less than 12.03 and therefore the hypothesis is accepted as true.

This is an important experimental observation because the derivation of parameters as described later is based on this finding. It is to be noted that the density distribution of heights of asperities have been determined for a C.I. ground surface. The grinding was done using the grinding wheel of type A-24-M-Vl. The other properties of the C.I class 35 are:

- (1) Brinel Hardness B.H. = 200
- (2) Modulus of Elasticity E * 105 GPa
- (3) Poisson's ratio = 0.29

2.5.2 Spectral Analysis

6

7,0

Nayak [24] has shown that useful statistical parameters can be obtained to characterize the surface if their power spectral density or amplitude function is known. It is well known from the observation of the ground surface that the irregularities are more closely packed in the direction perpendicular to the lay than along the direction of grinding. For lack of a more precise mathematical description it can be said that the first one is closer than the second one. This leads to the question, is there any other way that we can get more quantitative description? The answer to this question can be given by autocorrelation function. To construct this function a pair of ordinates separated by a horizontal distance $'\lambda'$ is considered as shown in Figure 2.13. If ' λ ' is large it is unlikely that these ordinates will lie on the same peak or valley. Therefore, the product of the ordinates at two points on the profile separated by a distance ' λ ' is equally likely to be positive or negative. And if their sums are obtained, the mean value will tend to zero. If on the other hand, a pair of ordinates whose separation is small is considered they are very likely to lie on the same peak or valley. Moreover, their product will be positive and the mean value of a large number of such products would be finite and positive. Therefore, one can define a statistic for a signal length 'L', i.e.,

$$G(x) = \lim_{L \to \infty} \frac{1}{L} \int_{0}^{L} Z(x) Z(x+\lambda) dx \qquad (2.2)$$

in which $Z(x) = z(x) - \langle z(x) \rangle$, which can be considered as a figure of merit of geometrical relationship. It will vary continuously with '\lambda', falling gradually to zero from an initial positive value at \lambda = 0. Its value at any given separation will be a measure of the average physical relationship of pairs of points on the profile with that separation. The length which it takes to decay to insignificance will be a measure of the average size of a peak. From the Figure 2.14 it is clearly evident that the autocorrelation function dies down faster for across the lay than for along the grains (lay).

It is a familiar concept that any profile, however complex its waveform, can in principle be represented by Fourier analysis as the sum of the number of pure sinusoids. Because of the large number of terms (Fourier) needed in practise to describe the random surface, the graph obtained with amplitude against its frequency would be continuous. By analogy with other frequency distribution (light, sound) it is called an amplitude spectrum. Since the amount of labour involved in calculating the large number of Fourier terms (even for a computer) is very great, it is desirable to consider the power over a small range of frequencies from f to Δf and with

the limit δf tending to df. This function can be defined as Power spectrum A(f). Therefore, this function gives the information about the frequency distribution on the surface considered. The area under the power spectrum between two given frequencies is the total power present in that frequency band and is statistically known as variance. Mathematically, it can be written as

$$A(f) = (2 \pi) \sum_{-\infty}^{\infty} G(x) \exp(-\pi 2 \pi f x) dx,$$
 (2.3)

 2π in which $f = \frac{2\pi}{\omega}$, ω = radial frequency.

In general, higher moments can be expressed by:

$$m_n = \{(2)^n\} \int_{-\infty}^{\infty} f A(f) df.$$
 (2.4)

In the present study, a significant parameter [24] is defined by:

$$\alpha = \frac{m_0 m_4}{m_2^2} - \frac{m_4}{m_2}$$
 (2.5)

This defines the width of the power spectrum of the random process forming the surface from which the profile is taken.

2.5.3 Practical Computations.

The estimation of the roughness spectrum A(f) for the random process Z(x) was done by computing first the ACF and then its Fourier transform. This procedure was adopted because of the following reasons:

- (1) The computation of the ACF as an intermediate result allows the incorporation of a lag window W(x) which corresponds to a spectral window w(f) in the spectral domain.
- (11) It'is possible to perform an arbitrary amount of smoothing in the spectral estimate.

Referring to Figure 2.15, the method [25] can be described as follows:

- (a) The sequence z(j) (supposed to be a power of 2) is split in N/M sequences of length M.
- (b) The sequences $z_i(j)$, $i=1,2,\ldots$, q is considered of length 2M overlapping by M.
- (c) At each sequence $z_i(j)$, the sequence $z_i^0(j)$ is associated, i.e.,

$$z_{i}(j) = z_{i}^{0}(j)$$
 for $j = 0,1, ..., M-1$.

0 for $j = M_{1}, ..., 2M-1$.

- (d) 2M discreet Fournier transforms (DFT's) $Z_i(f)$ and $Z_i(f)$ are computed.
- (e) $X(f) = \sum_{i=1}^{i=q} z_i(f) z_i(f)$ is formed.

(f) By using the FFT algorithm $G_{FT}(m) = DFT^{-1} [X(f)], m = 0,1, ..., 2M-1$ (2.6)

is computed.

(g) To obtain M auto-correlation points the last half of $G_{\rm FT}m$ is discarded.

In order to estimate the roughness spectrum A(f) from G(x), a smoothing window W(x) [26] must be used to reduce the undesirable effects of using a finite length record (i.e., M values of ACF) instead of the infinite correlation sequence. To make a selection from among the collection of possible windows, it is necessary to apply some goodness criterion or figure of merit for windows. Unfortunately, no single figure of merit could suffice for all possible underlying spectra and no single window can be best with respect to all the possible criteria. In practice it has been found that when the sample size is large enough to achieve adequate resolution with good stability most of the windows yield comparable estimators when properly matched for resolution and stability. After many attempts the simplest of windows, namely, the Bartlett window was chosen,

$$W(x) = \begin{cases} 1 - |x|/M, & |x| \leq M \\ 0, & |x| > M \end{cases}$$
 (2.7)

which yields in the spectral domain,

$$w(f) = M[\sin(fM/2)/(fM/2)]^{2}$$

In order to determine the number of lags M for which the ACF's have to be computed, the variation in the spectral estimates was examined as the truncation point was increased. If only minor changes occur in the estimates when M is changed beyond certain value M* then it can be concluded that the window closing procedure has revealed most of the detail in the spectrum. Figure 2.16 shows the spectral density obtained by using M = N/4 which is perfectly suitable according to Jenkins and Watts [27]. The parameters obtained from this spectrum are as shown in Table 4 which is presented in Section 2.6.2.

2.6 Determination of mean intercept length and its distribution.

In order to obtain the mean intercept length and its distribution, a test section of 200 x 500 microns² was selected. This section was considered as best to represent the whole surface on the assumption of statistical homogeneity. Before going into its experimental determination, it would be worthwhile to consider Figure 2.17. This figure shows a small test section scanned by eight lines using OGT technique. Another increment along 'X'-direction results in the total scan of 16 lines. It is to be noted that this procedure is necessary as a single line cannot represent the whole surface. It is evident from the figure that the asperities are more closely packed along Y-direction than along X-direction, this shows that the surface is anisotropic in character. In order to analyse this type of surface to yield parameters, Quantitative Stereological principles are invoked.

2.6.1 Application of Quantitative Stereology:

The principles of quantitative sterology [28] involves the determination of 3-D characteristics from two dimensional measurements. It determines the relationship between the point fraction, lineal fraction, areal fraction and volume fraction. In the study of surfaces the relation between the lineal fraction and areal fraction is important. This is because the lineal fraction is determined for a test section using OGT and using the proper relationship with the areal fraction, the mean bearing area could be determined. Therefore, before proceeding with the determination of areal fraction it is necessary to determine the relation between lineal fraction and areal fraction.

Consider a cube containing asperities on the surface, and let it be cut by a plane passing across these irregularities at any height from the mean line. The Figure 2.18 represents the square cross-section of Area $A = L^2$ parallel to the x-y plane which contains the irregularly shaped areas, and a thin strip of width ' δ x' across the section parallel to the y-axis. The area of contact in the thin strip is given by

 $\delta A_{C} = E \times \delta \times \times (A_{A})_{C}$

and, for 'δx' sufficiently small by

1

 $\delta A_{C} = 1_{X}$ (x) δx (2.8) where $i_{X}(x)$ is the length of bearing intercepted by strips as a function of strip position 'x'. $i_{X}(x)$ may vary with 'x' as indicated in Figure 2.18, and the average value between '0' and 'L' is

$$\langle i_{x} \rangle = -\frac{1}{L} \int_{0}^{L} i_{x}(x) dx = i_{x}^{-}$$
 (2.9)

In the limit, the total bearing area in the test section is given by

$$A_{C} = \int_{0}^{L} dA_{C} = \int_{0}^{L} 1_{x}(x) dx$$
 (2.10)

which becomes,

$$A_{C} = L_{1x}$$
 (2.11)

dividing both sides by AT we get,

$$\frac{A_C}{A_T} = \frac{1}{2} \times \text{ or } A_A = \overline{L}_L = \lambda \qquad (2.12)$$

Thus, it can be seen that the fractional length of lines through the irregularities gives an estimate of areal fraction of the surface.

An example [29] demonstrating this relationship can be given (as referring to Figure 20):

line density of contact along 'X'-direction

$$= (0 + 0.5 + 0.25 + 0.5)/4 = 5/16$$

line density along 'Y' direction

=
$$(0 + 0.75 + 0.5 + 0)/4 = 5/16$$

= $^{\circ}5/16 = A_{A}$.

The deviation of the lineal fraction can be given by the

equation [28]:

$$\left\{\begin{array}{ccc} 2 & 2 & 2 \\ \frac{D(\lambda)}{\lambda} & = & \frac{1}{N_{i}} & \left\{\begin{array}{ccc} D(1) & 2 \\ -\frac{1}{2} & + & 1 \end{array}\right\}$$
 (2.13)

where $i = mea_i n$ intercept length

D(i) = standard deviation of the intercept length

 N_{i} = No. of intercept length

 $D(\lambda)$ = deviation of the lineal fraction ''

 λ = lineal length fraction.

Depending on the degree of orientation of the irregularities which determines the degree of anisotropy, the parameters like the areal fraction and deviation would change. Incorporation of this term or factor is also possible and is discussed in reference [28].

Thus the characterization of surface however anisotropic may be done using the theory of quantitative stereology. Even though this does not give the nature of distribution of the bearing length, the parameters determined for far could give enough description about the morphology of surface for valid comparison and probably provide the type of information needed in surface systems.

2.6.2 Density distribution of intercept length and bearing area.

Having discussed the concept of quantitative stereology, its relevance in the characterization of surface would be clear when the intercept length and lineal fraction is defined.

Referring to Figure 2.19, the intercept length is the length of the line intercepted by the crest of the profile at any height 'Z' from the mean line of the profile. The sum of all the intercept lengths divided by the total length of line scanning the surface is the lineal fraction i.e.,

$$\lambda_{x} = -\frac{i_{x}}{L}, \quad \lambda_{y} = -\frac{i_{y}}{L}$$
 (2.14)

Using the principle of quantitative stereology, one gets

and the second of the second o

$$\lambda_{\mathbf{X}}$$
 or $\lambda_{\mathbf{Y}}$ z Af (Areal fraction).

The distribution of the intercept length along 'x' and 'y' direction is as shown in Figure 2.20. The intercept length distribution has been obtained at the mean level. Referring to the Figure 2.29 it can be seen that the lineal length fraction along 'X' or 'Y' direction is given as:

$$\lambda_{\mathbf{x}} = \frac{\mathbf{i}_{\mathbf{x}}}{\mathbf{L} \times \mathbf{n}}$$
 (2.15)

where

L = length of profile along 'x' direction

= 200 microns

n = number of lines scanning the surface

= 16

$$\begin{array}{c} \lambda_{x} = \frac{2176}{200 \times 16} = 0.68 \end{array}$$

Similarly,

$$\frac{\lambda}{y} = \frac{iy}{t \cdot x \cdot p}$$

Therefore, the areal fraction can be given as,

$$A_{A} = -\frac{a_{b}}{A} = 0.67 \tag{2.16}$$

On the assumption of the standard Gaussian Process, it has been shown by Papoulis [30] that the number of intercepts/unit length ' $N_{i,x}$ ', can be expressed in the following form:

$$N_{ix} = p_{x}(Z) E \{ |Z'(x)| \}$$

$$N_{iy} = p_{y}(Z) E \{ |Z'(y)| \}$$
(2.17)

in which p_X (Z), p_Y (Z) are the probability density function of the 'Z'-coordinate heights, Z'(x) and Z'(y) are the first derivatives of the variation in heights of the random profile and 'E' their expected values. Knowing the number of intercept length it is possible to determine the mean intercept length along 'X' and 'Y' direction. This can be used to determine the mean individual bearing area. Thus, for any surface the mean individual bearing area can be given as:

$$a_b = c(i_X . i_Y)$$
 (2.18)

where 'c' = shape factor depending on the shape of individual bearing area. For example, for an isotropic surface it would be $\pi/4$ with $\langle i_x \rangle \simeq \langle i_y \rangle$.

From the Figure 2.20, the mean intercept length along 'X' axis is equal to 28 μ m and that along 'Y'axis is equal to 13 μ m. Therefore, $a_b = \pi/4 \times 13 \times 28 = 285.7 \,\mu$ m². It is seen from the same Figure 2.20 that the intercept lengths 'ix' and 'iy' are

random variables and hence its density distribution have been obtained. The density distribution of intercept length at various scan levels is shown in Figure 2.21. In order to arrive at a single density function in terms of the density function of $^{1}_{x}$ and $^{1}_{y}$ and the shape factor, it is necessary to obtain the joint density of $p_{x}(1_{x})$ and $p_{y}(1_{y})$, i.e.,

$$P_{xy}(1_x) = P_2(1_x) \cdot P_y(1_y)$$
 (2.19)

The calculation procedure of the joint density and hence the density distribution of individual bearing area is given in Appendix A. The density distribution of individual bearing area as shown in Figure 2.22. From this figure one can observe that the mean value of the IBA is equal to 301µm². Using equation 2.16, the total IBA is given by,

$$\Sigma a_b = Af \times 500 \times 200.$$

= 0.668 x 500 x 200
= 66800 um²

The total bearing area can also be obtained from Figure 2.22. Since the mean IBA is equal to $301\mu\text{m}^2$, the total number of IBA is given by

n = 222.

Other parameters like the CLA, RMS, mean slope and curvature as obtained using spectral analysis is shown in Table No. 4. The Table No. 5 shows the statistical value obtained for the

Table 4

Numerical values of surface parameters of a casting iron gound surface.

Dimensions in micrometers(").

	Variance of height [*]	Variance of slope	Variance of curvature	CLA R _a *	Mean slope	Mean curvature*	Bandwidth
X Scan	3.371	0.03	0.00394	1.46	0.123	0.09	14.75
Y Scan	5.682	0.0692	0.0052	1.78	0.209	0.16	6.17

40

Table 5

Comparison of values obtained from the OGT technique and the Talysurf profilometer.

Description	OGT	Talysurf
Sampling length, µm	250.0	250.0
CLA	1.78	1.27
RMS	2.23	1.56
Mean intercept length	11.37	12.25
Mean slope	0.209	0.217
No. of crossings/ μm	0.031	0.22
No. of IBA/mm ²	2220.0	
Mean IBA, μm ²	3010.0	

methodology adopted in using the OGT technique was not applied using Talysurf profilometer, and hence the last two values have not been determined.

2.7 Error Analysis of OGT.

The errors introduced in the measurement of OGT were mainly due to:

- (i) the effect of diffraction at the straight edge of the shadow;
- (11) the effect of digitization due to 0.1mm resolution stylus of HIPAD DT 114S;
- (1ii) the effect of calibration.

2.7.1 Effect of diffraction at the straight edge of the

shadow.

It is well known that, due to diffraction, when a ray of light passes through a slit or a hole, it bends at the edges of the slit causing a gradual variation in the intensity of light from the light band to the dark region of the screen. This region, also called the grey region, is formed due to the wave nature of light. The extent to which the grey region exists depends on the wavelength of light used, width of the slit and the distance of the slit from the image on the screen. Therefore, this grey region is the cause of loss of sharpness at the straight edge of the shadow. While doing the profilometric trace of the delineated grating profile obtained from OGT,

there is an uncertainty in the reproduction of the profile due to the grey region. The amount of uncertainty can be determined referring to the Fig 2.23 obtained from reference [19]. It can be seen that for irregularities .76_m deep, the blurring of the edge of the shadow from this cause occurs over a region some .76_mwide. However, the height of the shadow can be estimated to a considerably smaller error (5_" = 0.127_m), as will be seen from Figure 2.23. Therefore, the diffraction at the edge would seem to limit the use of this technique to the study of the shape of irregularities of depth greater than 30m" (0.762_m) [19].

2.7.2 Effect of digitization using O.lmm, resolution stylus.

The photograph of the delineated grating profile obtained by using OGT is magnified 1000x. This photograph is then considered for the digitization of the delineated grating profile. The digitization procedure involves the use of stylus of 0.1mm resolution. Since the magnification is 1000x, the error due to stylus is 0.1µm, which corresponds to 2% (for a maximum height of rough ground surface = 5µm). The errors due to digitization and diffraction can be further minimized by the proper use of filters (either optical or in the image processing technique). The use of filters (digital) in the image processing of such photographs has been discussed in reference [31]. The technique employed by Kaneko S. et al could be useful in the automated digitization of grating line image and also in the minimization of errors due to diffraction.

2.7.3 Effect of calibration.

As discussed earlier, the delineation of grating line is obtained due to the effect of observing the grating line at an angle to the incident light. Therefore, the accuracy of measurement of the delineated grating profile depends on the accuracy of measuring the incident and observation angles of light ray. In order to accurately assess these angles, known steps in the form of highly accurate reflection type diffraction grating and slip gauges were used. The angles determined this way were then used to determine the unknown steps. The accuracy with which these measurements were made were of the order of 0.1µm. One typical example is as shown in Figure 2.8.a. Calibration error is caused by diffraction and as such it is included in the error due to the latter.

2.7.4 Results of error analysis.

To summarize for the types of error introduced and their effect on profile measurements, the following can be stated:

- 1. Diffraction at straight edge limits the measurement to the surfaces of $R_m \gg 0.76 \, \mu m$ (30 μ "). The error introduced into the profile measurements is of the order of 0.25 μm max (5-16(μ ").
- 2. Digitization introduces an error of about 2% or 0.1 μ m for R_m = 5 μ m.
- 3. The combined inaccuracies amount to 0.35µm (0.25+0.1) which is the maximum range of measurement error.

2.8 Discussion of results obtained from OGT.

The density distribution of heights determined using OGT technique yielded Gaussian type of distribution. was confirmed for both along the direction of grinding and perpendicular to it. This substantiates the earlier claims [32] [33] made in this context. However, based on this distribution many other useful parameters have been otained using the spectral analysis. Referring to Table 4, it can be seen that the characteristics for X-direction are different compared to those along Y-direction. The bandwidth parameter for X-scan is almost double compared to the value for y-scan. This suggests the degree of openness of irregularities along xscan as compared to that along y-scan. Moreover from the spectrum obtained along these two directions, it can be seen that the higher frequencies and larger amount of power exists in 'Y'direction as compared to that along 'X' direction. This is obvious from the anisotropic character of the surface. characterization of surfaces in terms of the parameters like CLA, RMS, mean slope, mean curvature and correlation function is not sufficient for its use in the functional behaviour of surface. This is due to the fact that it is possible to generate millions of types of profiles having similar Therefore, the characterization of surface in characteristics. terms of intercept length and its distribution is necessary. From this it is quite obvious that the potential contact areas can be easily assessed for the description of functional

behaviour in contact problems. The intercept length distribution as shown in Figure 2.20 shows that it is of an exponential type. The exact nature of the distribution will be determined later when the nature of distribution is determined analytically. Referring to Figure 2.20, it can be seen that the mean intercept length along 'X' axis is approximately twice as large compared to that along 'Y' direction.

The density distribution of individual bearing areas obtained by using the exponential density distribution of intercept length along 'X' and 'Y' direction again shows the exponential characteristics with mean around 300 m. Thus, the results so obtained experimentally can be used for the description of functional behaviour of surface in contact problems. The computational procedure described in this chapter is quite general in nature, and can be used for both Gaussian as well as non-Gaussian surfaces.

2.9 Summary.

The OGT technique was described along with its advantages and limitations. It was found that this technique was best suited to surfaces having average height of irregularities greater than 30 μ " (0.762 μ m). Subsequent computation of the digitized data obtained by this technique yielded not only, the conventional parameters like CLA, RMS, and correlation function, but also the density distribution of individual bearing areas. The latter was determined using the principle

of Quantitative Stereology. Other parameters can be obtained using this principle for the study of morphology of surfaces. This is not discussed here as it is irrelevant to the characterization of surfaces for the description of functional behaviour of surfaces in contact.

Having obtained these parameters, it is now necessary to review the earlier approaches to characterization of surfaces. This literature survey will now be the main substance of the next chapter.

CHAPTER 3

REVIEW OF SURFACE CHARACTERIZATION MODELS

3.1 Introduction.

Recognizing the characteristics of the surface and assessing them numerically in the form of paramaters is essential to describing the functional behaviour of surface. Since the surface is considered to be random, the number of parameters required to describe the surface completely is very large. Therefore, it is essential that the characterization be done taking into consideration its relevance to the application. Here an attempt will be made to describe previous models which characterizes the surface to describe its functional behaviour in contact problems. The characterization is achieved by numerical assessment of two main types of descriptors:

- 1. Profile descriptors.
- 2. Surface descriptors.

3.1.1 Profile descriptors.

It is well known that the profile can be characterized by means of two components; one of them varying vertically about the mean line called vertical descriptors, and the other horizontally which describes the openness and closeness of the profile, called as horizontal descriptors.

A. <u>Vertical descriptors</u>: The two most widely used parameters belonging to this category are the root mean

square (RMS) and arithmetic or centre line average (CLA) or R_a . The RMS which involves minimizing the sum of the squares defines the same mean as the R_a condition of equal areas or volumes of surface and void, above and below the mean [22]. Of these two parameters, the RMS roughness is not as extensively used as the R_a value. The R_a value may be defined mathematically as:

$$R_{a} = -\frac{1}{L} \int_{0}^{L} |z| dx$$
 (3.1)

where 'Z' is measured from the mean line and 'L' is the profile sample length in 'X' direction. This parameter can'also be considered as the first moment of the probability density distribution of heights of the profile to be discussed later. It can very well be seen that one can describe millions of different types of profile having the same average roughness value viz. Ra or CLA. Therefore, its usage in the contact problem and surface characterization is highly restricted.

B. Horizontal descriptors: In order to study the openness or closeness of the texture, it is necessary to describe the profile in terms of horizontal descriptors. The most common approach is to study the number of peaks/unit length of profile or the zero crossing density of the profile. Unfortunately, neither of them is the intrinsic property of the profile. It is because they are the function of the

measuring instrument. Therefore, to circumvent this difficulty an average wavelength as a parameter [34] was introduced. Average wavelength for some typical surfaces are shown in Figure 3.1. It is interesting to note that this corresponds to feed mark of the tool used in the manufacturing process and is particularly noticeable in turned surfaces [22]. It can be shown that these parameters are not truly representative of the surface and are not sufficient to describe functional behaviour of surface. Thus, statistical methods were introduced [24] to obtain more useful information about the profile. The statistical methods to evaluate the profiles in terms of vertical and horizontal descriptors are:

Probability distribution functions. The probability function P(h) associated with the random variable 'Z' which could take any value between - ∞ and ∞ is defined as the probability of the event Z(y) or Z(x) h and is written:

$$P(h) = Prob \{Z \leq h\}$$
 (3.2)
 $P(-\infty) = 0 \text{ and } P(\infty) = 1$

Probability density function: If the probability function P(h) is differentiated, the probability density function is obtained. Thus,

$$p(z) = \frac{d P(h)}{dz}$$
 (3.3)

Obtaining the distribution of heights of the profile in the probabilistic sense gives the following information.

first moment of the density.

b. the measure of the spread of the distribution and therefore of the data by means of the variance which is the second moment of the density.

- c. the measure of the skewness and the peakedness of the distribution (Kurtosis) which are the third and the fourth moment of the density respectively. The skewness and Kurtosis effect obtained from density distribution could be attributed to the sampling process itself [35]. Therefore, its usage as the significant property of the profile is restricted.
- d. the bearing length curve or the Abbott curve, as shown in Figure 3.2.

The probability distribution curve can be used to get the bearing length fraction for the profile as first suggested by Abbot(t and Firestone [36]. The information obtained from this curve gives some description of the profile horizontally, but its usage is still restricted as it cannot give information about deviation to arrive at the nature of distribution of the bearing line fraction.

3. Auto- covariance or Auto-correlation functions: The description of the profile by means of correlation function has been the most popular way of representing

spatial variation. Whitehouse and Archand [37] derived their significance from the distance over which it decays. Peklenik [38] used this decay length (auto covariance length) to classify typology. It will be seen in the next chapter how this function was used to determine the cut-offs relevant to the contact problem. Another significant use of parameter called autocovariance length and the rms also obtained from this function is in the experiments related to the theory of scattering and its conversion to surface plasma oscillation of photons normally incident upon rough surface [39]. The mathematical properties of ACF and their usage in the analytical determination of intercept length will be discussed in the next chapter. Usually, in order to obtain the useful parameters characterizing the profile, power spectral density (PSD) is used which is the Fourier transform of the ACF.

4. Power Spectral Density Function (PSDF): The spectrum is another form of spatial representation which is useful when the aim is to use the information as the harmonic input to a physical system [40]. The parameters like mean slope and mean curvature are obtained from this PSDF in the form of second and fourth moment of this function. This significance of a various moments of PSDF in surface studies was obtained

by Nayak [4]. The cross correlation analysis [24] is applied in the context of surface description which will be described later.

3.1.2 Surface descriptors.

The statistical parameters obtained for a profile cannot actually represent the surface. This is evident in the case of anisotropic surface. Moreover, a profile will more often than not pass over the shoulder of an asperity on the sufrace instead of its summit. The shoulder will, nevertheless, appear as a peak on the profile, though one of reduced height. Thus the profile indicates the presence of far fewer high peaks than are actually existing on the surface. A similar error occurs in the determination of the mean surface gradient. Therefore, most of the existing models are based on two assumptions:

- (i) The statistics of the surface are the same as the statistics of the profile of the surface, and
- (ii) The asperities have regular geometry (asperity models).

Based on the second assumption, there are various models wherein the surface is replaced by spheroids, paraboloids, elliptic paraboloids and hyperboloids.

Replacing the irregularities (asperities) with simple geometric shapes facilitates easy solution for an elastic contact problem. The derivation of bearing area corresponding to each load acting between two surfaces in contact is based on basic solutions for the governing elastic equations existing

for these shapes. Therefore, the description of the surface in terms of population of these simple shapes has been the most popular approach.

13

The most important contribution was made by J.A. Greenwood and J.B.P. Williamson [41]. In their model the rough surface is represented by a population of identical paraboloids having a Gaussian distribution of peak heights. For the contact between this surface and a smooth flat, composed entirely of elastic micro-contact, they derived an expression for the total normal load and contact area. This expression was the function of the distance 'd' between the flat and the mean peak level and in terms of three topographical parameters:

- a. peak radius of curvature
- b. standard deviation of peak heights, and
- c. number of peaks/unit area.

Greenwood and Tripp [42] extended the model to take into account the random misalignment of each pair of contacting peaks, and derived contact area and/loads as functions of distance between the mean peak levels of the two surfaces.

The simplifications in the above two theories of using a constant radius of curvature was removed by Whitehouse and Arhard [43]. Experimentally, it was found that on an average higher summits are sharper than the lower ones. This was incorporated into the surface statistics. Their theory was based on the assumption that surface profiles have an exponential auto-correlation function.

For an isotropic random Gaussian surface defining each peak by its height and its two principal curvatures, Bush et al [44] derived, in effect, the joint probability density distribution of these variables. Each peak was replaced by elliptic paraboloids having the same height and two radius of curvatures. The elastic contact of the population of the elastic elliptic paraboloid with a smooth flat was investigated. The resulting functions 'a' contact area and 'W' load were expressed in terms of the standard deviation of height, slope and curvature. Finally, they even investigated the elastic contact with flat surface for an anistropic surface. This investigation is mathematically attractive, but they come into the category of asperity models where in the peak shape is a deterministic function.

Hisakado and T. Tsukizoe [45] attempted to resolve this problem by working backwards from a Gaussian surface height to derive the peak height probability density function, given a deterministic peak shape function— either paraboloid or conical. It was assumed that both the paraboloid radius and the cone slope are independent of height. However, this approach resulted in an unrealistic probability density function of height distribution which is strongly dependent on the peak shape. The distribution was negatively skewed for heights less than zero with paraboloids and for heights less than the standard deviation of heights with cones. This shows that the basic assumption of having asperity models does not validate the true representation of the surface.

5

Perhaps the most remarkable effort made in the surface profile characterization was by Nayak [24]. He discussed the importance of structure function or ACF in surface studies. He proposed the model of surface roughness based on the theory of statistical geometry developed by Longuet-Higgins [46] for the analysis of ocean surfaces. The validity of this theory is dependent on one assumption, namely that the surface heights, slopes and curvature possess a multi-Gaussian probability density. In order to assess the non-Gaussian and/or anistropic surface, he suggested the cross-correlation technique, which is discussed later.

Osman and Sankar [5] employed the theory of stochastic excursion to characterize the surface texture in terms of vertical descriptors and mean intercept length. This was a good step in the characterization of surface, but the analysis fails for non-Gaussian surfaces.

Later on, Elgabry, Osman, and San kar [47] proposed a simplified probabilistic model to represent the intercept length of crest and valleys for surfaces machines by grinding or lapping processes. This procedure is based on three assumptions.

- The probability density distribution of heights is Gaussian.
- 2. The surface profile is considered to be a series of attached linear segments whose slopes w.r.t. the 'X' direction could be positive or negative.

The stylus faithfully follows the asperities on the surface.

Having obtained mean intercept length and its deviation by the procedure developed by Osman and Saukar [5], they determined the scale and shape parameter of Weibull distribution. They assumed that the distribution could be of Weibull type. It is interesting to note that the distribution developed analytically in terms of moments of PSDF in the next chapter was of Weibull type for heights of asperities close to the peak. Their usage in surface studies is restricted because profile statistics does not give surface statistics, which will be evident later on in this chapter.

In order to characterize the surface which is anisotropic and non-Gaussian, Nayak [24] proposed a cross-correlation technique to obtain useful parameters. The method involves the determination of correlation function for profiles obtained at various angles to each other. The resulting moments from the PSDF then gives parameters, as in the case of isotropic Gaussian surfaces.

3.2 Surface and profile characterization based on PSDF

A simple example of an isotropic surface shows that the profile PSD can seriously distort the spectral content of the surface roughness by giving undue weight to long wavelength at the expense of short wavelength. The relation between the surface and profile PSD is due to Nayak [24].

Auto covariance function may be defined as [24]:

$$G(r) = \lim_{\substack{1 \\ 4L_1 \ L_2}} \int_{-L_1}^{L_1} \int_{-L_2}^{L_2} z(x_1, x_2) z(x_1 + \lambda_1, x_2 + \lambda_2) dx_1 dx_2$$

$$\lim_{\substack{-L_1 \ -L_2}} \int_{-L_2}^{L_1} (3.4)^{-L_1} dx_2$$
when $L_1 + \infty$,

where
$$r = (\lambda_1 + \lambda_2)^{1/2}$$

 $Z(x_1,x_2)$ is the height of the surface at x_1 and x_2 position in the cartesian plane and $\langle Z(x_1,x_2) \rangle = 0$.

The PSDF of the profile

$$A_{p}(\omega_{1}) = \frac{1}{2\pi} \int_{-\infty}^{\infty} G(r) \exp(-\tau \omega_{1} r) dr$$
 (3.5)

and that for the surface:

$$A_{s}(\omega_{1},\omega_{2}) = \frac{1}{4\pi^{2}} \int \int G(x_{1},x_{2}) \exp\{(-\tau(\omega_{1}x + \omega_{2}x_{2}))\} dx_{1}dx_{2}$$

$$= -\infty -\infty$$
(3.6)

If the auto covariance function is considered as

$$-\beta(r)$$
 e [37] (3.7)

$$A_{p}(\omega_{1}) = \frac{1}{2} - \frac{1}{2}$$
 and, (3.8)

$$A_{s}(\omega) = \frac{\beta}{2\pi(\beta^2 + \omega^2)^{3/2}}$$
 (3.9)

where,

$$\omega^2 = \omega_1^2 + \omega_2^2$$
 (3.10)

In general, the PSD for these two cases lying in the range $(|\omega_0|, |\omega_0+d\omega_0|)$ will be given by:

$$A_{p}(^{\omega}) = \frac{2 \beta d \omega}{(\beta^{2} + \omega^{2})} \text{ and,}$$
 (3.11)

$$A_{S}(\omega) = \frac{\beta \omega_{0} d \omega_{0}}{(\beta^{2} + \omega^{2})^{3/2}}$$
(3.12)

Therefore,

$$\frac{\Delta A_{s}(\omega)}{\Delta A_{p}(\omega)} = \frac{\pi \omega_{0}}{2(\beta^{2} + \omega_{0}^{2})^{1/2}}$$

$$0 \text{ as } \omega_{0} \rightarrow 0$$
(3.13)

From this relation it is clear that the profile distorts the surface in such a way as to give undue weight to long wavelengths at the expense of short wavelengths. All the models discussed so far, thus, emphasize the profile characterization rather than the surface characterization. In order to characterize the anisotropic surface it is necessary to examine the cross-covariance of parallel profiles. This will be the subject of investigation in the next chapter.

3.3 Summary.

It was observed that the characterization of surface different from that of the profile. Most of the existing models deal with either profile characterization or asperity models for the surface. Nayak has shown that cmoss-covariance of the parallel profile should be examined in order to obtain useful parameters for surface characterization. Experimentally, it is difficult to determine the twodimensional ACF. Therefore, it is possible to deal with one dimensional ACF in which co-variance is determined over a line This is consistent with our assumption of instead of an area. isotropic surface statistics. If surface statistics are not isotropic, valid results can be obtained by averaging over a large number of lines scanning the surface. It is this method which has been adopted to characterize the anisotropic surface which will be the substance of the next chapter.

The experimental determination of intercept length and its distribution have been otained using the OGT technique. The other conventional parameters have also been determined using the concepts already discussed. But the exact nature of the distribution of intercept length and individual bearing area have not been determined. Therefore, the next chapter will be concerned with the determination of these parameters. Their application in determining the high and low pass cut-off and hence, its usage in contact problems, will also be discussed.

CHAPTER 4

3-D Characterization of Surfaces Based on Individual Bearing
Area.

4.1 Introduction.

In recent years an extended surface characterization of machined surfaces has been the subject of considerable interest its possible applications in the description of In general in the surface functional behaviour. phenomenological approach to the functional behaviour, parameters like area of contact, curvature and slopes of the surface asperities become significant. However, these quantities are random in nature, and hence must be determined from the probability density distributions in terms of their well-defined local values. This chapter considers the required parameters for the surface characterization in form of the probability density distribution of heights, curvatures, slopes, bearing lengths and bearing areas. The latter is referred to as local bearing areas or individual bearing areas It has been shown that these parameters can be obtained experimentally by using "Optical Grating Topography." It was established on the basis of statistical analysis of the made observations that the probability density distribution of Hence, it is possible to define a heights are Gaussian. "Bandwidth" parameter and intercept lengths between peaks of the profile by employing the multiple scanning method of the

OGT technique. The determination of these parameters and their significance for their subsequent surface characterization is discussed.

4.2 Auto-covariance Function (ACF) of the surface.

It is evident that the machined ground surface considered has a topography as indicated schematically in Figure 4.1. Any point on the surface chosen at random can be analytically characterized by its surface co-ordinates (x,y) and its position as a function of height co-ordinates 'z' measured from a chosen datum surface. It has been discussed in the previous chapter how, by double scanning procedure, it is possible to characterize surface asperities with reference to a mean value of the height co-ordinates. Thus in the double scanning procedure an 'X' or 'Y' scan is performed at a certain scan level (z₁) indicated in Figure 4.1. It is also apparent that the scanning which is performed in a discreet manner leads to a surface characterization in terms of "adjacent points AA'" on the surface. Considering that z(A) is a random function, the auto-covariance function G(AA') can be given as

$$G(|AA'|) = \langle z(A)z(A') \rangle - \langle z(A) \rangle \langle z(A') \rangle \qquad (4.1)$$

or in terms of (x.,y) coordinates by:

$$G[(x^2+y^2)^{1/2}] = \langle z(x',y') z(x+x',y+y') \rangle - \langle z(x',y') \rangle \langle (z(x+x',y+y')) \rangle$$
(4.2)

The variance of the surface height function z(A) can be

expressed in terms of G-function by

$$G(0,0) = [z(x,y)]^2 - \langle z(x,y) \rangle^2$$
 (4.3)

in which z(A) is taken w.r.t. an ideal in finite plane "AT" at the level $\langle z(x,y) \rangle = 0$ or for the height function:

$$z(x,y) = z(x,y) - \langle z(x,y) \rangle$$
 (4.4)

The above auto-covariance function with respect to the ideal surface $^{\prime}A_{T}^{\prime}$ (extending to $^{\infty}$) can also be written as:

$$G(x,y) = \langle Z(x,y) Z(x+x',y+y') \rangle$$

$$G(x,y) = \lim_{A_{T}} \int_{A_{T}} \int_{X} Z(x,y) Z(x+x',y+y') dx dy$$

$$A_{T} \rightarrow \infty$$
(4.5)

where ' A_T ' is the area of test sample considered.

It was mentioned earlier that 2-dimensional ACF is difficult to obtain experimentally. Therefore, a given sample of surface is scanned by 16 lines which corresponds to double scan of OGT technique. This test sample surface then is assumed to be statistically homogeneous over the entire sample surface. This suggests the application of the parameters so obtained for surface studies as more representative than those obtained by profile characterization. Hence by using equation (4.5), the auto-covariance for a profile if considered to be a continuous function over the sample length or when datum line is taken to be infinite along x-direction is given by:

$$G(x') = \lim_{L \to \infty} \frac{1}{L} \int_{0}^{L} Z(x)Z(x+x')dx'$$

$$(4.6)$$

, in which
$$Z(x) = z(x) - \langle z(\hat{x}) \rangle$$
 (4.7)

Due to the finiteness of the test sample and, hence, of a finite datum area A_T , the calculations have to be performed from discreet data as obtained from OGT. Hence for each line (j=1, ..., N) the mean height will be:

$$\langle z \rangle = \frac{1}{N} \sum_{j=1}^{j=N} z_j$$
(4.8)

and the discreet form of equation is,

$$G(m \triangle) = \frac{1}{N-M} \sum_{j=1}^{N-M} z_{j} z_{j+m}$$
 (4.9)

where ' Δ ' denotes a chosen digitizing distance and the number of correlated points is m = 0,1,2, ..., M. The ACF is then calculated for several regularly spaced lines on the anisotropic surface. On the application of the OGT method to the surface under consideration, the total number of points were 200 with a digitizing distance of lµm. The ACF for the

surface is as shown in Figure 4.2. The dashed curve is the Gaussian function:

$$G(x) = G(0) \exp(-x^2/3^2)$$
 (4.10)

This is an important finding and is useful in surface studies to determine the cut-offs relevant to the application which is discussed later. The validity of the observation is also discussed separately in this section.

For the further characterization of surfaces it becomes necessary to find the variance of the slopes of the profile which leads to the so-called intercept lengths that form the bearing areas. Thus considering the first and second derivative of G(x) denoted by G'(x) and G''(x) these, quantities can be obtained from equation (4.6) as follows:

$$G'(x) = \lim_{L \to \infty} \frac{1}{L} \int_{0}^{L} Z(x')Z'(x+x')dx$$
 (4.11)

$$dG(x) dZ(x+x')$$
if which $G'(x) = ----- \text{ and } Z'(x+x') = ----- \text{ dx}$

$$(4.12)$$

Letting $\theta = x+x'$, one obtains the ACF along the x-direction:

$$G'(x) = \lim_{L \to \infty} \frac{1}{L} \int_{0}^{L} Z'(\theta) Z(\theta - x') d\theta \qquad (4.13)$$

A second differentiation and introducing another change of variables, i.e., $x = \theta - x'$ yields

$$G''(x) = -\lim_{x \to \infty} \frac{1}{L} \int_{0}^{L} Z'(x) Z'(x+x') dx.$$
 (4.14)

in which $G_1^{"}(x)$ represents the ACF of the slopes of the profile. The variance of the slopes being given by $G^{"}(0)$. In an analagous manner the ACF of heights and slopes of the profile along 'y' direction can be obtained.

4.3 Power Spectral Density Function (Amplitude spectrum) of the surface.

The significance of this function in surface studies and the computational procedure of determining this function was already discussed in Chapter 2. In this chapter the changes observed in the PSDF of the surface loaded axially is considered. In this context it is worthwhile to consider the amplitude spectrum as:

$$A(f) = (2\pi)^n \int_{-\infty}^{\infty} G(x) \exp(-\tau 2\pi f x) dx$$
, (4.15)

in which $f = \frac{2\pi}{\omega}$, $\omega = \text{radial frequency}$.

and, the higher moment can be expressed by

$$m_n = (2\pi)^n \int f^n A(f) df.$$
 (4.16)

The amplitude spectrum for various loads is as shown in Figure 4.3. The corresponding density distribution of heights for different loads is shown in Figures 4.9.

4.4 Determination of intercept length and its distribution.

The computational procedure of determining the distribution of individual bearing areas has been discussed previously. However, it might be instructive to briefly mention the lineal fraction, its deviation and number of intercepts/unit length, which leads to the density distribution of intercept length in terms of conventional parameters. Using the concept-of Quantitative Stereology, the lineal fraction ($\lambda_{\rm x}$

, y) and its deviation can be expressed by:

$$\lambda_{\mathbf{x}} = -\frac{\mathbf{i}_{\mathbf{x}}}{\mathbf{L}}, \quad \lambda_{\mathbf{y}} = -\frac{\mathbf{i}_{\mathbf{y}}}{\mathbf{L}}$$
 (4.17)

$$\lambda_{x} \text{ or } \lambda_{y} \equiv A_{A}$$
 (4.18)

where ' $A_{\mbox{\scriptsize A}}$ ' is the area fraction.

In accordance with the assumed Gaussian process, the lineal fraction can also be written as [48]:

$$\lambda_{x} = \int_{z}^{\infty} p_{x}(z) dz = -\frac{1}{2} \left[1 - erf\left(\frac{z}{\sqrt{2G_{x}(0)}}\right)\right]$$
 (4.19)

$$y = \int p_{y}(z) dz = \frac{1}{2} - \left[1 - e^{r} f\left(\frac{z}{----}\right)\right]$$

$$z = \int p_{y}(z) dz = \frac{1}{2} - \left[1 - e^{r} f\left(\frac{z}{----}\right)\right]$$

$$(4.20)$$

The deviation of the lineal fraction is given by

$$D(\lambda_{X}) = \left\{ \frac{D(\lambda)}{-\lambda} \right\}^{2} = \frac{1}{N_{1X}} \left\{ \left[\frac{D(1)}{-\frac{1}{2}} \right]^{2} + 1 \right\}$$
 (4.21)

where $'N_{1x}'$ is the number of intercept/scanning line.

$$E_{1X} = p_{X}(Z) E_{\{Z'(X)\}}$$

$$= \frac{1}{T} \sqrt{\frac{-G_{X}(0)}{G_{Y}(0)}} \exp \frac{-Z^{2}}{2G_{Y}(0)}$$
(4.22)

In terms of these functions which are obtainable from the A&F or the amplitude spectrum as already discussed, the average intercept length in x, y scanning direction will b:

$$\langle 1_{x} \rangle = 1/2 \{1 - \text{erf} \frac{Z_{x}}{\sqrt{2G_{x}(0)}} \} / p_{x}(Z) E \{|Z'(x)|\}$$
 (4.23)

and correspondingly for the 'y' direction,

$$\langle i_x \rangle -1/2[1-erf \frac{z}{\sqrt{2G_y^{(0)}}}]/p_x(z) E \{ |z'(y)| \}$$
 (4.24)

In order to extablish a distribution of the intercept length required for the definintion of individual bearing areas, it is to be recognized that the 0th moment and second moment as obtained from the power spectrum are now designated for the (x,y) scanning direction as by $m_{0x} = G_x(0)$, $m_{2x} = G_x(0)$, $m_{0y} = G_y(0)$ and $m_{2y} = G_y(0)$.

When 'Z' is very large, the length of the intercept made by the profile Z(x) at any level 'Z'. i.e., Z(x)>Z is very short. The intercept length starting at $x=x_1$ is to a second degree of approximation,

$$i_x = \frac{2Z'(x_1)}{[-Z''(x_1)]}$$
 (4.25)

The joint probability density of Z(x), Z'(x) and Z''(x) can be given as [49],

$$p(Z(x),Z'(x),Z''(x)) =$$

$$\frac{1}{(2\pi)^{3/2}} \left[m_{2x} \left(m_{0x} m_{4x} - m_{2x} \right) \right]^{1/2} = \exp \left[-\frac{1}{2} \right] \left\{ \begin{array}{ccc} m_{0x} m_{4x} & z^2(x) & z''(x) \\ ----- & m_{0x} m_{4x} - m_{2x} & m_{0x} & m_{4x} \end{array} \right]$$

Since Z"(x) is a random variable whose mean value -m2Z is large compared to the standard deviation, we may put, using equation 4.25,

$$i_x = \frac{2Z'(x_1)}{m_{2x}Z}$$
 (4.27)

The probability that Z(x) will pass upwards through the value Z(x) in the interval x_1 , x_1 + dx with a slope between Z' and Z'+dZ' is equal to the probability that, at x_1 , Z(x) lies between Z(x) and Z-Z'dx and has a slope in Z', Z' + dZ'. This probability is:

$$p(Z,Z^{4}(x)) = \frac{Z^{1}dx(dZ^{1})}{2\sqrt{m_{2}x^{m_{0}x}}} \exp \frac{1}{2} \left(\frac{Z^{2}}{m_{0}x^{m_{2}x}}\right)$$
(4.28)

Expressing Z' in terms of i_X shows that the probability of Z(x) passing up through Z in z_1 , x_1+dx and starting at Z(x)> Z interval whose length lies between i_X and i_X + d_{1X} is:

$$\frac{m_{2x}}{3} = \frac{z^{2}}{1} \frac{1}{x} \frac{d_{1}x^{2}dx}{d_{1}x^{2}dx} = \exp\left(\frac{-z^{2}}{2m_{0x}} + \frac{m_{2x}}{8} + \frac{z^{2}}{1} + \frac{z^{2}}{1}\right) \qquad (4.29)$$

The probability density for the intercept length i_x of the Z(x) = Z '2' very large is obtained by:

$$p(1_{x}) = \frac{m_{2x}^{3/2}}{2m_{0x}} \frac{z^{2}}{2} \frac{1_{x}}{4m_{0x}} \frac{d1_{x} dx}{dx} = \exp\left(\frac{-z^{2}}{2m_{0x}} - \frac{m_{2x}}{8} \frac{z^{2}}{1^{2}}\right)$$

$$= \frac{m_{2x}^{1/2}}{2\pi} \frac{z^{2}}{4m_{0x}} \frac{1_{x}}{2\pi} \exp\left(\frac{-z^{2}}{8m_{0x}} \frac{m_{2x}}{1^{2}}\right)$$

$$= \frac{m_{2x}}{4m_{0x}} \frac{z^{2}}{4m_{0x}} \exp\left(\frac{-z^{2}}{8m_{0x}} \frac{m_{2x}}{1^{2}}\right)$$

$$= \frac{m_{2x}}{4m_{0x}} \frac{z^{2}}{4m_{0x}} \frac{1_{x}}{8m_{0x}}$$

$$(4.30)$$

Similarly, that along the 'y' direction is given by:

$$p(i_{y}) = \frac{m_{2y}}{4m_{0y}} \frac{z^{2}}{4m_{0y}} \exp\left(\frac{-z^{2}}{8m_{0y}} \frac{m_{2y}}{i_{y}} \frac{i_{y}}{2}\right)$$
(4.31)

The density distribution of the intercept length obtained experimentally is compared with the density distribution of

Intercept length obtained analytically in terms of the moments of PSD in Figures 4.4, 4.5, 4.6.

4.5 <u>Determination of individual bearing area and its</u> distribution.

Consider the consideration and the second second

Having obtained the distribution of the random variables ix and iy, it is now necessary to determine the density of the function $g(i_X,i_Y)$, i.e.,

$$g(i_{x}, i_{y}) = c. i_{x}. i_{y}. = a_{b}$$
 (4.32)

Since i_x and i_y is a random variable, $a_b = g(i_x, i_y)$ is also a random variable and the function is a Baire function (see Glossary).

Its value
$$a_b(Z)' = g(i_x(Z), i_y(Z))$$
 (4.33)

In order to determine $P_{ab}(a)$ for a given a, it is necessary to determine the probability of the event $\{a_b \leq a\}$. Denoting by D_2 the region of the (i_x, i_y) plane s.t.

$$g(i_X,i_Y) \le a \tag{4.34}$$

It is easy to see that

$$\{a_b \le a\} = (i_x, i_y) \in D_2$$
 (4.35)

$$P(a_b \le a) = P\{(i_x, i_y) \in D_2\}$$

=
$$\iint P_{ix,iy} (i_x,i_y) di_x.di_y$$
 (4.36)

The density $p(a_b)$ can be found by differentiating $P(a_b)$ or directly, by determining the region D_2 of the i_x i_y plane s.t.

$$a < g(i_X, i_Y) < a+da$$
 (4.37)

Since,

$$a < ab > (a+da = (i_x, i_y) \in D_2$$
 (4.38)

therefore,

$$p(a) da = P \{ a < a_b \le a + da \} = (i_x, i_y) \in D_2$$

 $p(a)da = P\{a < a_b < (a+da)\}$

therefore,

$$= \iint_{\Delta D_2} p_{xy}(i_x, i_y) d_{ix} d_{iy}. \qquad (4.39)$$

For the sake of simplicity, assuming the area to be of elliptical shape, let

$$a_{b}' = \pi / 4 i_{x} \cdot i_{y}$$
 (4.40)

The distribution of ab is now obtained by using the transformation given by equation (4.40) in the distribution in equations 4.30 and 4.31, i.e.,

$$f(a_b) = \frac{16a_b}{\pi^2(K_1K_2)} K_0(\frac{(4a_b)}{\pi^{K_1K_2}}), \qquad (4.41)$$

where
$$K_1 = \frac{4m_0 x^2}{m_{2x} z^2}$$
 $K_2 = \frac{4m_{0y}^2}{m_{2y} z^2}$

where κ_0 is the second order modified binel function. The derivation is shown in the appendix [50] [51]. Normalizing the area yields

$$a^* = \frac{a_{b} \cdot z^2 /\{m_2 \times m_{0y}\}}{\pi m_{0x} m_{0y}}$$
 (4.42)

$$f(a^*) = a^* K_0(a^*)$$
 (4.43)

where a is the normalized individual bearing area. It can be seen that this is a density since the total area = 1.

The normalized density distribution of individual bearing area is as shown in Figure 4.7.

4.6 Determination of mean intercept length and density distribution of bearing areas for different loads.

There are a number of factors to be considered when dealing with surfaces in contact. The two most important of them are (i) the effect of surface film and (ii) the effect of size on strength properties. Both these factors may have a pronounced effect on the real situation as will be discussed later.

The simplest model one can consider to describe the deformation of the irregularities (asperities) is when the plastic flow occurs. It turns out that the local plastic yield pressure 'Y' is very nearly constant [52], and is comparable to the indentation hardness of the metal. Under these conditions,

the total area of contact formed for two surfaces in contact can be given as:

$$A_{C} = W/H$$
 [52] (4.44)

where Ac = total area of contact

W = total normal load

H = hardness of the metal surface.

It is to be noted that this is a very simple model assuming ideal physical properties that extend to the outermost surface layers. The sample having a nominal CSA of 400mm^2 was loaded up to 77.3MPa. Knowing the distribution of the individual bearing area at various scan levels of the surface, it is possible to get the contact area growth with load applied. To arrive at the contact area, one can consider two distinct ways of deformation [52].

- (1) The number of asperities in contact remains constant.
- (2) The average area of each asperity remains constant and only the number of regions of contact increases with load appreciation.

Referring to the Figure 4.8, it is seen that the growth of the number of crossings is fairly flat over a wide range except the initial portion. This suggests the applicability of the first case as suggested by Tabor. For example, the mean contact area

$$a_{C} = (W/H) \times n \times A \qquad (4.45)$$

where,

A = nominal CSA in mm²; n = number of contacts/mm². For W = 10.5MPa , H = 200BHN , n = 221 and A = 400mm², a_C = 23.7 μ m² which corresponds to a scan level of 0.8 μ m.

The zero scan level corresponds to the level of point contact between two surfaces in contact. Therefore, the mean plastic deformation is equal to 0.8 µm. Similarly, the variation of the intercept length with various scan levels and hence load is shown in Figure 4.10. The probability density distribution of IBA corresponding to these loads is shown in Figure 4.11 and the variation of ab in Figure 4.12.

4.7 Determination of cut-offs.

It was shown by Attia [53], and then by Abrams [54], that it is necessary to confine measurement to the portion of the spectrum of wavelengths which is relevant to the deformation of the interface. For example, at very high loads it is obvious that the irregularities having short wavelengths, and hence higher frequencies, will be flattened out and will disappear from the spectrum. This is evident from the Figure 4.3. Moreover, investigations of machine tool joints when subjected to many load reversals (see Archard (55)) have shown that whilst an initial plastic deformation in the contact surface will occur, the material response nevertheless will be an elastic one as long as the initial load is not exceeded. Therefore, from the point of view of present analysis it is important to recognize

a certain frequency of the occurring asperities below which the contact problem between two surfaces can be analyzed in terms of elasticity theory. Thus individual bearing areas as defined earlier which depend on the frequencies of the occurring asperities will have to be considered as contact area through which a contact force can be transmitted. This particular frequency for a given load is known as a cut-off frequency, and therefore the problem reduces to the determination of the cut-offs which define the pass-band.

The cut-off-which rejects the long wavelengths is the easier one to select, as it clearly must be related to the largest horizontal dimension of the surface interaction. contact problems, usually the high pass cut-off is set by the dimensions of the normal contact area of the size of spectrum. On the other hand, the low pass cut-off is rather difficult to determi/he. In the context of the contact problem one can obtain such a cut-off by assuming a certain initial plastic The knowledge of the distribution of bearing area permits the Aretermination of the extent of the plastic deformation that can take place for a given load. It can be further assumed that all asperities with dimensions of a pearing area smallen than that corresponding to an area capable of holding the particular load will be deformed plastically with reference to the interface in the contacting bodies. Hence, it will disappear from the power spectrum.

4.7.1 Low pass cut-Off:

As discussed earlier, the high pass cut-off can be given by [56], π

$$\omega_{H} = -\frac{\pi}{d_{s}}$$
 (4.46)

where ds = diameter of specimen.

Instead of considering the bandwidth between ω_H and ω_L (low pass-cut-off) of a spectrum of unknown constants, by filtering at ω_H the problem is reduced to that of a bandwidth between 0 and ω_0 of the spectrum when constants are known or can be determined provided that G(x) function continues to hold.

Before proceeding to the determination of low pass cut-off, it is necessary to determine the density of contact spots for that particular load. This relation between the hardness H(BHN), and the yield strength of the material given by Tabor [57] is,

$$H = 2.7Y$$
 (4.47)

. . total area supported by load 'W'

$$= W \times 2.7/H$$
 - '(4.48)

The knowledge of the distribution of individual bearing area permits the determination of height of asperities at which the total bearing area is equal to that given by equation (4.48). Knowing this height of asperity ${}^{1}Z_{C}^{1}$, one can calcutate the density of contact spots N from equation (4.22).

$$N = \frac{1}{4\pi^{2}} \left(\frac{m_{2x} m_{2y}}{m_{0x} m_{0y}} \right)^{1/2} \exp\left(-\frac{z_{c}^{2}}{2m_{0x}} - \frac{z_{c}^{2}}{2m_{0y}} \right)$$
 (4.49)

Having calculated the density of contact spots corresponding to a particular load, it is now necessary to determine the moments of the PSDF valid between limits '0' and ω_L . According to the equation (4.10), the ACF is given as:

$$G(x) = G(0) \exp\left(-\frac{x^2}{\beta^2}\right) = D^2 \exp\left(-\frac{x^2}{\beta^2}\right)$$
 (4.50)

where ' β ' is the auto-covariance length. D = total RMS roughness of the surface.

Taking the Fourier transform of the equation (4.50),

$$A(f) = D^2 . \sqrt{\pi} , \beta \exp(-f^2 \beta^2 / 4)$$
 (4.51)

where $f = frequency in \mu m^{-1}$. Therefore the moments of the A(f) can be given as:

$$\dot{m}_{n} = \int_{0}^{L} \omega^{n} A(f) d\omega \qquad (4.52)$$

Using equations (4.51), (4.52), m_{0x} , m_{2x} can be determined knowing G(y), and can be used in the equation 4.49 to determine the unknown ω_L . Therefore, corresponding to this pass band of ω_H and ω_L , the moments so obtained can be used to determine the individual bearing area distribution. This distribution can be employed together with the well defined local stress to formulate a solution for the elastic contact problem using the concept of probabilistic mechanics [58] to take care of other factors like the effect of size and surface film.

4.8 Discussion of results.

Referring to the Figure 4.2, it can be seen that the initial portion of the ACF for the surface is of the form

$$G(x) = G(0) \exp(-x^2/\beta^2)$$
 (4.53)

This curve is the most representative of the entire surface and this determines the behaviour of A(f). For it is the initial portion of the ACF (G(x) curve that determines the shape and magnitude of A(f). Most of the difficulties associated with the exponential ACF [3] do not exist with this form of the initial portion of ACF. This can be proved by considering the Gaussian or more generally, a Gaussian curve ACF model,

$$G(x) = D^2 \exp(-x^2/\beta^2) \cos(\sigma x) d>0.$$
 (4.54)

. The F.T. of this equation gives:

$$A(f) = [\pi^{1/2} \cdot D^2 \cdot \beta \cdot \exp(-f^2 \beta^2)] + \pi[(\delta_D(f^{-\sigma}) + \delta_D(f^{+\sigma})]$$

$$= \pi^{3/2} D^{2}. \beta \{ \exp(-(f + \sigma)^{2} \beta^{2}) + \exp[(f - \sigma^{2})] \}$$

$$\frac{1}{4} \beta^{-2}$$
(4.55)

In this case, it can be verified that $f^2Af \rightarrow 0$ as $f \rightarrow \infty$. Now, if we consider the general cosine ACF, i.e.,

$$G(x) = A_e e^{-b(x)} |\cos(\sigma x)$$
 (4.56)

and obtain its F.T.,

$$A(f) = 4\pi A_e b [f^2 + (b^2 + \sigma^2)]/[f^4 + 2(b^2 - \sigma^2)f^2 + (b^2 + \sigma^2)^2]$$
 (4.57)

It can be seen that $f^2A(f)$ does not approach zero for large K. Therefore, G''(0) which is the variance of slope given by

$$G''(0) = -\frac{1}{\pi} \int_{0}^{\pi} f^{2} A(f) df$$
, tends to large value (4.58)

In both cases, the models give similar results when ' ' and is equal to zero, which represents the true Gaussian and exponential ACF respectively. Similar observation was made by Nayak [4]. It can be shown that by introducing equation (4.56) into equation (4.52) for a random process with exponential ACF, the moments mo and ma are undefined (theory of Markoff Process). It is to be noted that this result was obtained using OGT whose resolution is of the order of 0.5_m and wavelength range of irregularities of the order of 4 ms. According to Nayak, it is clear that the Whitehouse and Archand's model does not allow slopes and curvature to exist, though they proceed to obtain these data from profiles. reason why this does not amount to a contradiction in practise is that their sampling interval is finite; the effect of finite sampling interval is to filter out small wavelength components, and to change the behaviour of the ACF at the origin [4].

Considering Figure 4.9 for different loadings, it can be seen that as the load increases beyond 10.5MPa, the density distribution of heights tends to be more and more exponential. This suggests the range of application of the Gaussian model for the surface characterization in contact problems. Since, the static loads usually encountered in the engineering application rarely exceeds 8MPa [54], the Gaussian assumption is valid for all practical purposes.

The intercept length distribution obtained analytically is compared with the distribution obtained experimentally in Figures 4.4. It is interesting to note that the distribution is exponential, and the experimental as well as theoretical results obtained matches fairly well for higher value of levels from the mean line (CLA). The disparity between the two which results at lower value is due to the assumption made in the analytical development of the distribution (i.e., for large value of Z(x) and for Gaussian random process). This does not restrict its usage in contact problems. This is due to the fact that at loads less than 10MPa, the first encounter between asperities takes place at its peak, and the knowledge of IBA distribution near to peak is more relevant than that much below. Since the moments of the PSD of the profiles scanning the surface can be easily computed, the intercept length and IBA distribution can be directly obtained from the equation (4.30) -

If one looks carefully at the equation (4.30), it is clear that it can also be represented as

$$p(i_{X}) = \alpha_{W} \beta_{W} i_{X} e \qquad i_{X} > 0 \qquad (4.59)$$

$$= 0 \text{ elsewhere}$$

where parameters α w and β w of Weibull distribution are greater than zero. From the equation (4.30), is equal to '22'. It is interesting to note that similar observation was made by Elgabry, Sankar and Osman [47]. It is, therefore, quite evident that in spite of using a better resolution technique of

optical methods, the results obtained by them using Talysurf profilometer is similar, and hence, intercept length distribution in general can be given by equation (4.30). This is an important finding as this facilitates the determination of individual bearing area distribution.

The area distribution as shown in Figure 4.7 is of the type $a^*K_0(a^*)$ which has been derived in Appendix A. It is interesting to note that one can again arrive at this distribution by simply determining the moments m_0 and m_2 . This is again an important finding useful in contact mechanics.

The mean intercept length, mean bearing area and its distribution calculated for different loads shows that the contact area approaches the nominal area as the load increases. However, as the load increases the deformation at the interface might be so large that the asperities might overlap with the neighbouring asperities, distorting completely original profiles obtained before loading. Even though this case is rarely encountered in practise, it is not difficult to find such large plastic flow in contact problems related to high heat transfer rates (nuclear industry). In that case it is to be noted that the model developed here is not valid.

The two factors discussed in context to the simplified model presented to obtain the mean intercept length and mean bearing area greatly affect the contact between solid surfaces. The first factor is concerned with the presence of surface films (oxide layer, for example). These may undergo large

deformation at the region of contact. If the surface film is ductile they will deform with the metal and retain their integrity. In case of brittle surface, they will crack and metal will tend to flow through the cracks. These films are especially important in adhesion and friction but unfortunately, it is not easy to specify or quantify their strength and yield properties.

.The second factor is concerned with the effect of size of the asperities on local material properties. Size has little effect on elastic properties, but it can have a marked influence on brittle strength and plastic yielding (52). the volume being deformed is very small, it may not contain any mobile dislocations; and, in that case, Gane [59] has shown, the plastic yield stress may reach very high values representative of the "ideal" crystal lattice. This implies that asperities may undergo much larger elastic deformation before plastic flow occurs, and the area of true contact may be appreciably less than that calculated from bulk values of 'Y". Moreover, from the PSD curve obtained for different loadings it is apparent that the amount of plastic deformation is very small. This shows that the disappearance of asperities of higher frequencies at higher load is rather small and could be attributed to the statistical scatter inherent in the sampling This gives further credence to the occurrence of elastic contact at loads less than 10MPa.

There are no theoretical models of contact between solids that take these factors into account.

4.9 Summary

It has been shown that the distribution of the intercept length determined analytically on the basis of Gaussian Ramdon Process is $i^{*2} \exp(-i^{*2})$, where i^{*} is the normalized intercept length obtained from OGT for heights of asperities at or above the R_{a} value. Using the joint exponential density distribution of intercept length along 'X' and 'Y' direction, the IBA distribution was also determined analytically. It was found that it was of the form a^{*} $K_{0}(a^{*})$, where a^{*} is the normalized IBA and K_{0} the modified benel function. From equation (4.30) it is clear that the IBA distribution and hence the mean IBA, can be determined at various levels, knowing the 'zero' and 'second' moment of the PSDF. The moments of the PSDF are the average of the moments of all the profile PSDFs scanning the test area of the surface.

The determination of ACF of the surface leads to the evaluation of cut-offs which specifies the pass band taking part in the phenomenon under investigation. The dependence of application of load on cut-off reveals that as the load increases, the importance of considering the waviness increases. This suggests that there is an upper and lower bound of frequencies of PSD which will have to be considered to describe the functional behaviour of surface. It is well known that as the length or area of the sample is increased, one observes longer wavelength features. As a random process, this type of structure represents a form of non-stationarity that is termed

'stationary within an interval' [25]. This shows that depending on the upper and lower frequencies of PSDF, the moments of PSDF would also change. Therefore, to determine these moments corresponding to the pass band defined by the application of load, the higher and lower pass cut-offs are determined using the initial portion of ACF which is found to be of the Gaussian form.

CHAPTER 5

CONCLUSIONS AND RECOMMENDATIONS

5.1 Conclusions

On the basis of the present study, the following conclusions can be made:

On Surface Characterization:

- The characterization of surface in terms of Ra, RMS, mean slope, mean curvature and in terms of correlation function is not sufficient to describe its functional behaviour. Extended characterization in terms of IRA and its distribution, and not by simple geometric shapes (like spheroids, paraboloids, etc.) is necessary. The latter models give statistically unsound results as the peak shape function is deterministic.
 - 2. It was proved that the statistics obtained from a profile cannot represent the surface and that for effective characterization a representative test area be scanned by series of parallel profiles. The surface and profile PSDF showed that the profile distorts the surface in such a way as to give undue weight to long wavelengths at the expense of short wavelengths.

On Optical Grating Topography:

3. The OGT technique can be used to determine the

parameters like R_a, RMS, mean slope and curvature of the surface irregularities. The characterization of surface in terms of correlation function is also possible as the basic requirement of series of parallel profiles with a common origin and can be obtained by this technique.

4. The profile measurements can be obtained for surfaces having $R_m \ge 0.76 \mu m (30 \mu^n)$. The maximum resolution obtained using objective of NA 0.35 was $0.8 \mu m$.

On Computational Procedure:

- 5. Computation of the digitized data obtained by using OGT yielded parameters in the form of:
 - (i) the mean intercept length and its distribution;
 - (ii) the mean individual bearing area and its distribution.
- 6. The computational procedure is quite general in nature.

 It is applicable to surfaces showing:
 - (i) isotropic or non-isotropic;
 - (ii) Gaussian or non-Gaussian characteristics.
- 7. The intercept length distribution obtained from profile measurements showed that it is of exponential type:
- 8. The application of principles of Quantitative stereology also yielded the areal fraction and its deviation. The areal fraction gives the fraction of

the nominal cross-section-area which is the total bearing area at the chosen level.

9. The Auto-covariance Function (AFC) of the surface determined by scanning and then averaging over the test area of the surface yielded a Gaussian form, i.e.,

$$G(x) = G(0) \exp(-\frac{x^2 + \beta^2}{4})$$

It was shown that this function is the true representation of the surface. It did not display any of the basis limitations possessed by the exponential curve.

On Analytical Procedures:

- 10. The analytical determination of distribution of intercept length showed that it is of the form i* $\exp(-i^*2)$, where 'i*' is the normalized intercept length. This was observed to match well with the measured values obtained from OGT for heights of irregularities $\geq R_a$.
- II. From the density distribution of intercept length, the distribution of IBA was determined. It was found that it was of a* $K_0(a^*)$, where 'a*' is the normalized bearing area. Moreover, it was found that this distribution can be easily determined from the moments of the spectrum.

bearing area. Moreover, it was found that this distribution can be easily determined from the moments of the spectrum.

On Application to Contact Problems.

- 12. With the knowledge of the density of IBA and initial portion of ACF, the low pass cut-off relevant to the contact problem can be determined. By knowing this cut-off, it is possible to determine the wavelength of surface asperities which actually contributes to the formation of contact area on the application of load.
- 13. It was shown using a simplified model that as the load increases the contact area increases as it tends to the nominal area. The spectral analysis reveals the persistence of asperities and importance of waviness with the increase of load.
- 14. The density distribution of heights obtained for the surface subjected to increasing loads showed that the distribution exhibits the deviation from Gaussian characteristics and becomes more skewed (exponential). Therefore, the theoretical investigation of intercept length and pearing area which is based on Gaussian Random Process is not valid for very heavy loading (greater than 10MPa).
- 15. Using the individual bearing areas (IBA) and their

corresponding probability density function, together with the well-defined local stress, a stochastic theory of deformation can be formulated for the solution of an elastic contact problem.

5.2 Recommendations

- 1. It is recommended that OGT technique be automated to give the direct computerized read-out of parameters.
- 2. In the present study the density distribution of IBA can be used to predict the deformation of the interface formed by two surfaces in contact. It is recommended that the properties of the interface, for example stiffness and damping, be investigated using the concept of IBA and its distribution.
- 3. There is no theoretical model which takes into consideration the effect of size of asperities on the material properties. It is recommended that by defining a local stress with local material properties a stochastic theory of deformation be formulated for the solution of contact problems.
- 4. It is recommended that theoretical study be undertaken to characterize the surface which is anistropic and non-Gaussian. The effectiveness of cross-correlation techniques to arrive at useful parameters for such a type of surface should be verified through OGT measurement.

- 5. Using the 3-D characterization of surface developed in this work with the concept of IBA, the study of the interfacial behaviour relating to the following is recommended:
 - the thermal contact resistence
 - 2. the frictional behaviour of surface
 - 3. the bonding properties of the interface.

REFERENCES

- 1. Abrams, D.M. and Kops, L. 'Effect of waviness on normal contact stiffness of machine tool joints.' Annals of the CIRP, Vol. 34, 1985, pp. 327-330.
- 2. Peklenik, J. 'New developments in surface characterization and measurements by means of random process analysis.' Proc. Instn. of Mech. Engrs. 182 Part 3k, pp. 108-26.
- 3. Whitehouse, D.J. and Archard, J.F. 'The properties of random surfaces of significance in contact.' Ling, F.F. (ed.) in Surface Mechanics, ASME, N.Y., 1969, pp. 36-37.
- 4. Nayak, P.B. 'Random process model of rough surfaces.'
 Trans. ASME, J. Lub. Tech. 93F, 1971, pp. 398-407.
- 5. Osman, M.O.M. and Sankar, T.S. 'Profile characterization of manufactured surfaces using random function excursion technique.' Trans. ASME, Vol. 97, 1975, p. 190.
- 6. Bennett, J.M. 'Measurement of the rms roughness, autocovariance function and other statistical properties of optical surfaces using a FECO scanning interferometer.' A.O. Vol. 15, 1976, pp. 2705-2721.
- 7. Sprague, R.A. 'Surface roughness measurement using white light speckle.' A.O. Vol. 11, pp. 2811-16.
- 8. Ribbens, W.B., and Lazik, G.L. 'Use of optical data processing techniques for surface roughness studies.' Proc. IEEE Letters, 56, pp. 1637-8.
- 9. Kais, Almarzouk. 'Three beam interferometric profilometer.' PSA.AO, Vol. 22, 1983, p. 1893.
- 10. Sato and Hori, O. 'Surface roughness measurement by SEM.'
 Annals of CIRP 31, 1982, p. 457.
- 11. Clarke, G.M. and Thomas, T.R. 'Roughness measurement with a laser scanning analyser.' Wear, 57, 1979, p. 107.
- 12. Francon, F. and Mallick, S. 'Polarization interferometry.' Wiley-Interscience, N.Y., 1971.
- 13. Young, R., Ward, J. and Scire, F. 'The Topografiner: An instrument for measuring surface microtopography.' Rev. Sci. Instrum., 43, pp. 999-1011.

- 14. Bhusan, B., Wyant, James C., and Koliopoulus, C.R.
 'Measurement of surface topography of magnetic tapes by
 mireau interferometry.' 15th May 1985, Vol. 24, No. 10,
 Optical Society of America.
- 15. Mitsui, K., Ozawa, N., Kohno, T. 'Development of a high resolution in process sensor for surface roughness by Laser beam.' JSPE, Vol. 19, No. 2, 1985, pp. 142-144.
- 16. Radhakrishnan, V. 'Effect of stylus radius on the roughness values measured with tracing stylus measurements.' Wear, 16, 1970, pp. 325-335.
- 17. Thomas, T.R 'Stylus Instruments,' in 'Rouch Surfaces.'
 Edited by T.R. Thomas, Longman Inc., New York: 1982.
- 18. De Vries, W.R., and Li, C.J. 'Algorithms to deconvolve stylus geometry from surface profile measurements.' Trans. ASME, Journal of Engineering for Industry, Vol. 107, 1985, pp. 167-174.
- 19. Way, S. 'Description and Observation of metal surfaces.'
 Proc. Conf. on Friction and Surface Finish, 1969, MIT
 Press, Cambridge, pp. 44-75.
- 20. Biernawski, W. 'Teoria Obrobki Skrawaniem.' Metal cutting theory, PWN, Warsaw, 1956, p. 321; also 'Stankii Instrument,' in Russian, no. 8., 1951.
- 21. Zieler, H.W. 'The optical performance of light microscope.' Vol. II. Microscope publications Ltd., London: 1972.
- 22. Sayles, R.S. 'The profile as a random process,' in 'Rough Surfaces.' Edited by T.R. Thomas, Longman Inc., New York: 1982.
- 23. Leaver, R.H., Thomas, T.R. 'Analysis and presentation of experimental results.' Macmillan, London: 1974.
- 24. Nayak, P.R. 'Some aspects of surface roughness measurement.' Wear 26, 1973, pp. 165-174.
- 25. Bendat, J.S., and Piersot, A.G. 'Measurement and analysis of random data.' Wiley, New York: 1966.
- 26. Hamming, R.W. 'Digital Filters.' Prentice Hall, NJ: 1983.
- 27. Jenkin, G.M., and Watts, D.G. 'Spectral Analysis and its Applications.' Holden-Day, San Francisco: 1968.
- 28. Underwood, E.L. 'Quantitative Stereology.' Addisson, Wesley Publ. Co. Massachusetts: 1970.

- 29. Finkin, E.F. 'The bearing area of surfaces.' Trans. ASME, J. Lub. Tech., 90F, pp. 329-30.
- 30. Papoulis, A. 'Probability, Ramdom Variables, and Stochastic process.' McGraw-Hill, NY: 1965.
- 31. Shoichi, A., Takashi, S., Yoshitomo, O., Kaneko, S., and Shinji, H. 'Measurement of visualization images of unstable flow between two parallel rotating disks.' Flow Visualization Society of Japan, Vol. 5, No. 18, 1985. pp. 295.
- 32. Hisakado, T. Bulletin of JSME, 12, 1969, pp. 1591-1527.
- 33. Francis, H.A. 'Application of spherical indentation mechanity to reversible and irreversible contact between rough states.' Wear, 45, 1977. pp. 221-269.
- 34. Spragg, R.C., and Whitehouse, D.J. 'A new unified approach to surface metrology.' Proc. Inst. of Mech. Engineers, 185, 1970/71. pp. 697-707.
- 35. Pearson, E.S., 'A further development of tests for normality.' Biometrika, 22, pp. 239-249.
- 36. Abbott, E.J. and Firestone, F.A. 'Specify surface quality.' Mech. Engg. 55, 1933, pp. 569-572.
- 37. Whitehouse, D.J. and Archard, J.F. 'The properties of random surfaces of significant in their contact.' Ling, F.F. (ed.) in Surface Mechanics. ASME, N.Y. 1969, pp. 36-37.
- 38. Peklenik, J. 'New developments in surface characterization and measurements by means of random process analysis.' Proc. Instn. of Mech. Engrs. 182 Part 3k, pp. 108-26.
- 39. Rasigui, M., Rasigui, G. and Palmeri, J.P. 'Study of surface roughness using micro-densitometer analysis of electron micrographs of surface replicas. II: Autocovariance functions.' J. of Optical Soc. of America, Vol. 71, October 1981, p. 1230.
- 40. Pandit, S.M., Wu, S.M. 'Time series and System Analysis with application.' John Wiley and Sons, 1983.
- Greenwood, J.A. and Williamson, J.B.P. 'Contact of nominally flat surfaces.' Proc. Royal Soc. London, A295, pp. 300-19.
- 42. Greenwood, J.A. and Tripp, . 'The elastic contact of rough spheres.' Trans. ASME, J. Appl. Mech., 34E, pp. 153-9.

- 43. Whitehouse, D.J. and Archard, J.F. 'The properties of random surfaces of significance in their contact.' Proc. Roy. Soc. London, A316, 1970, pp. 97-121.
- 44. Bush, et al. 'Strongly anistropic rough surfaces.' ASME paper, 78-LUB-16.
- 45. Hisakado, T. and Tsukizoe, T. 'Effects of distribution of surface slopes and flow pressures of contact asperities on contact between solid surfaces.' Wear, 28, pp. 217-34.
- 46. Longuet-Higgins, M.S. 'The statistical geometry of random surfaces.' Proc. 13th Symp. on Appl. Maths. 1051, (Am. Math. Soc., Böston), 1962.
- 47. Elgabry, A.A., Osman, M.O.M., Sankar, T.S.. 'A simplified . Probabilistic Model for 2-D profile characterization of surfaces machined by finishing processes.' Transaction of the CSME, Vol. 5., No. 3, 1978-79.
- 48. Cramer, H. and Leadbetter, M.R. 'Stationary and related 'stochastic processes.' John Wiley and Sons, N.Y.: 1967.
- 49. Gibson, R.D. 'The surface as a random process.' In 'Rough Surfaces.' (T.R. Thomas ed.) Longman Inc., NY: 1982.
- 50. Barndorff-Nielsen, O. and Halgreen, C. 'Infinite divisibility of the hyperbolic and generalised inverse Gaussian distributions.' Z. Wahrscheinlichkeitstheorie Verw. Gebiete 39, 1971, pp. 309-311.
- 51. Letac, Gerard and Seshadri, V. 'A characterization of the generalized inverse Gaussian distribution by continued fractions.' Z. Wahrscheinlichkeitstheorie Verw. Gebiete 62 m 1983, pp. 485-489.
- 52. Tabor, D. 'Interaction between surfaces: Adhesion and Friction.' In 'Surface physics of materials,' Vol. II. (J.M. Blakely, Ed.) Academic Press, NY: 1975.
- 53. Attia, M.H. and Kops, L. 'Nonlinear thermoelastic behaviour of structural joints solution to a missing link for prediction of thermal deformation of machine tools.' Trans. ASME, J. of Engg. for Industry, Vol. 101, No. 3, 1979, pp. 348-354.
- 54. Abrams, D.M.A., 'Effect of joints under combined loading on thermal deformation of machine tools.' Master's Thesis, McGill University, 1984.
- 55. Archard, J.F. 'Single contacts and multiple encounters.'
 J. Appl. Phys., 32, 1961, pp. 1420-1425.

- 56. Thomas, T.R. and Sayles, R.S. 'Random process analysis of the effect of waviness on thermal contact resistance.'
 In 'Progress in Aeronautics and Astronautics.' Vol. 39, 1975, pp. 3-20.
- 57. Tabor, D. 'The Hardness of Metals.' Clarendon Press, Oxford: 1951.

V

- 58. Axelrad, D.R. 'Foundations of the Probabilistic Mechanics of Discrete Media.' Pergamon Press, Oxford: 1984.
- 59. Gane, N. 'The direct measurement of the strength of metals on a sub-micrometer scale.' Proc. Royal Soc. London, A317, 1970, pp. 367-391.

Tracing stylus tip

Traced profile

Original profile

Fig. 1.1 Distortion of profile reading due to finite dimension of stylus tip (exaggerated) [17].

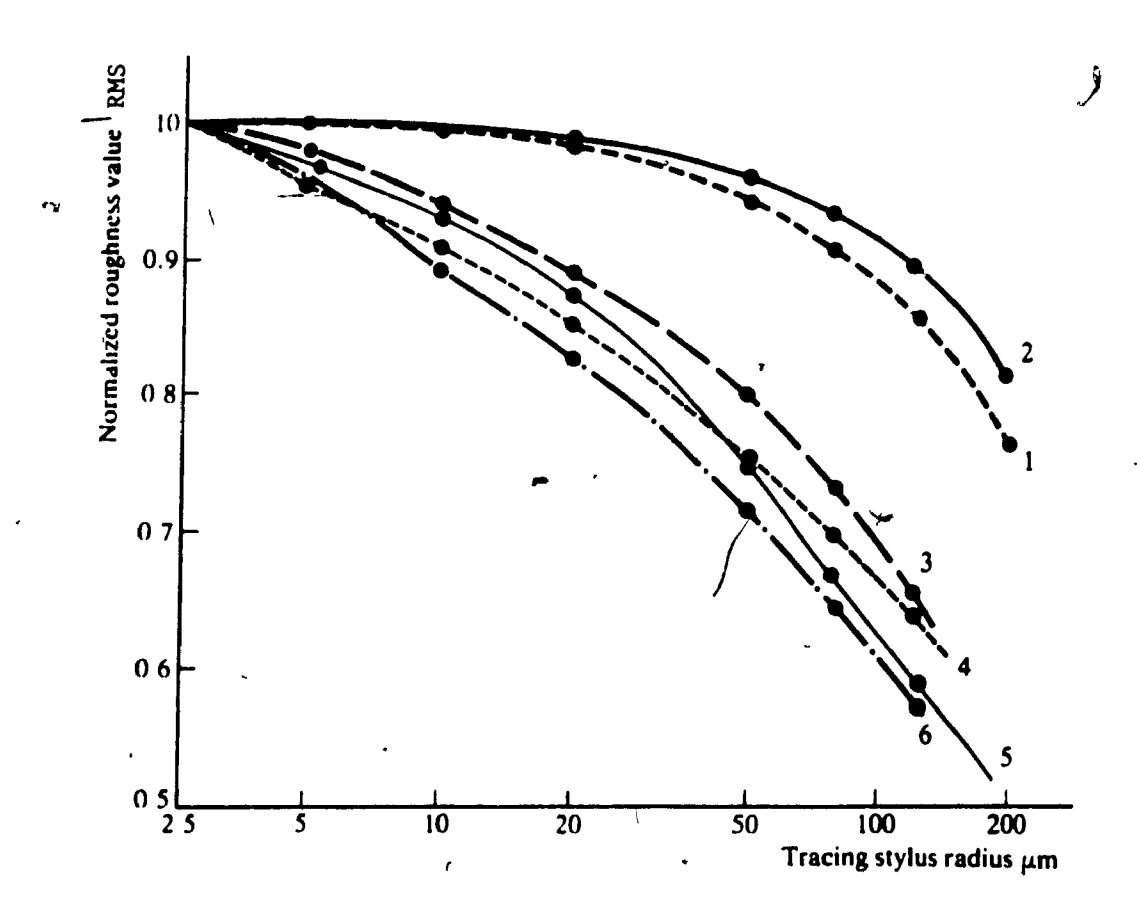


Fig. 1.2 Effect of stylus tip radius on measured roughness of various surfaces [17].

- 1. Planed 2. Electo-eroded 3. Milled 4. Ground
- 5. Electrochemically sunk 6. Honed.

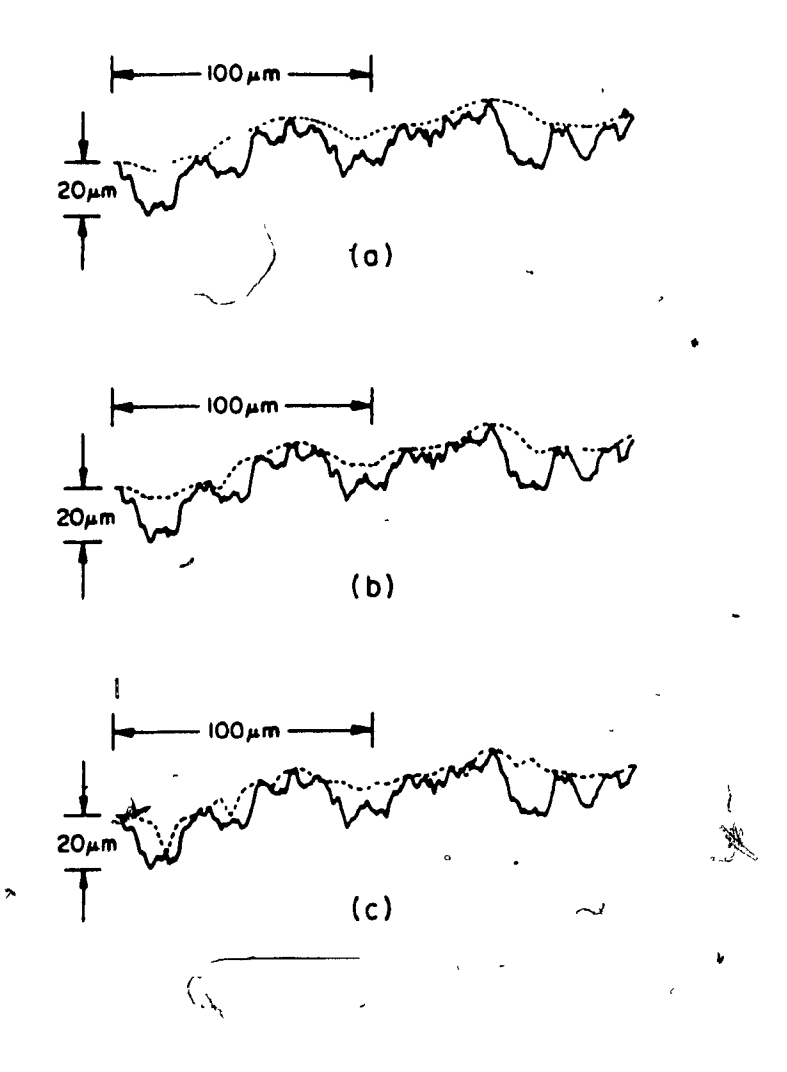


Fig. 1.3 Simulated profile with RMS = 10 μm , L = 100 μm and radius of stylus tip = 25 μm , illustrating:

1. measured profile 2. compensated profile 3. Using
further compensation [17].

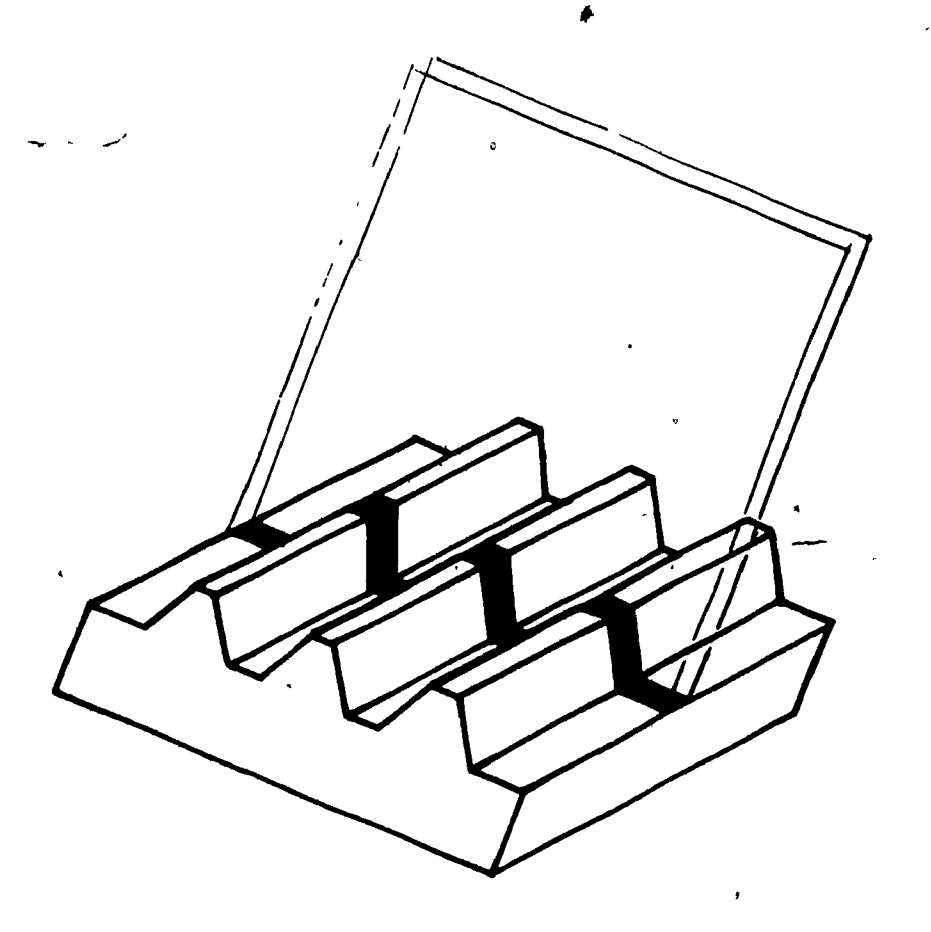
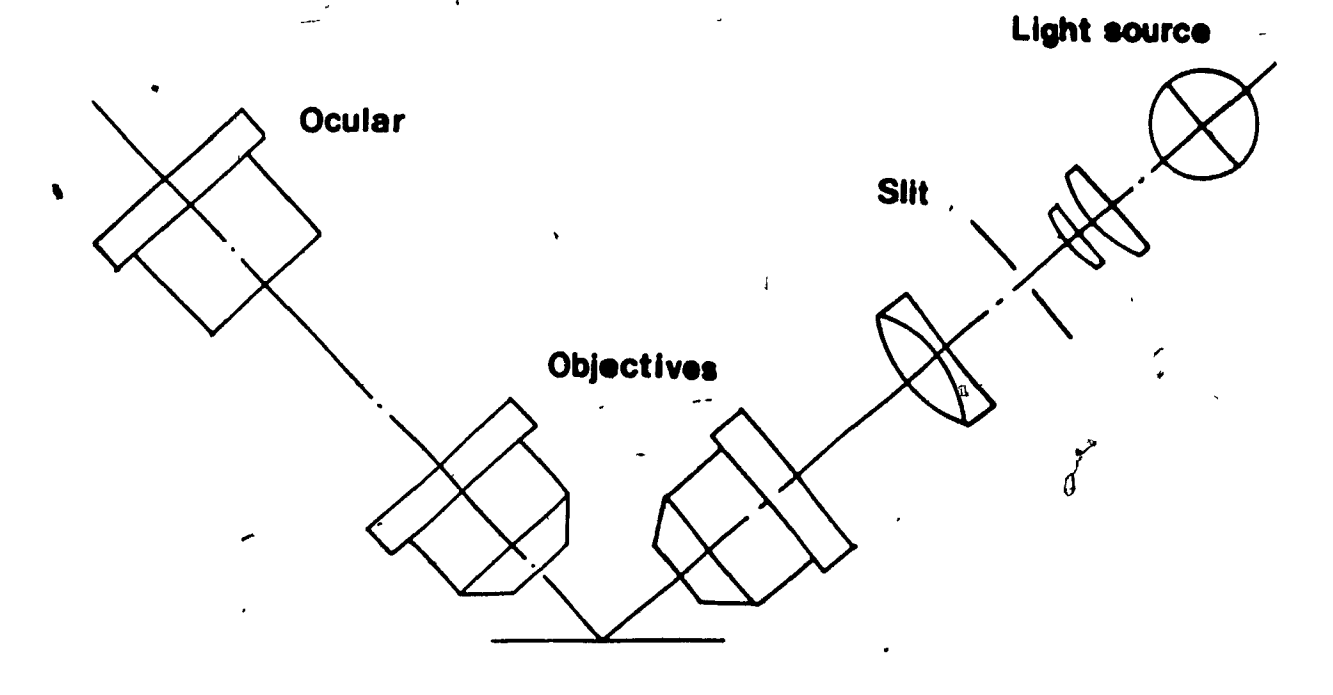


Fig. 2.1 Principle of Schmaltz microscopy

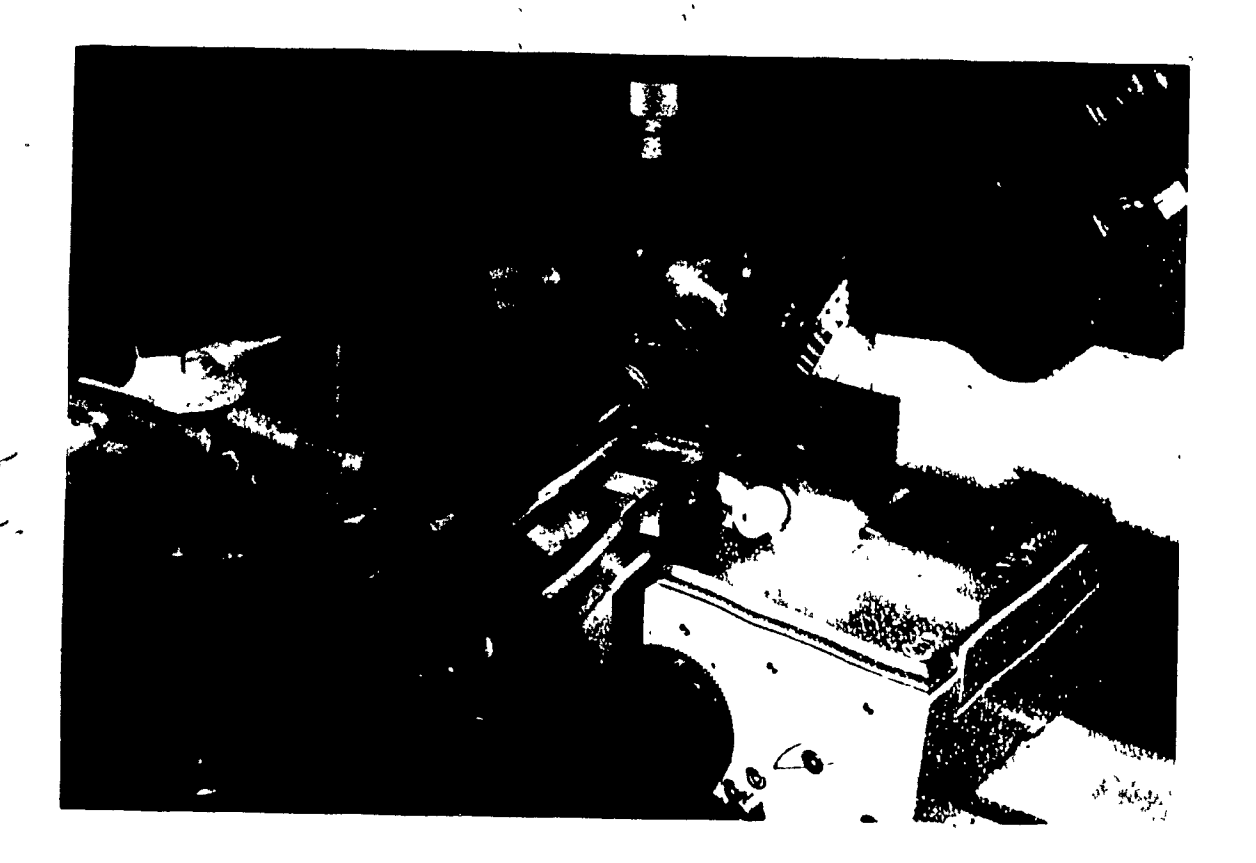


OPTICAL SYSTEM

Fig. 2.2 Optical system used by Schmaltz [19].

7. 5.

Fig. 2.3 Schematic of optical Grating Topography, OGT.



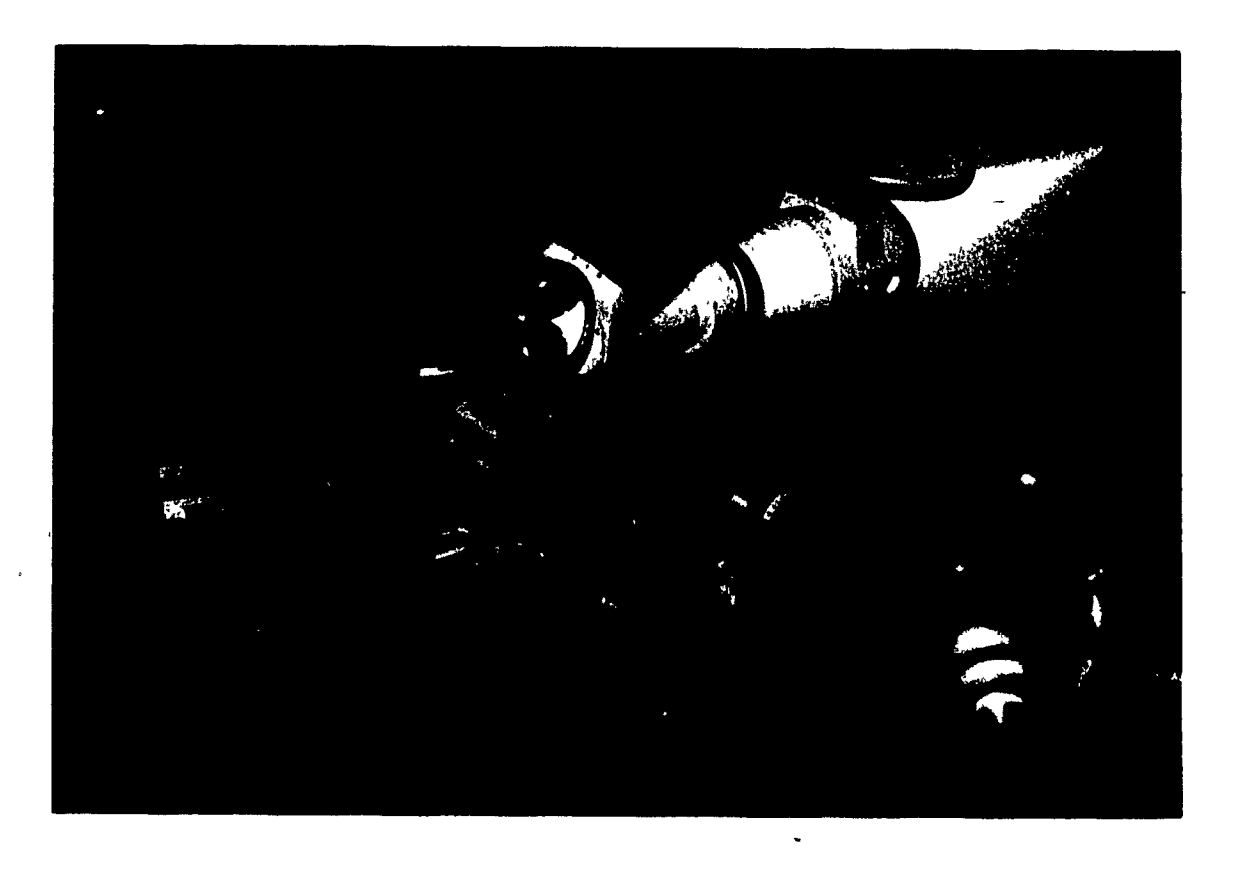


Fig.2.4 General arrangement of OGT set up

۱ ۵`

Fib. 2.5 Flow chart for the operation of OGT system.

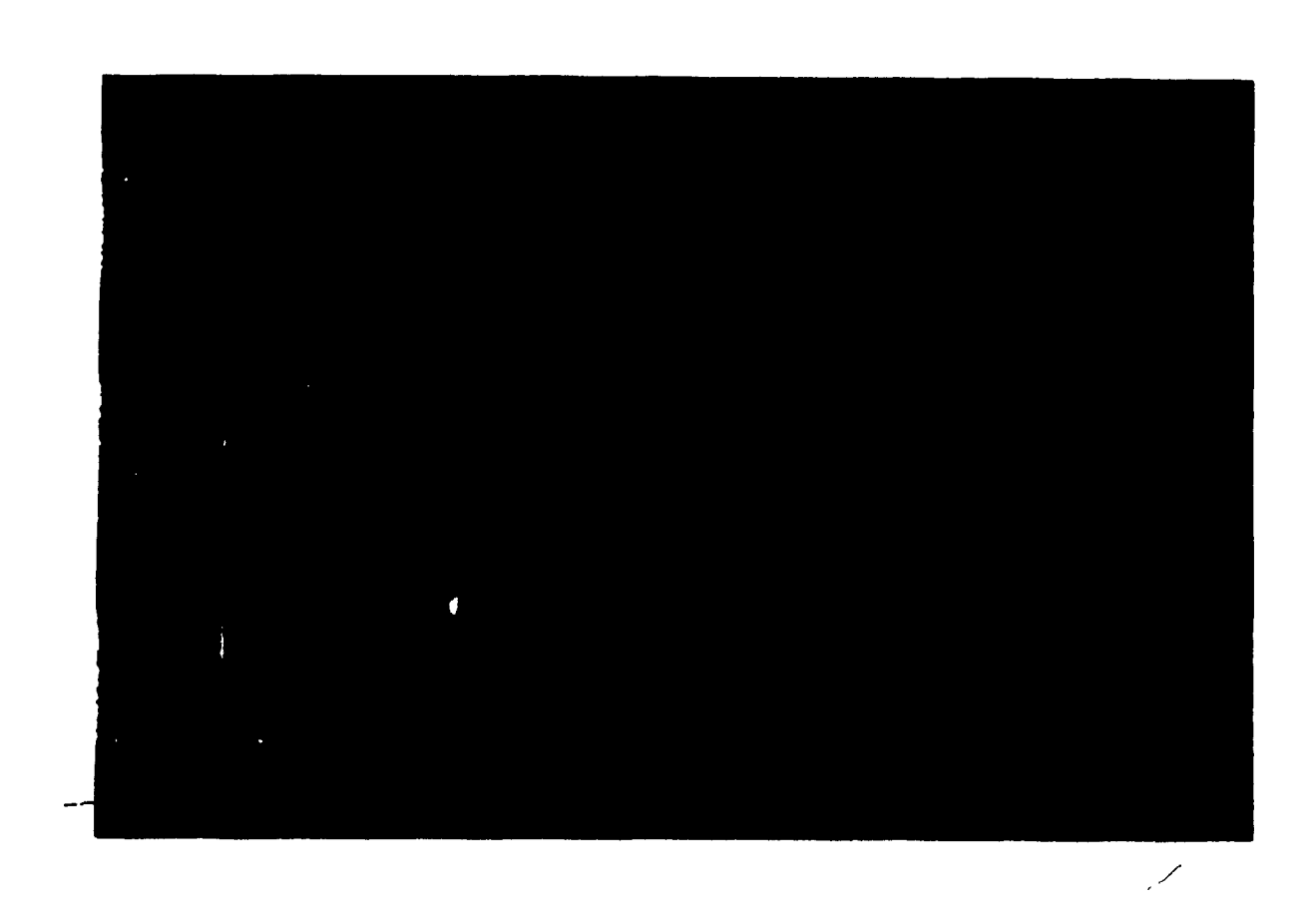


Fig. 2.6 Grating lines on optically flat mirro'r.



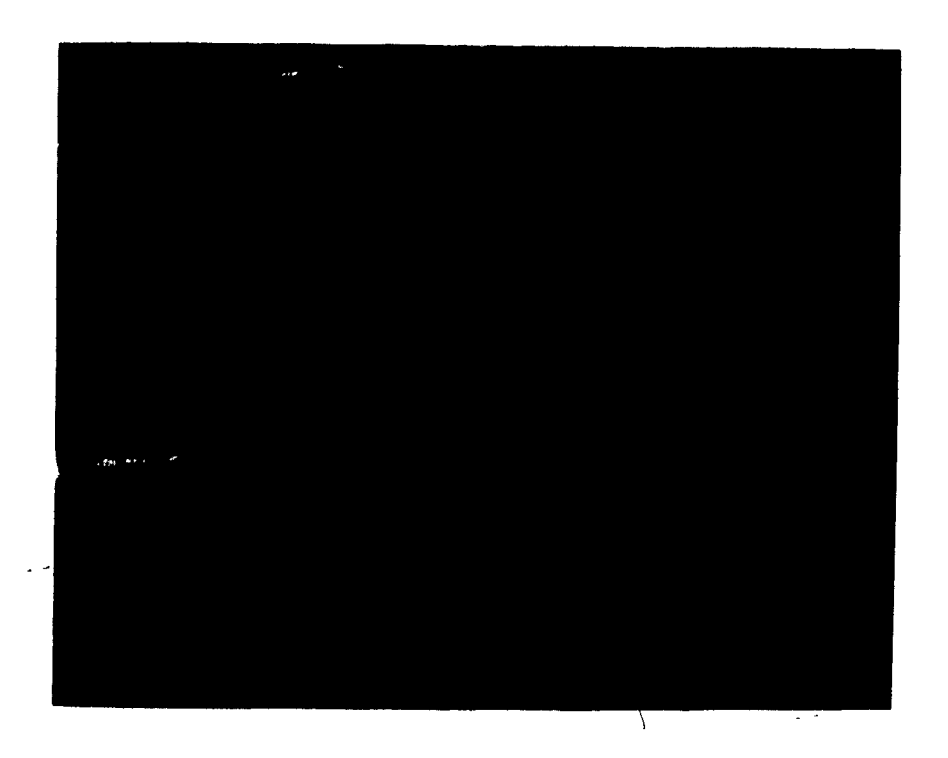
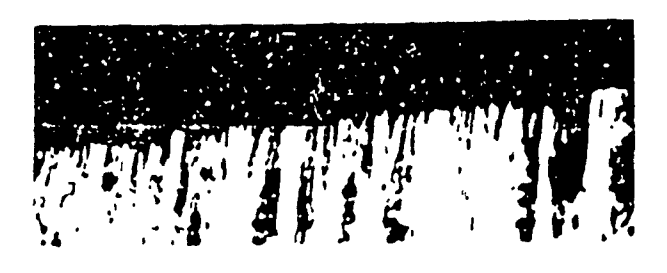


Fig. 2.7 Grating lines on machined ground surface



а



b



C

Fig. 2.8 Examples of application of OGT

- a) OGT photograph of 0.001" step
- b) OGT photograph of the belt ground sufface
- c) OGT photograph of the surface, obtained on the surface grinder

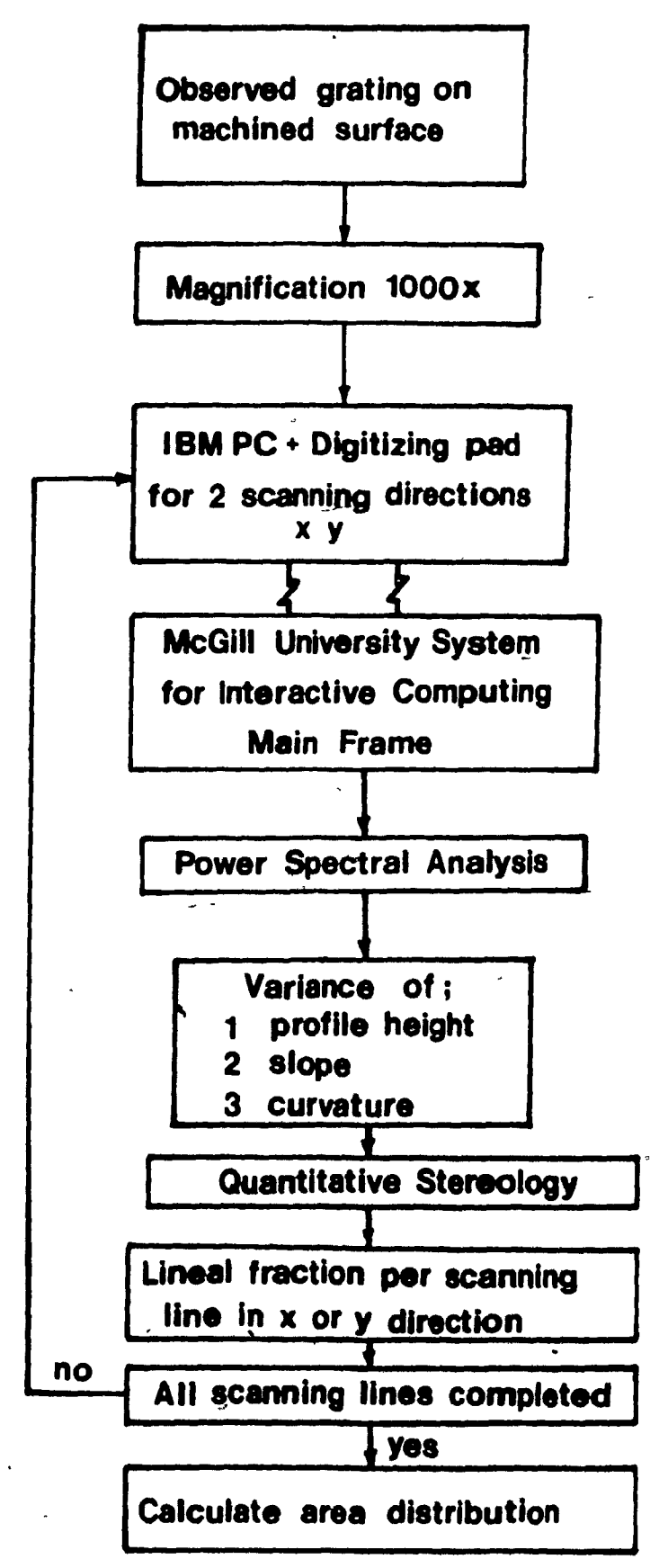


*Fig. 2.9 Computational flow chart.

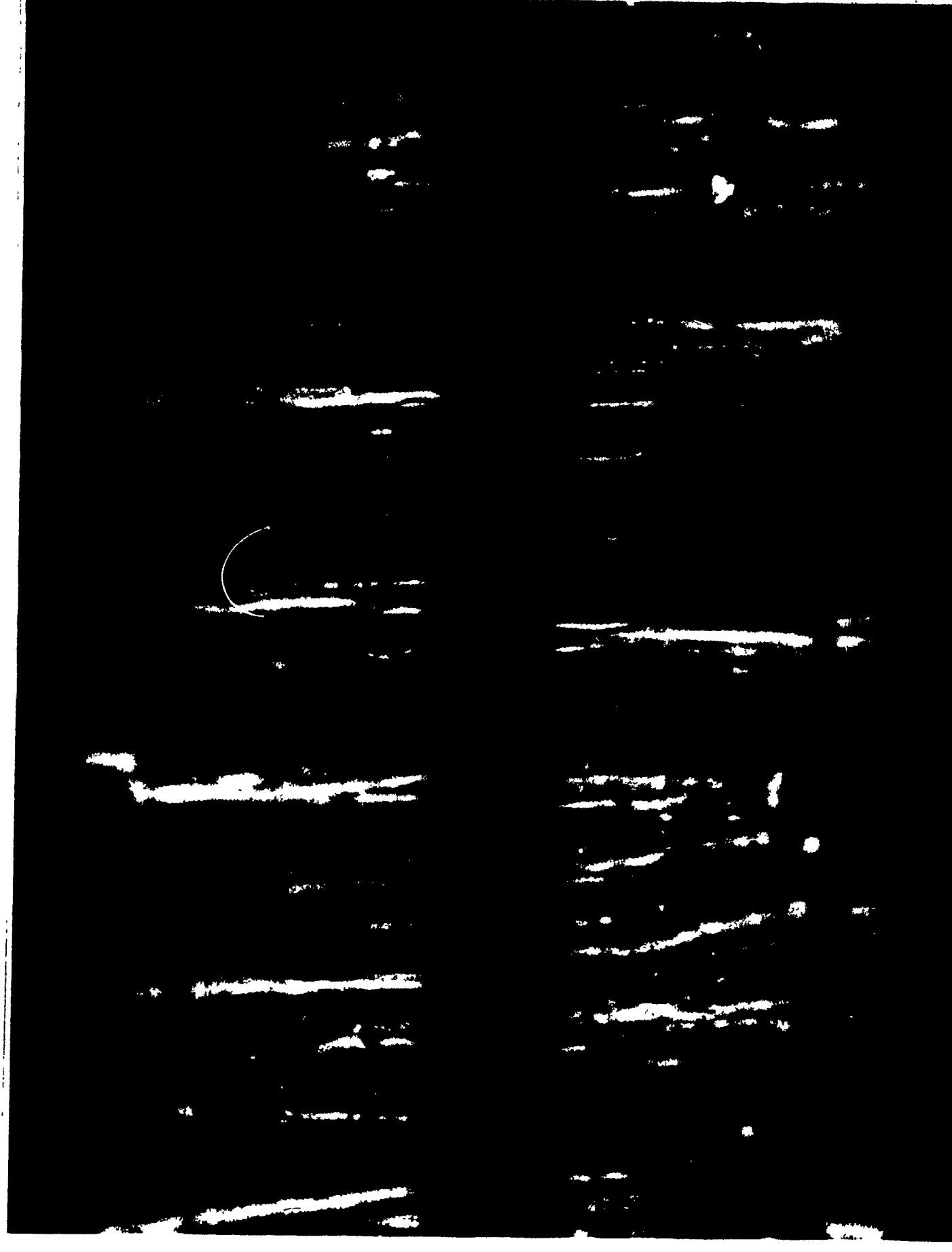
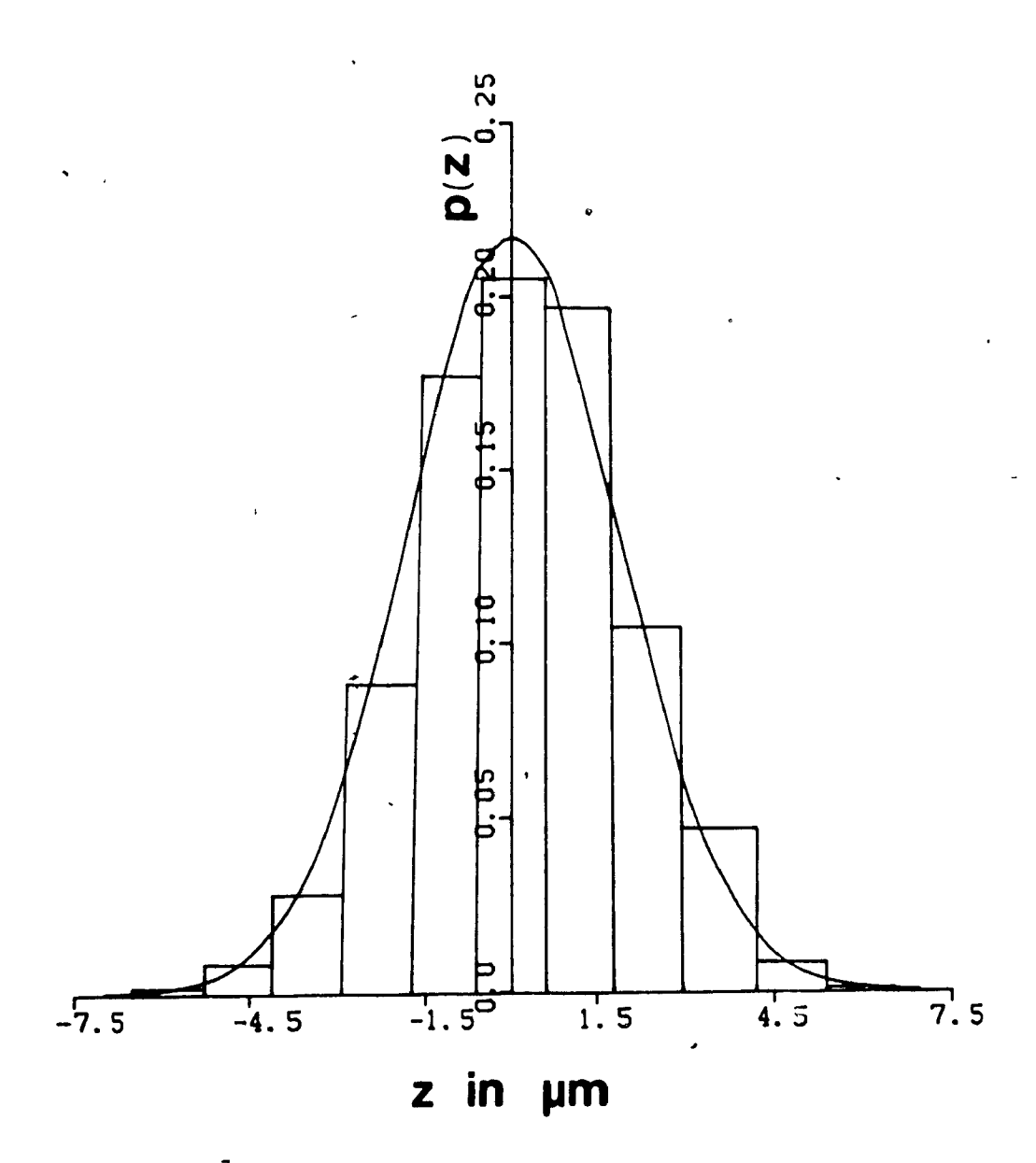
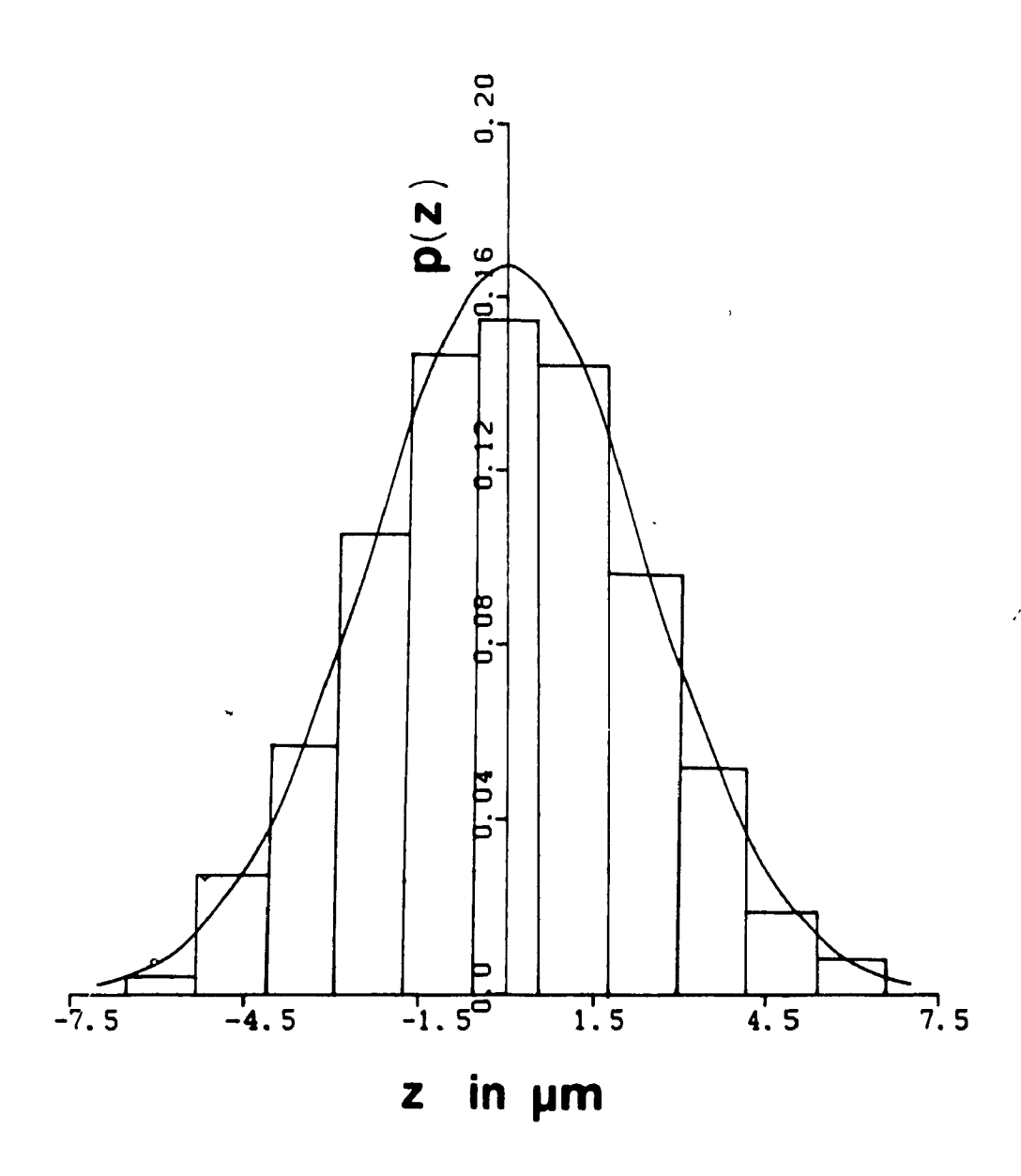


Fig. 2.10 1000x magnified photograph of the delineated grating profile



PROBABILITY DENSITY DISTRIBUTION OF HEIGHTS

Fig. 2.11 Density distribution of heights of the profile obtained along the direction of grinding.



PROBABILITY DENSITY DISTRIBUTION OF HEIGHTS

Fig. 2.12 Density distribution of heights of the profile obtained across the direction of grinding.

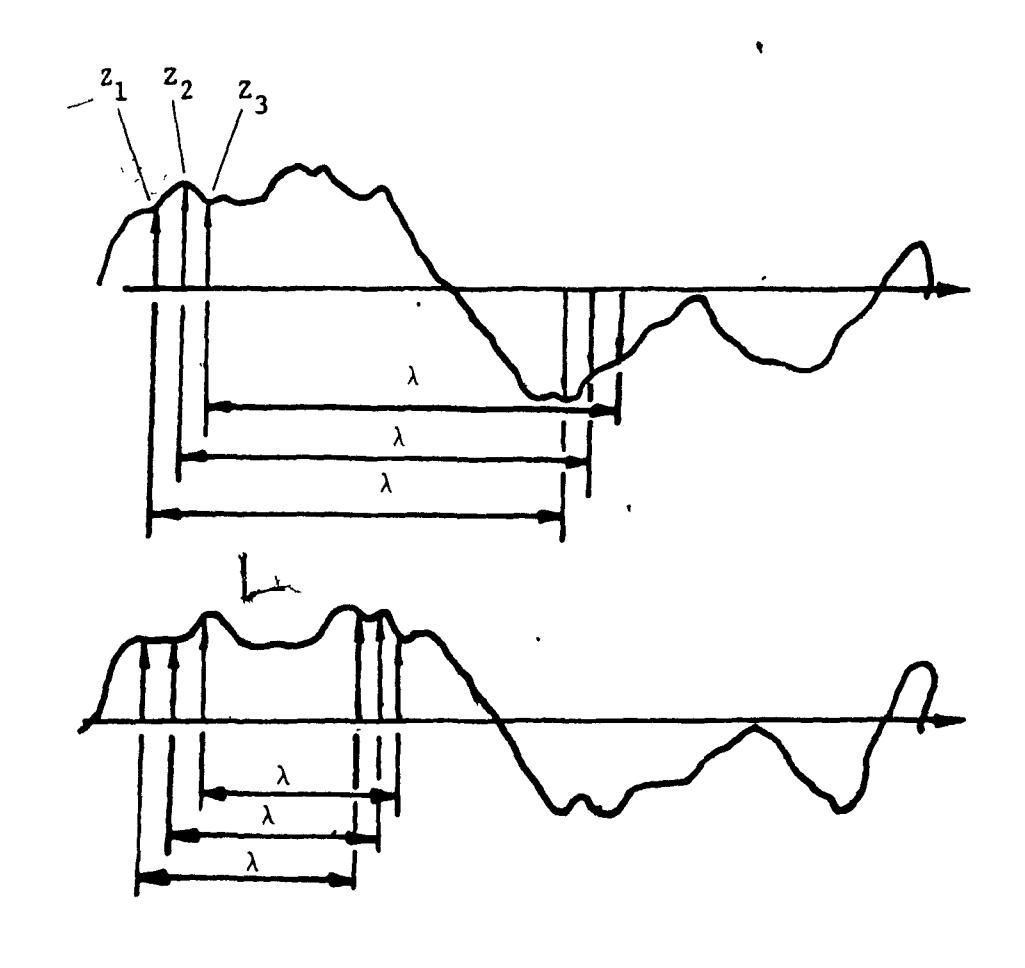
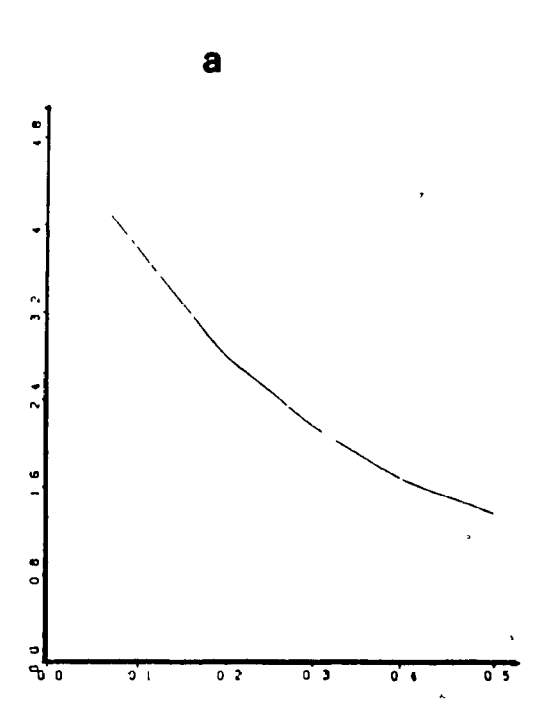


Fig. 2.13 Concept of auto-correlation function.



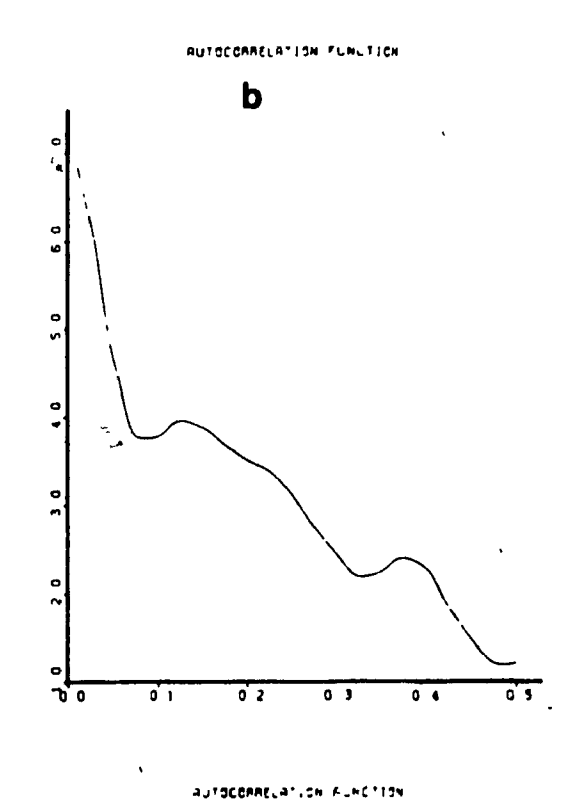


Fig. 2.14 Auto-correlation function for the surface profile

- a) along the direction of grinding -
- b) across the direction of grinding.

Fig. 2.15 Principle of auto covariance computations by means of Discreet Fourier-Transform

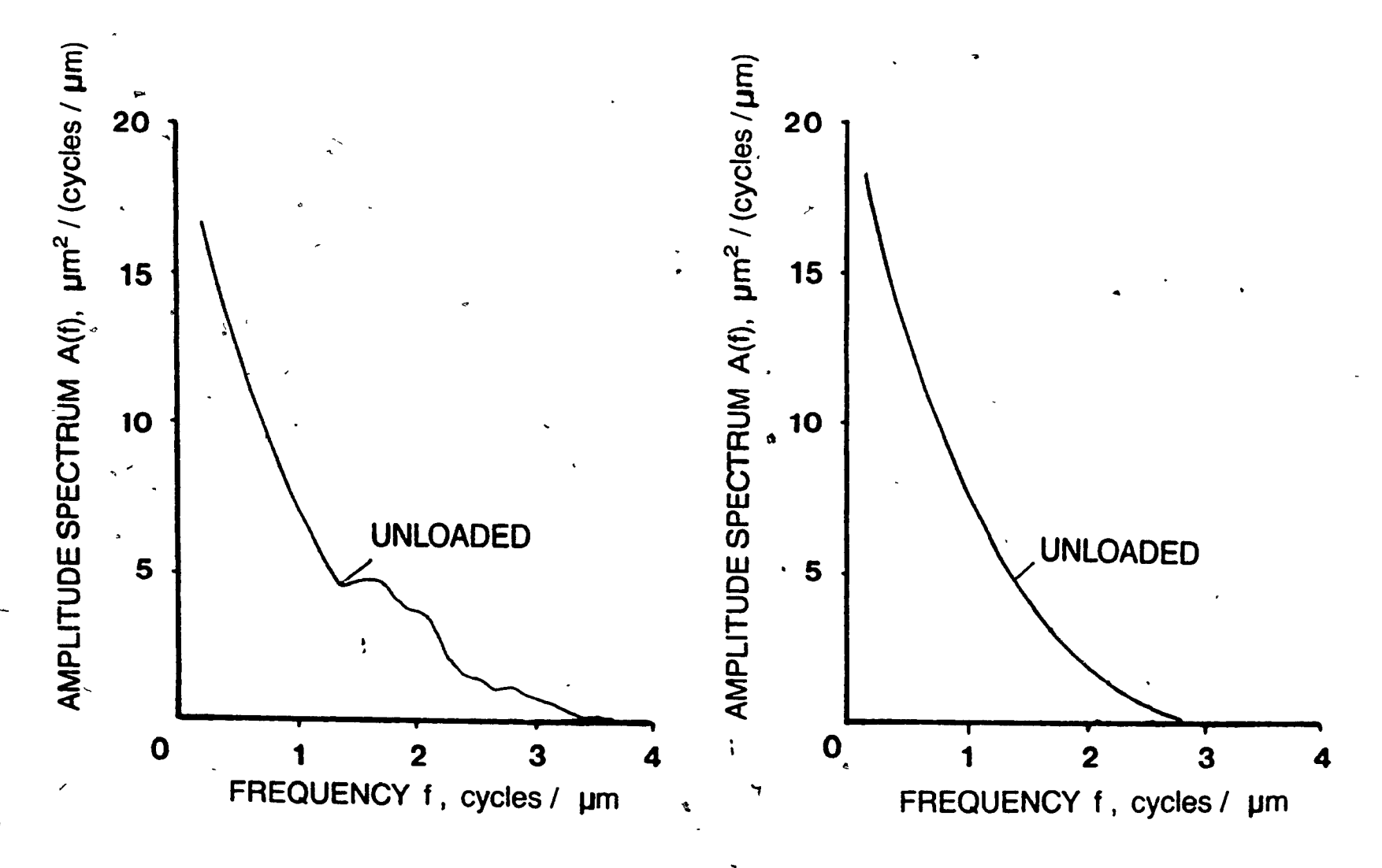


Fig. 2.16 Amplitude spectrum of the surface profile

- a) along the profile
- b) across the profile

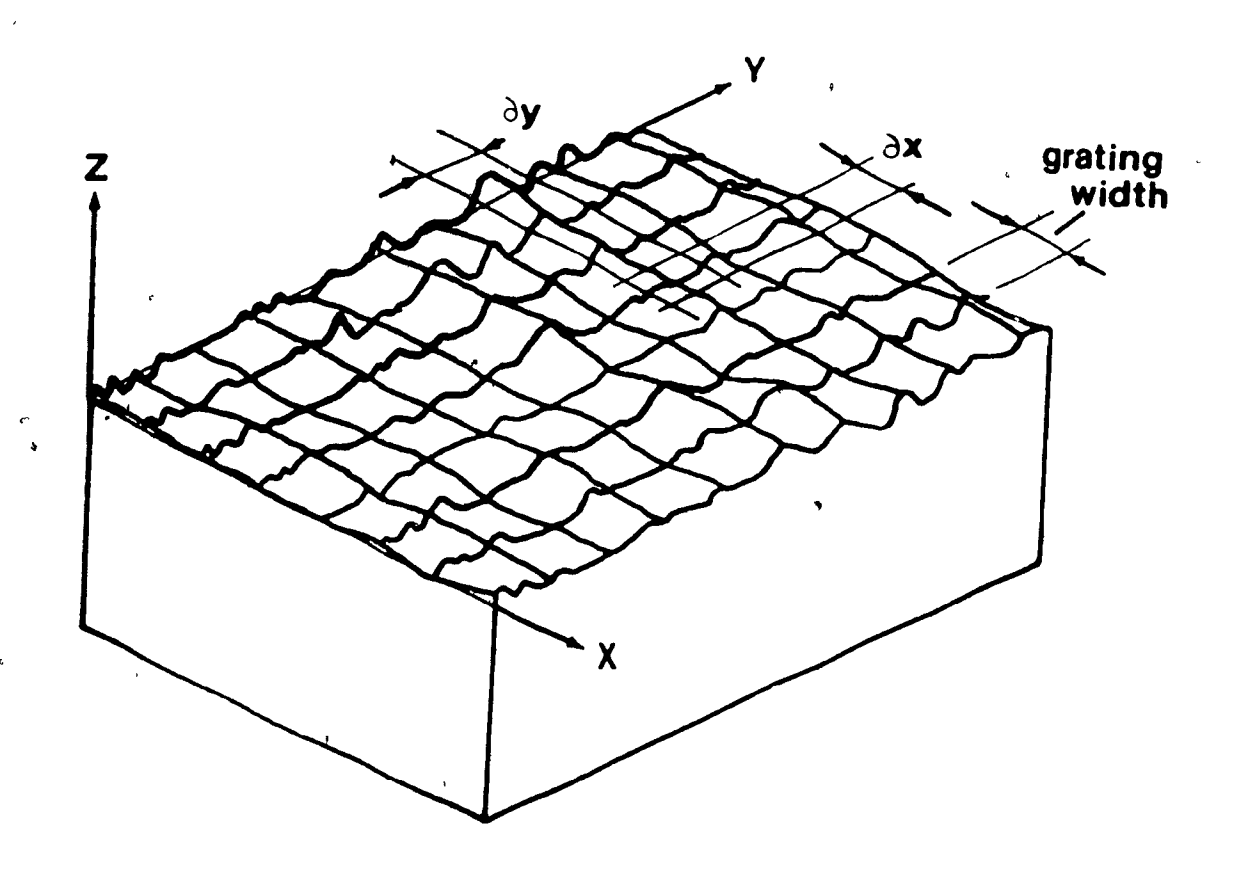
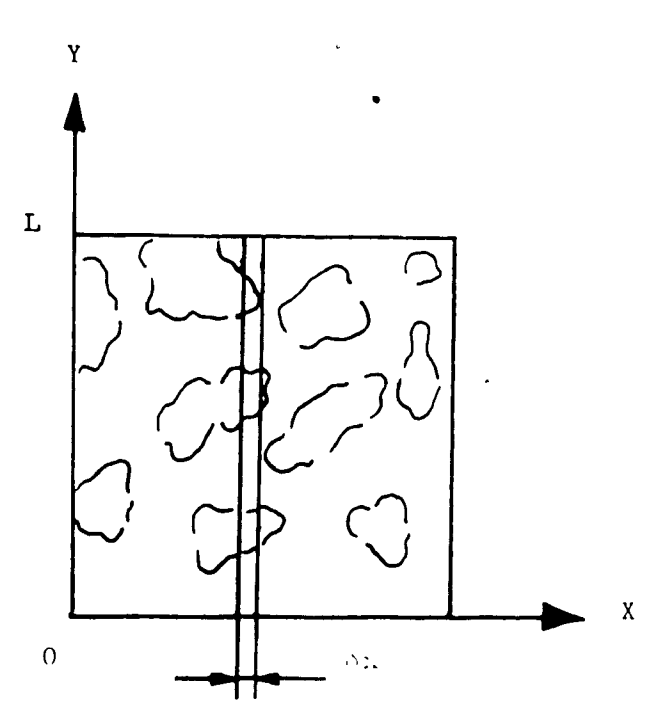
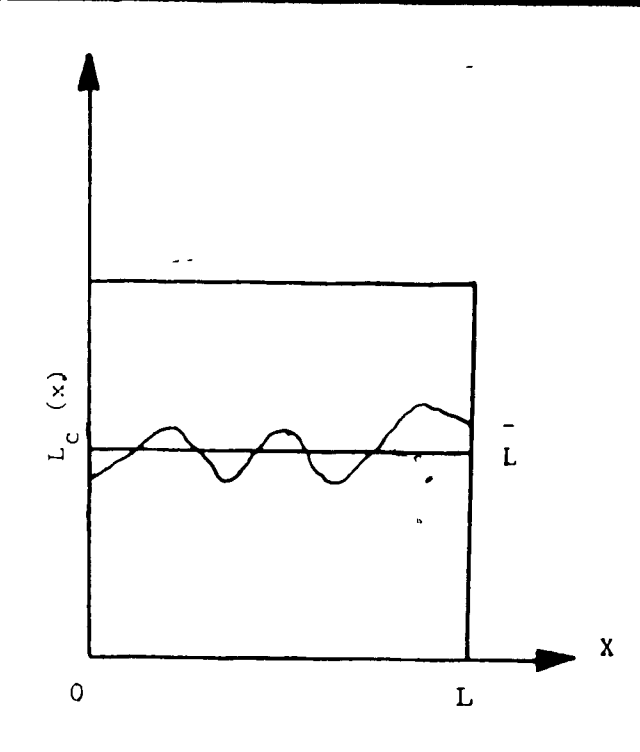


Fig. 2.17 3-D surface representation by means of parallel scanning lines.



Section plane showing small microcontact areas cut by test lines of width δx to form bearing length



Variation of bearing length in thin strip $L_c(\mathbf{x})$ as a function of strip position \mathbf{x}

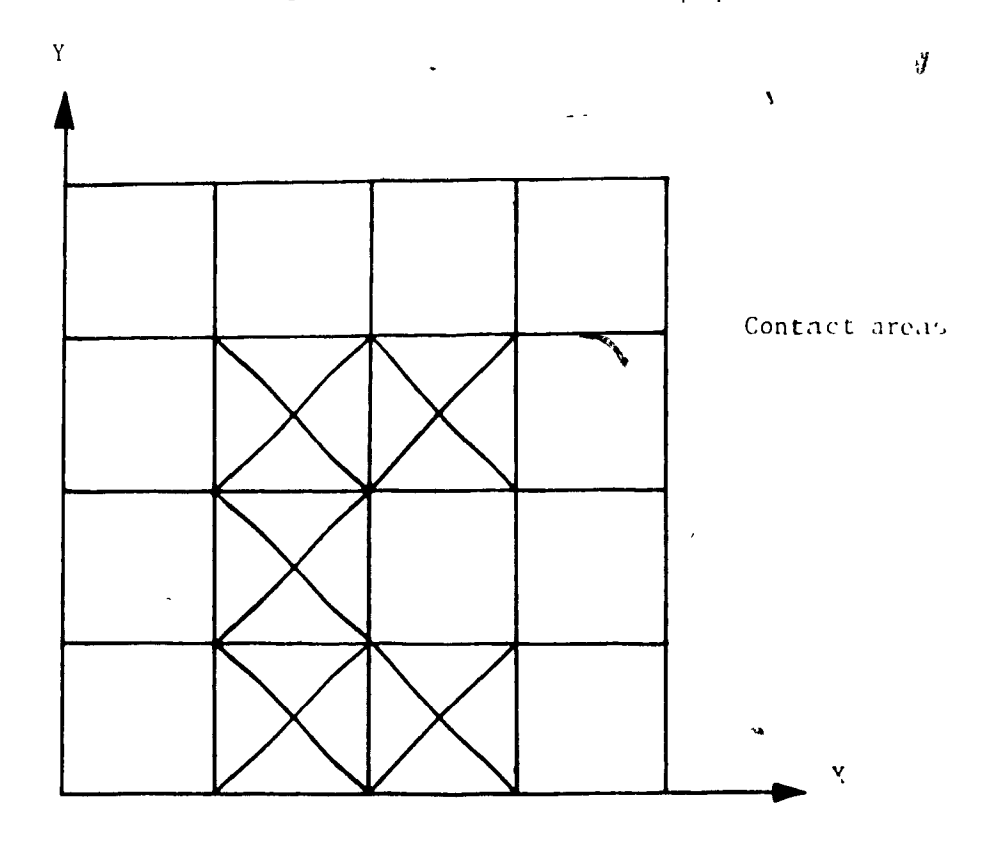


Fig. 2.18 Concept of lineal fraction and its relationship to the area fraction.

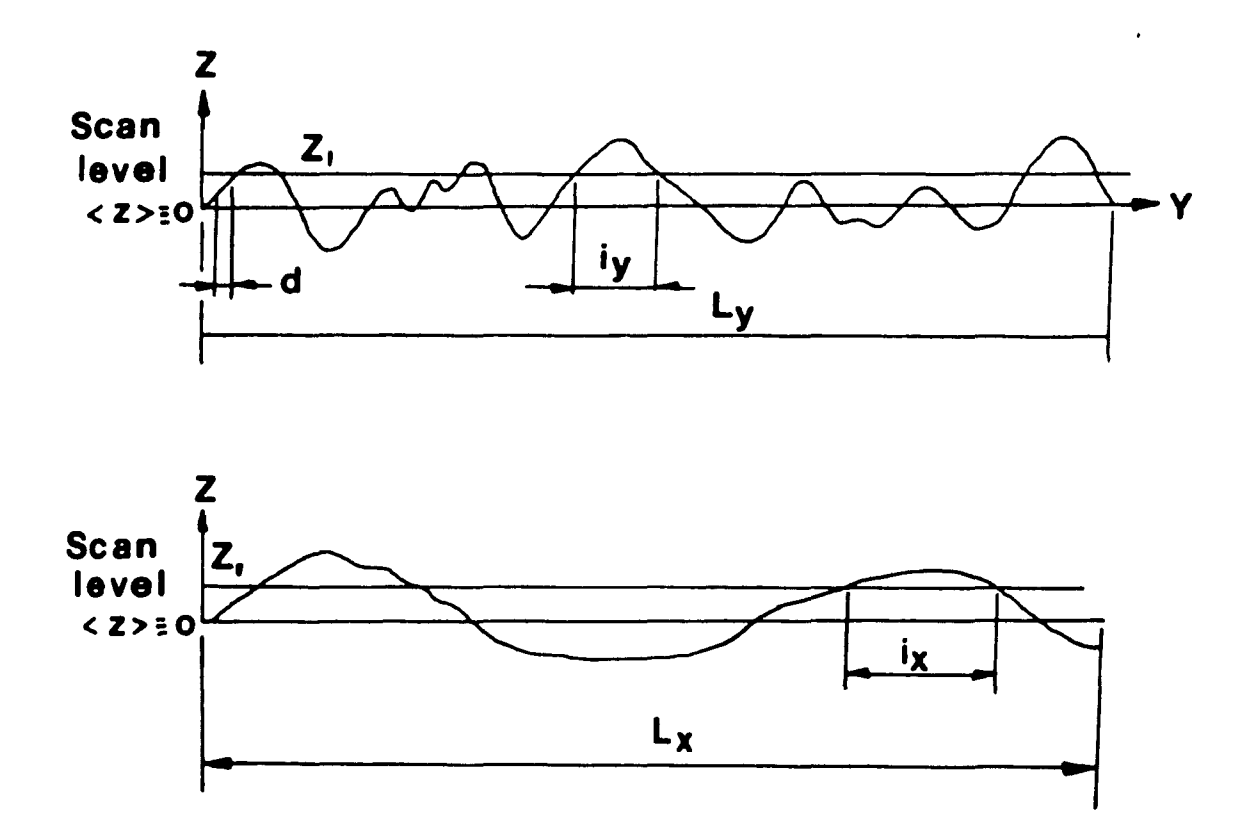


Fig. 2.19 Definition of intercept length: $^{1}\mathbf{x}$ and $^{1}\mathbf{y}$ for along and across the direction of grinding.

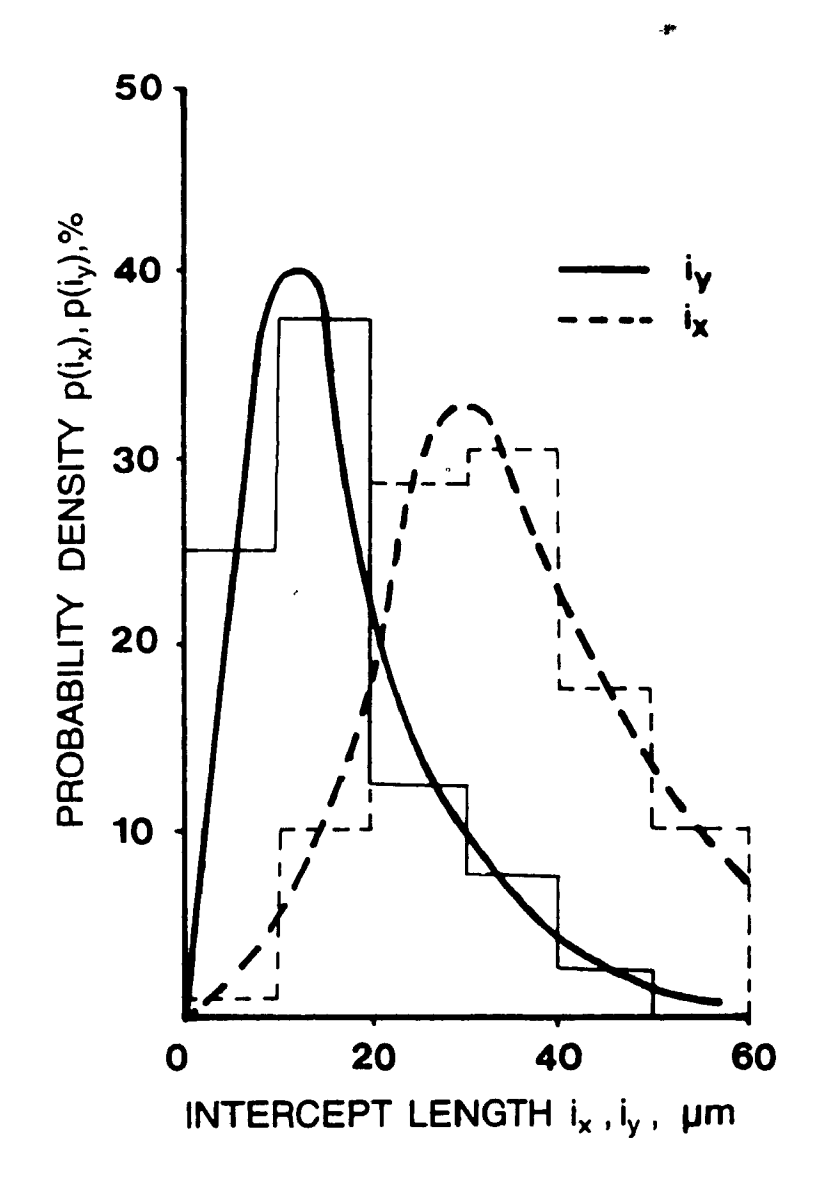


Fig. 2.20 Distribution of intercept length along 'X' and 'Y' direction.

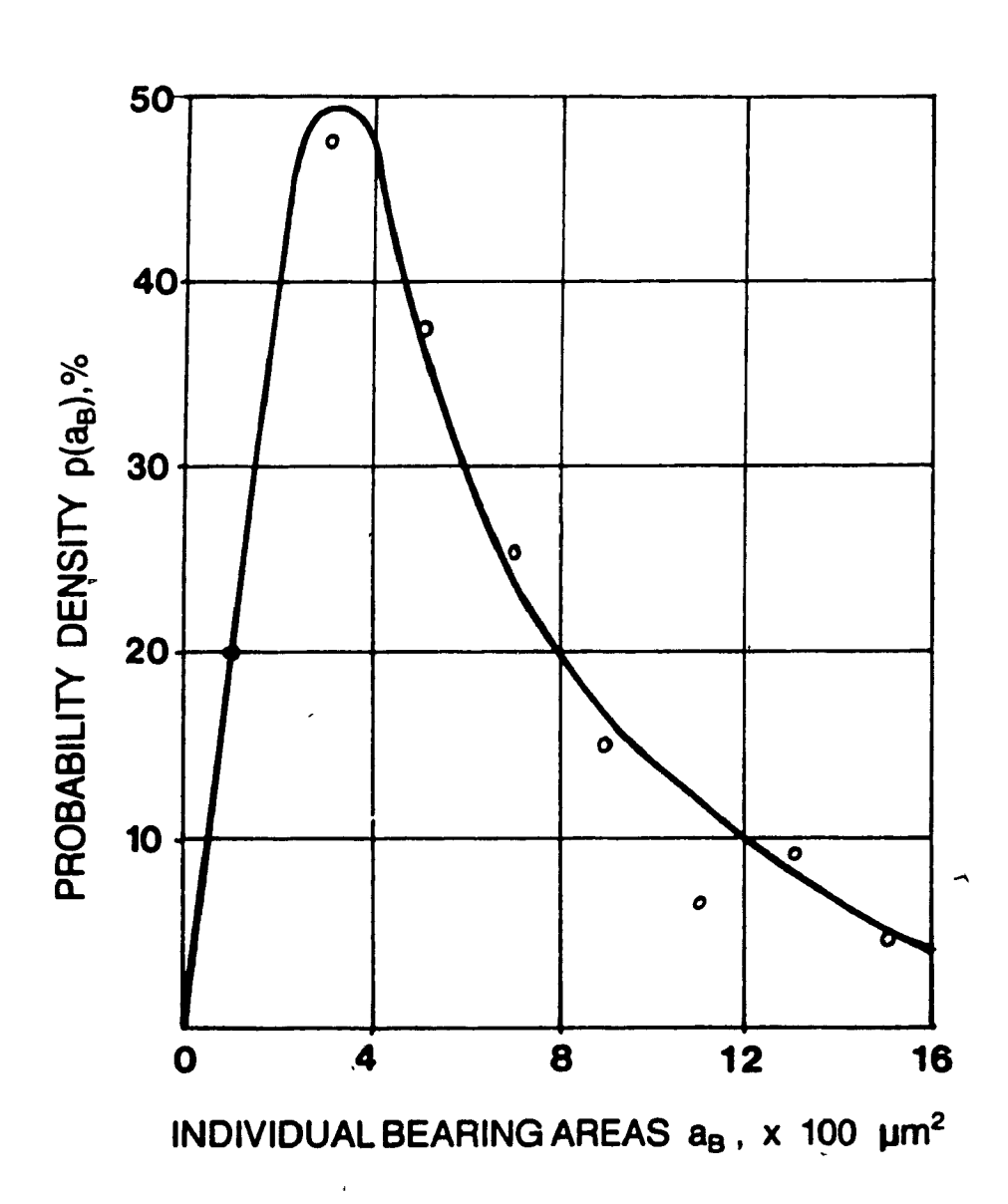


Fig. 2.22 Distribution of individual bearing area.

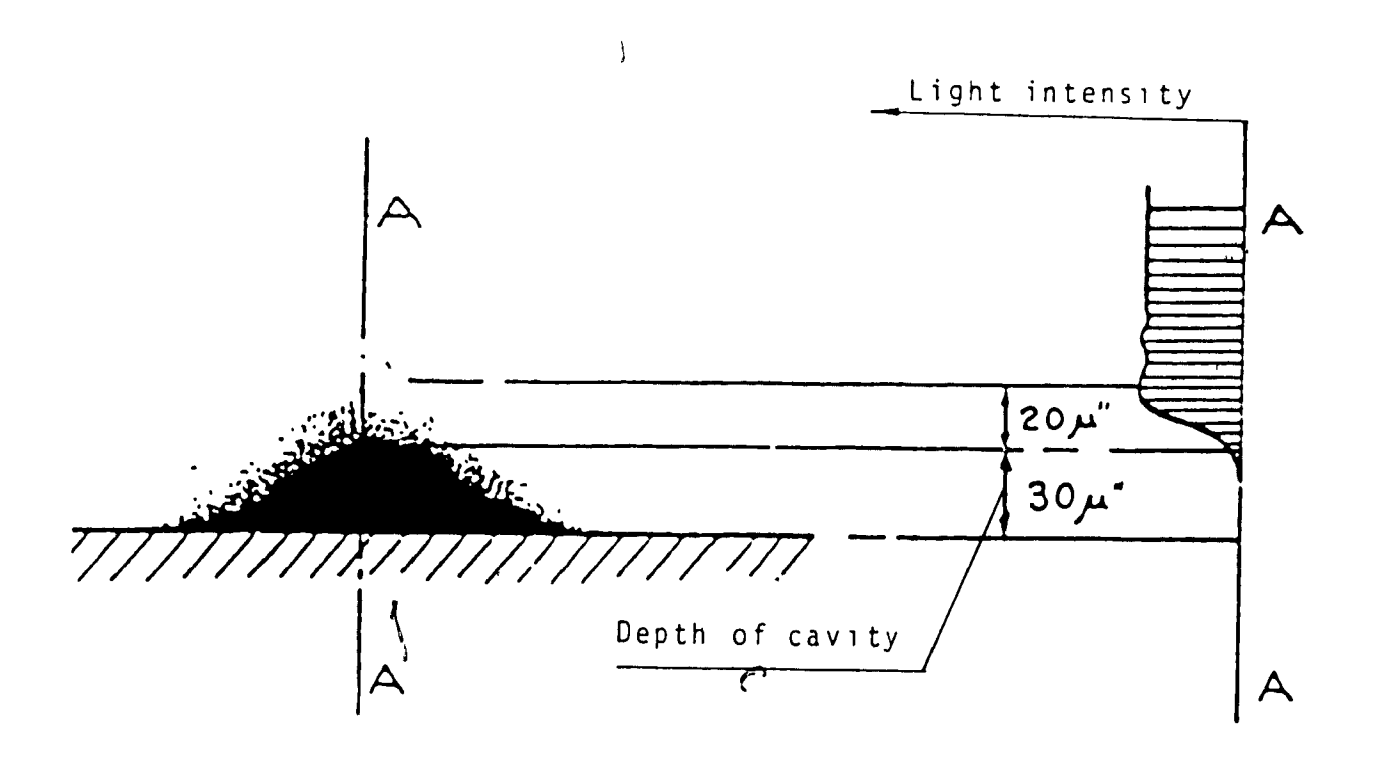


Fig. 2.23 Effect of diffraction at straight edge [19].

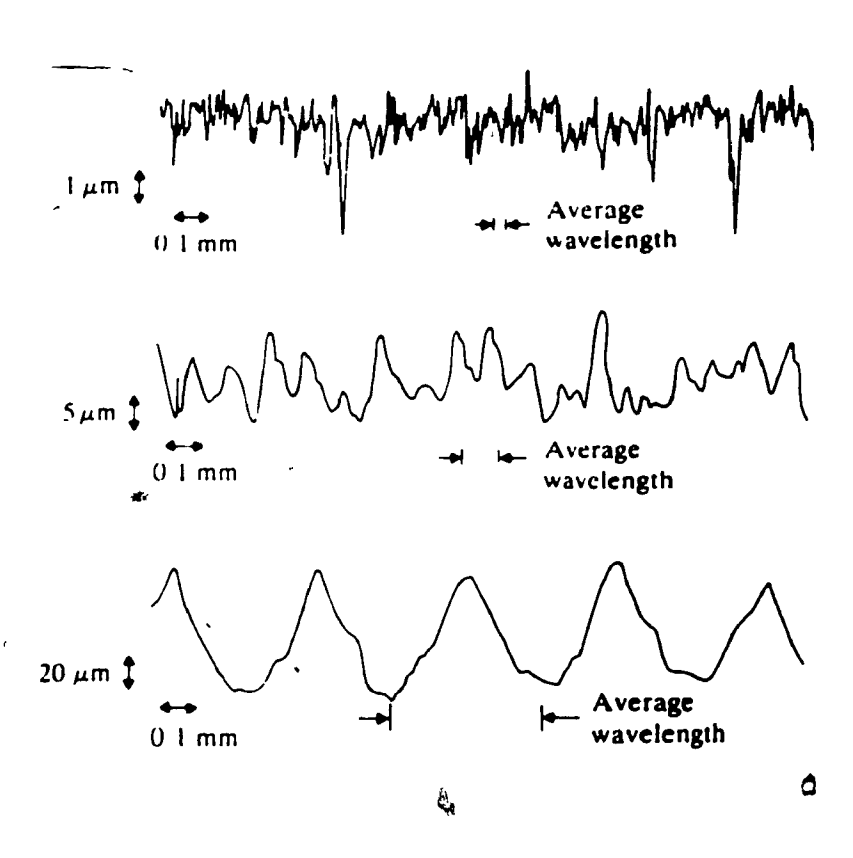


Fig. 3.1 Average wavelength for different surfaces [17].

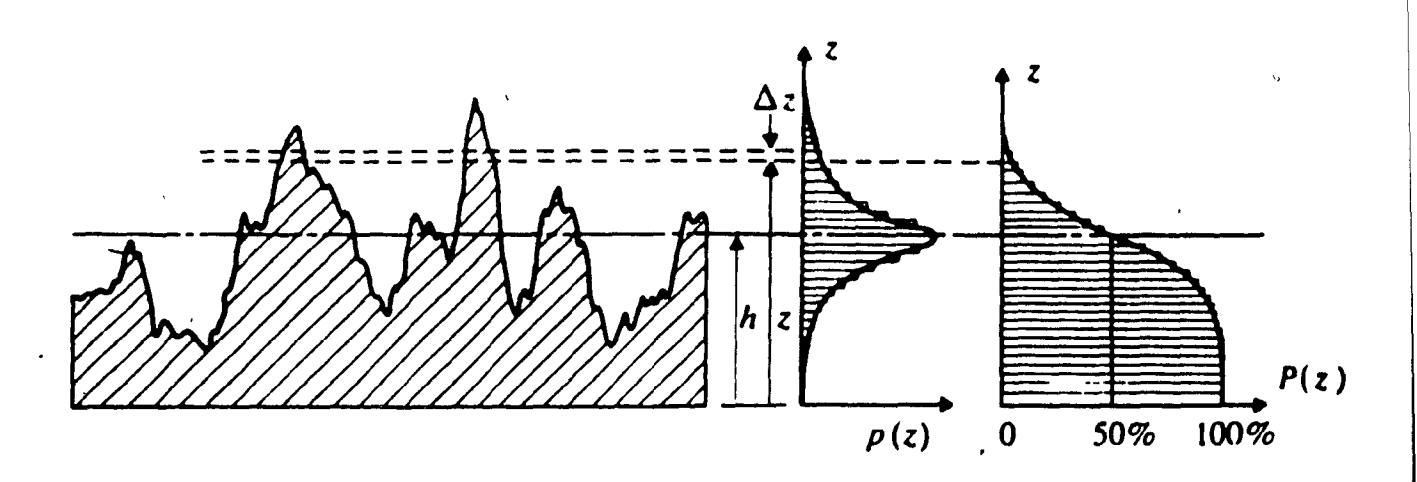


Fig. 3.2 The bearing length curve or Abbott curve [22].

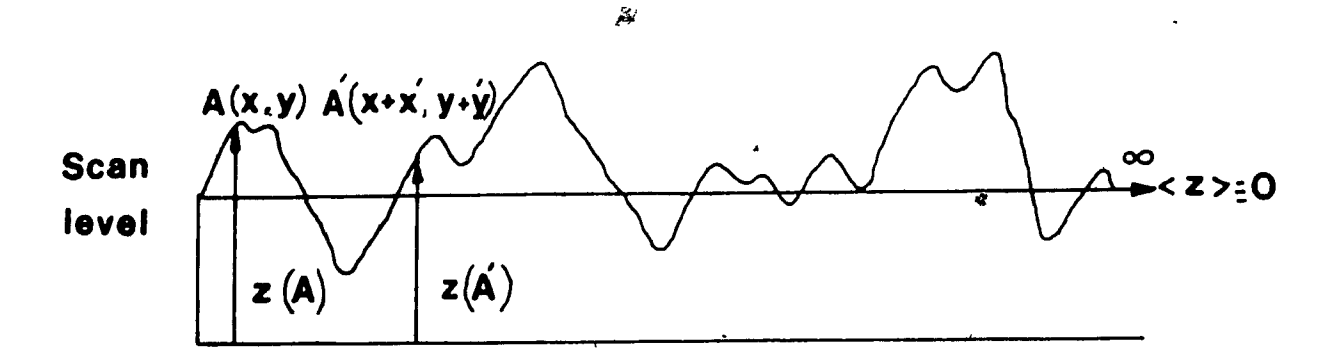


Fig. 4.1 Definition of ACF to determine the intercept length.

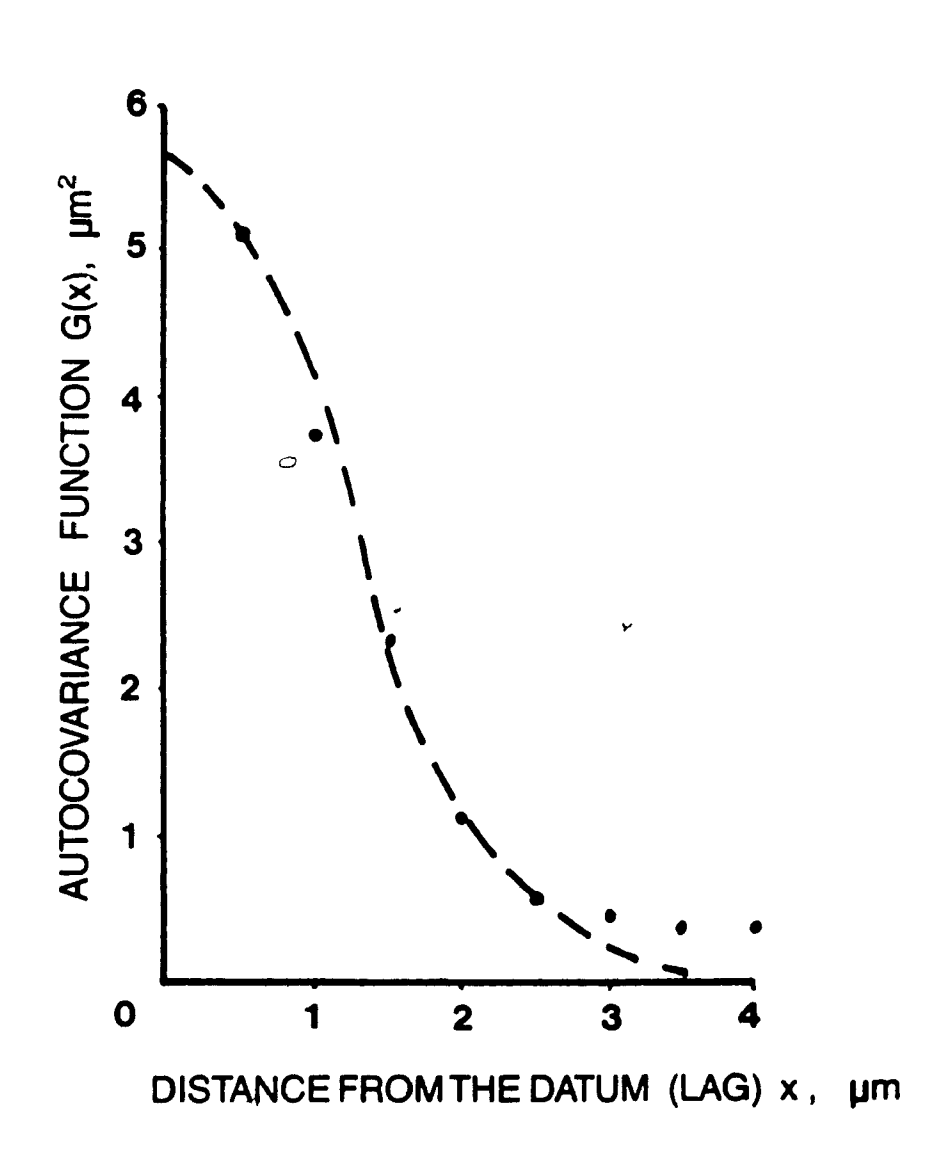


Fig. 4.2 The ACF of the surface.

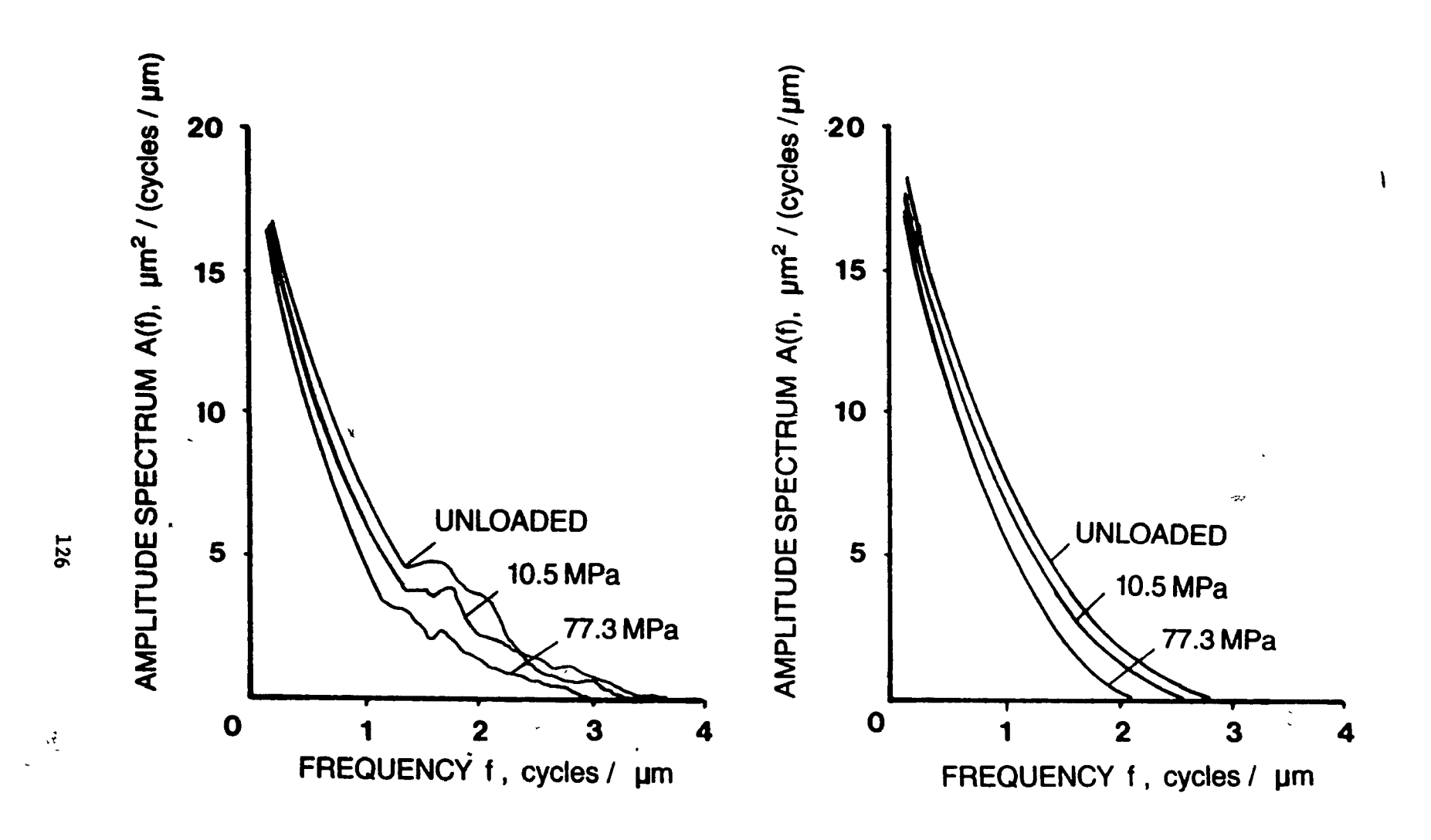


Fig. 4.3 Amplitude spectrum at various loads.

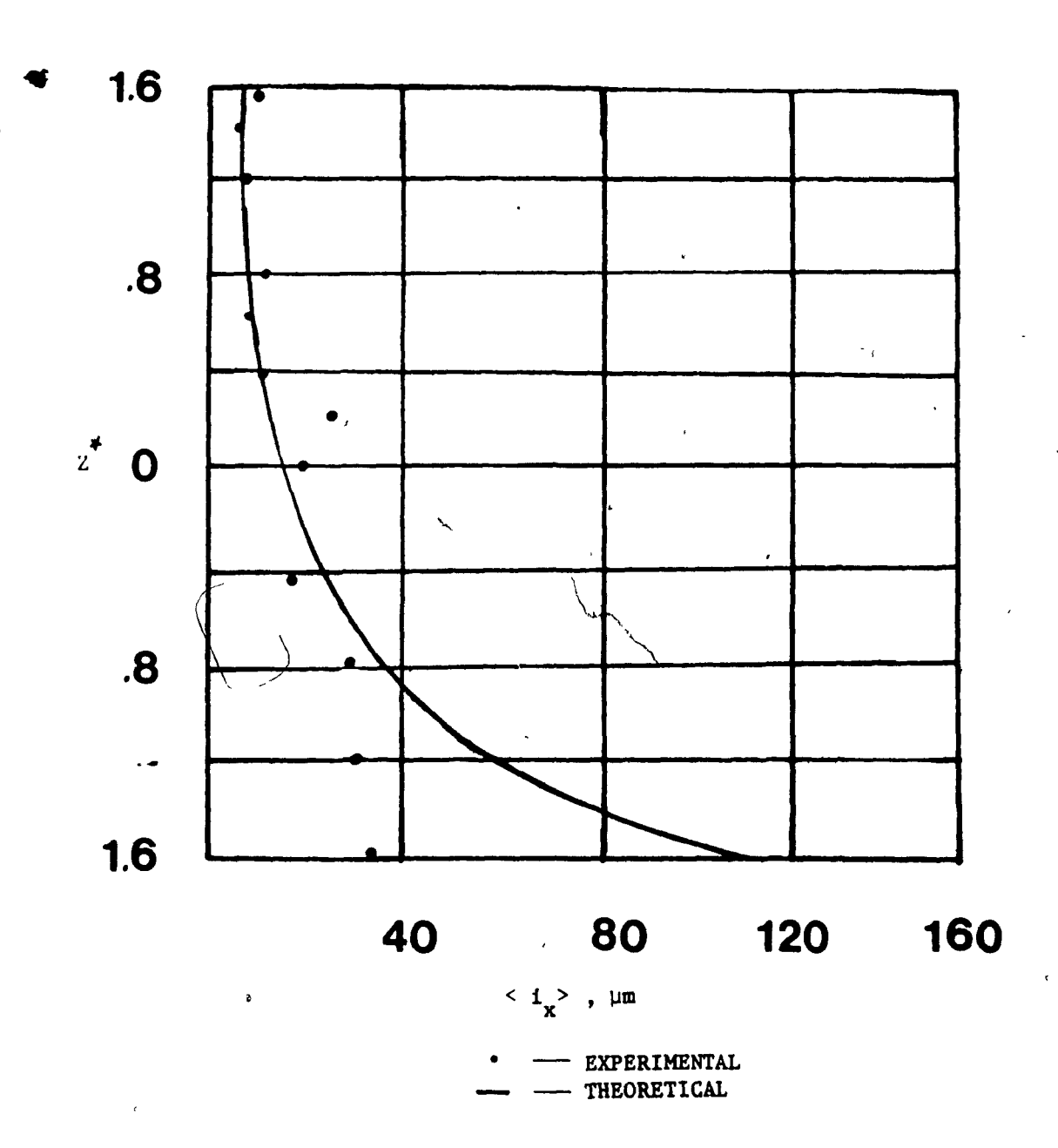


Fig. 4.4 Comparison of mean intercept length determined from measurement as compared to that obtained by equation 4.23.

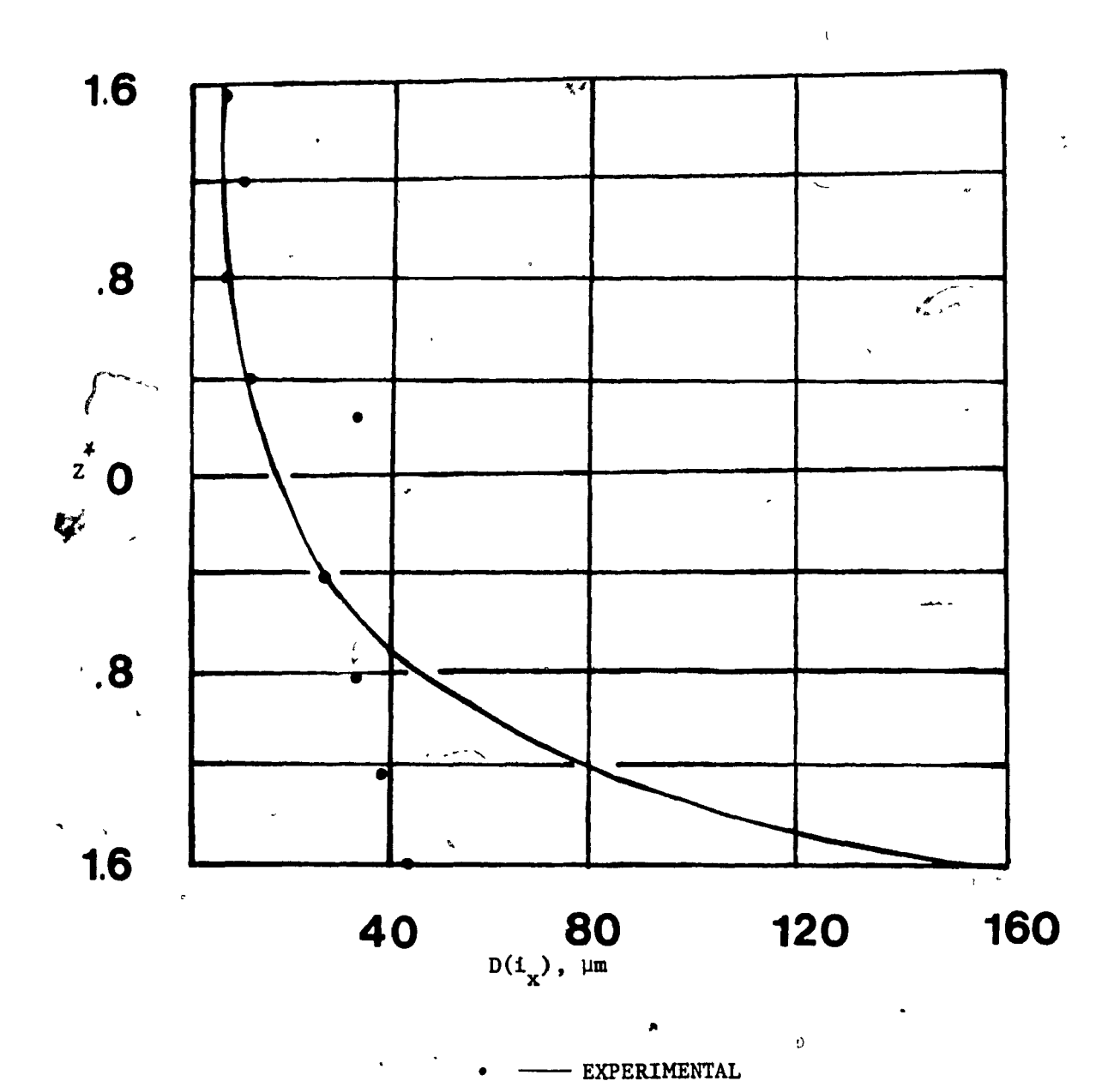


Fig. 4.5 Comparison of the deviation of the intercept length obtained from measurement as compared to that obtained using density distribution given by equation 4.30.

THEORETICAL

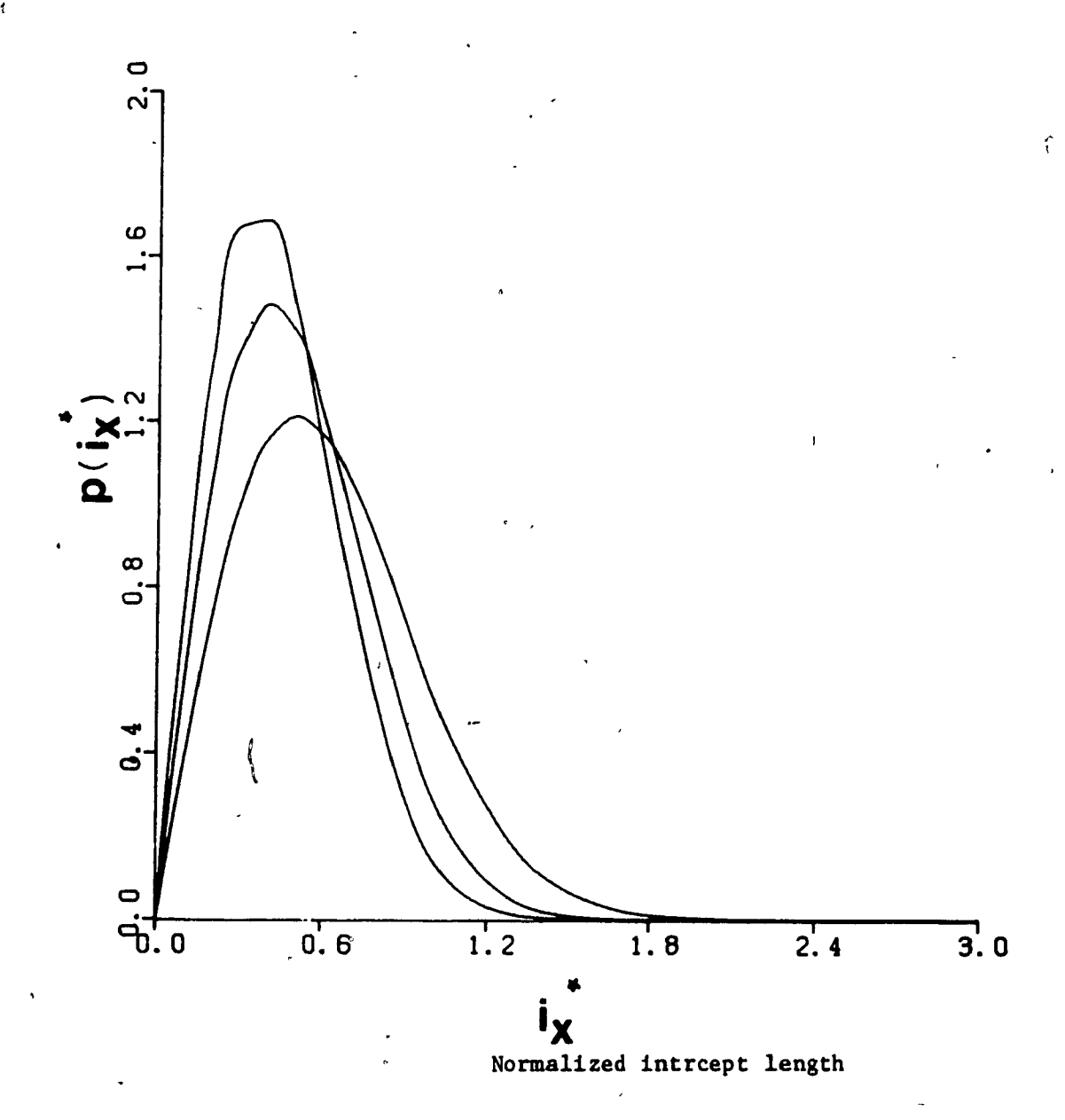


Fig. 4.6 The distribution of intercept length at various levels.

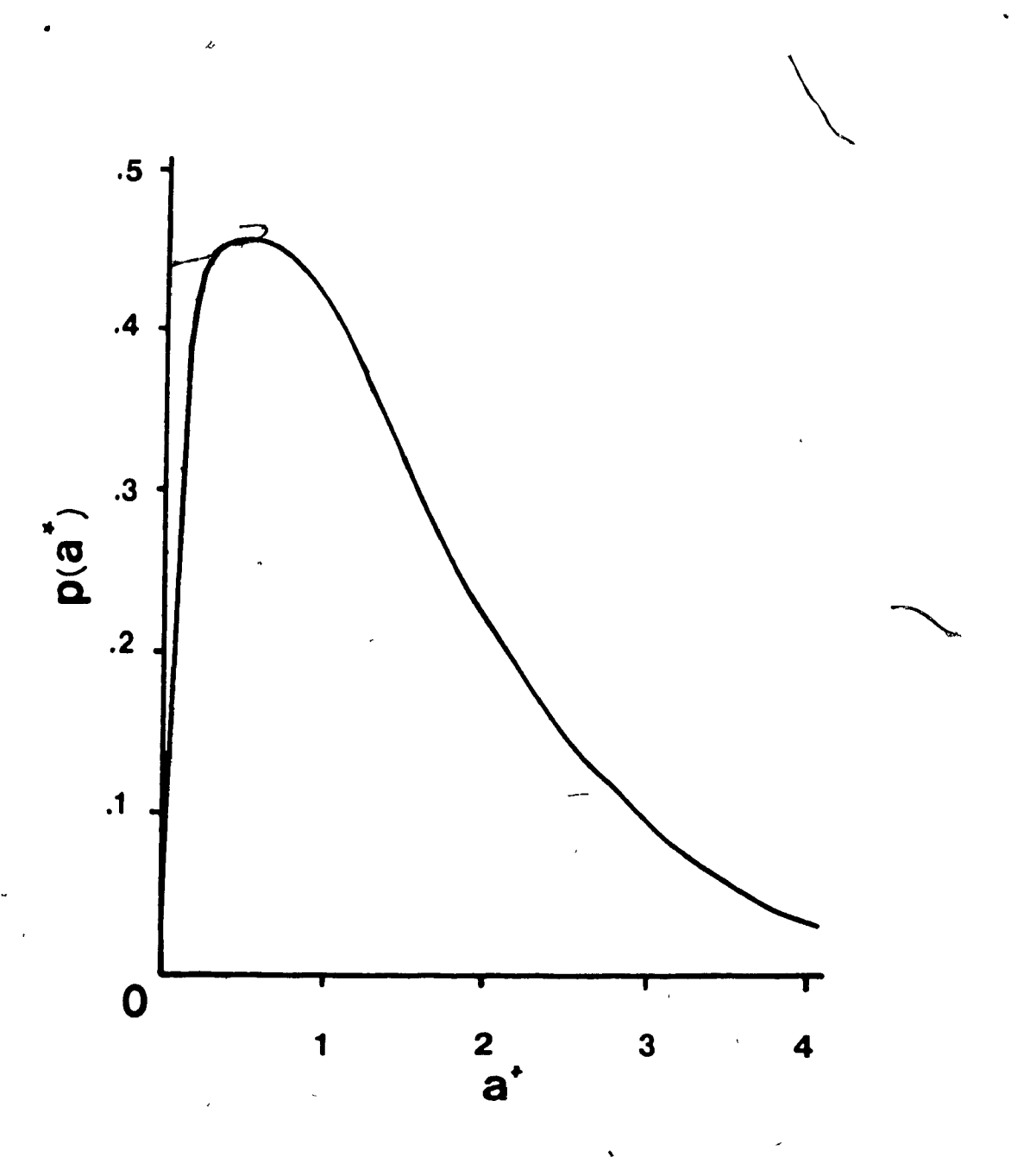


Fig. 4.7 The normalised density distribution of IBA.

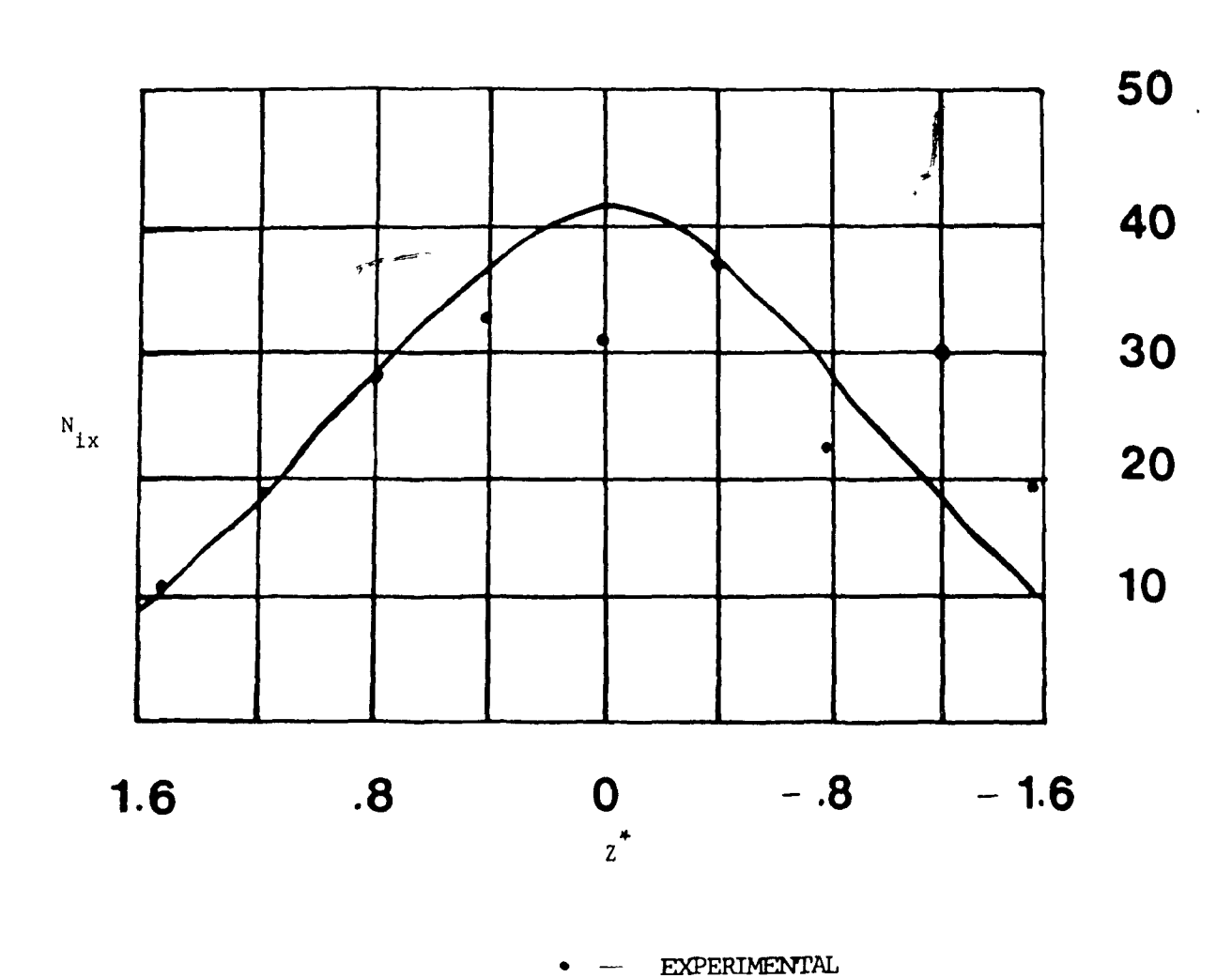


Fig. 4.8 Growth of number of intercept lengths compared to that obtained by equation (4.22).

THEORETICAL

٢

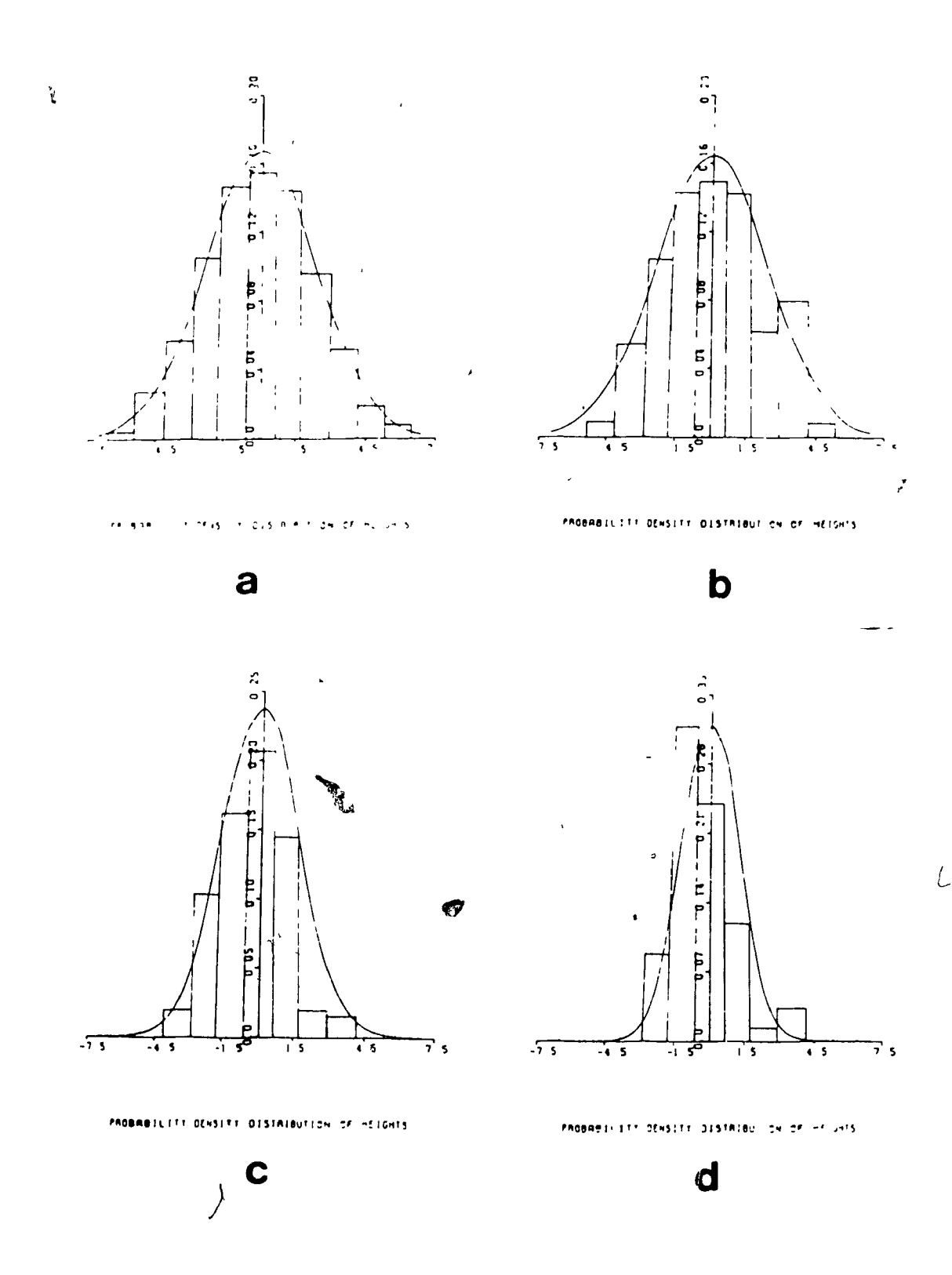


Fig. 4.9 Density distribution of heights: a) unloaded b)

10.5MPa c) 44 MPa d) 77.3 MPa

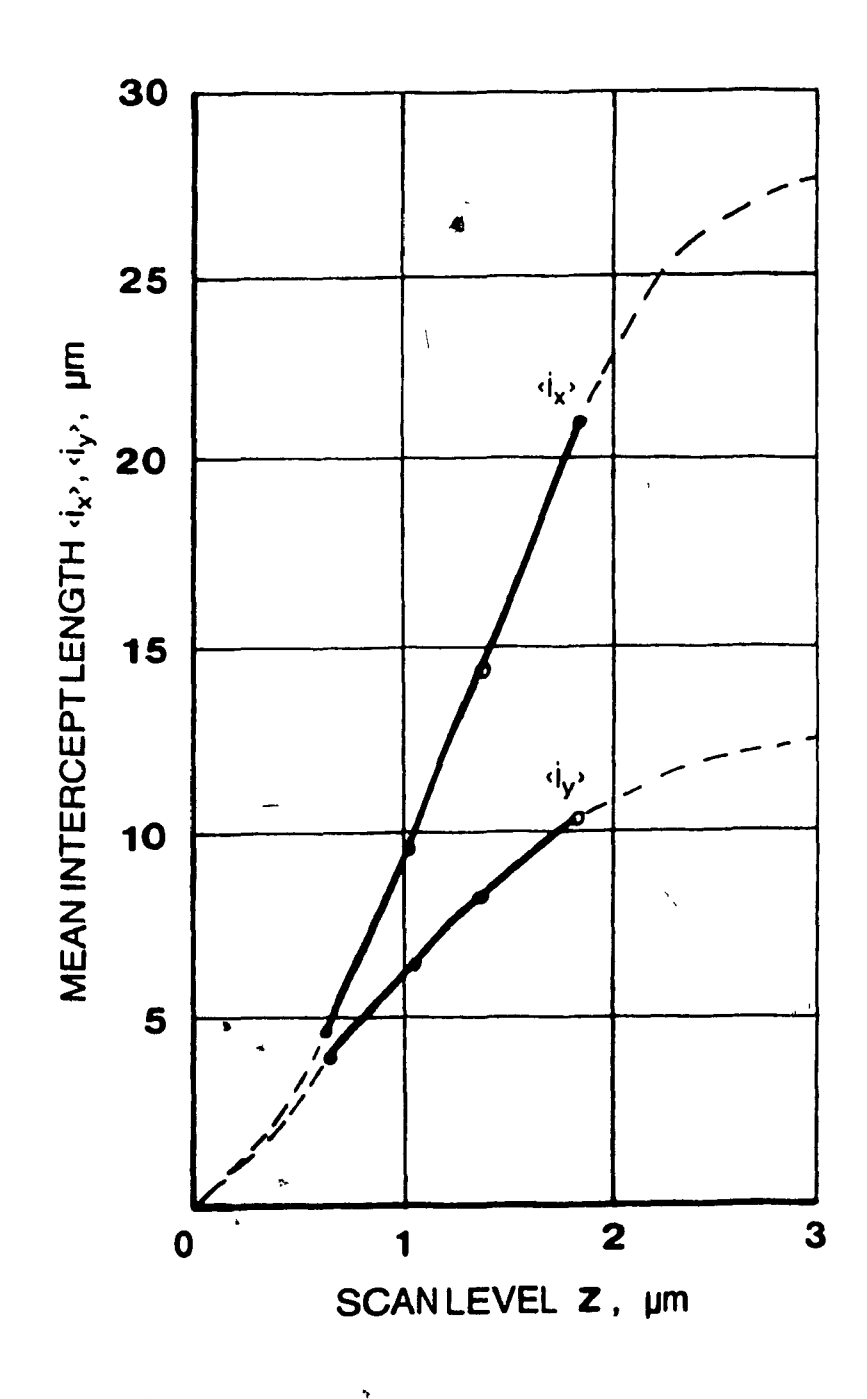


Fig. 4.10 Variation of mean intercept length with various scan levels and hence load.

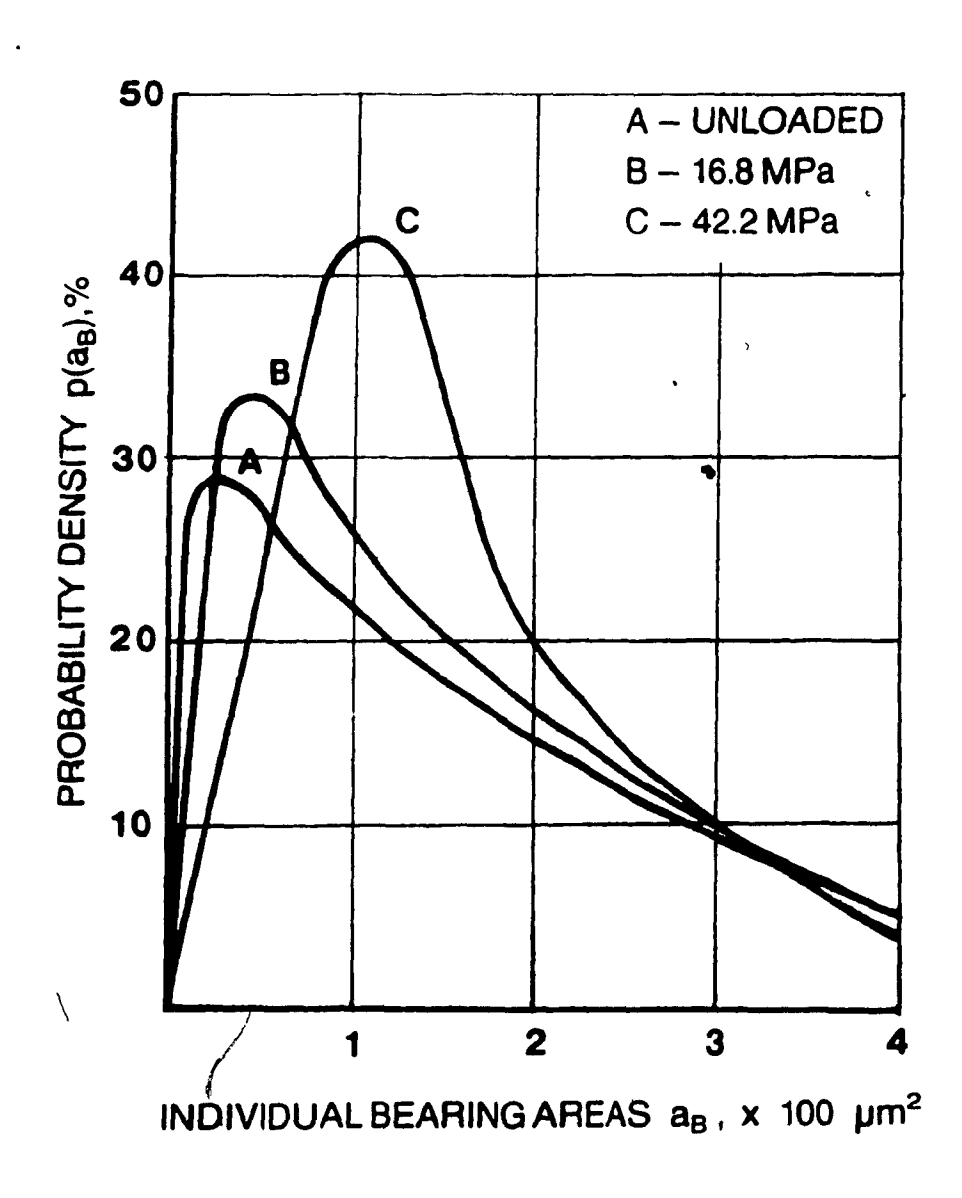


Fig. 4.11 Density distribution of bearing areas at various scan levels

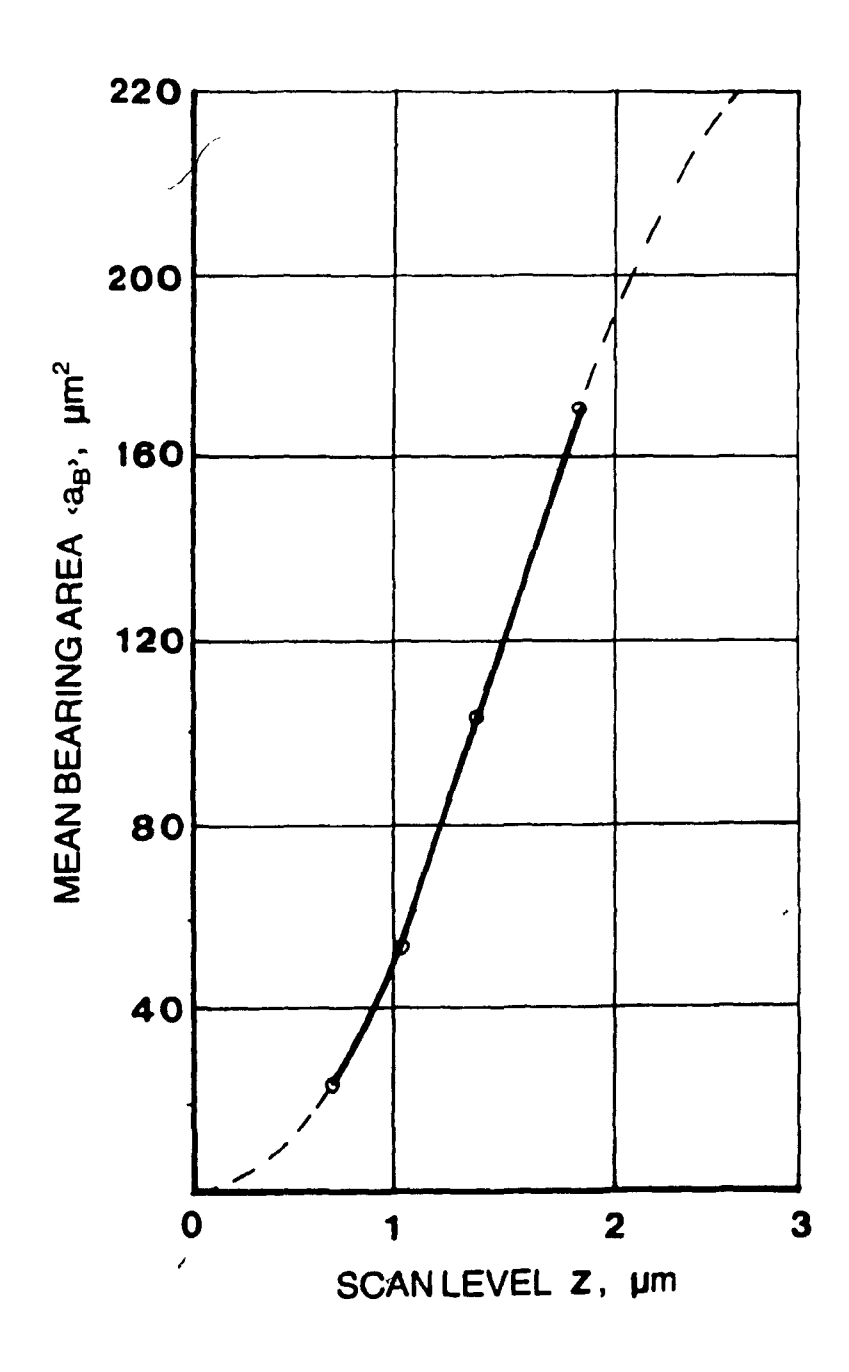


Fig. 4.12 Variation in the IBA of various scan levels and hence load.

APPENDIX A

From equation ,4.30 we get,

$$f(i_{x},z) = \frac{m_{2}z^{2}i_{x}}{-4m_{0}z^{2}} \exp\left(\frac{-z^{2}m_{2}z^{1}x}{8m_{0}z^{2}}\right) ... A.1$$

This is the probability density distribution of bearing lengths $^{1}x^{1}$ along the direction perpendicular to the direction of grinding.

Let
$${}^{1}K_{1} = {}^{4}m_{0}{}^{2}$$
 so that ${}^{2}m_{2}x^{2}$ = ${}^{2}K_{1}$

.. equation A.1 becomes

$$f(i_{x}, z) = \frac{1}{K_{1}} \cdot i_{x} \cdot \exp \frac{-i_{x}^{2}}{2K_{1}} \cdot \dots \cdot A.2$$

Similarly, letting
$$K_2' = \frac{4m_0y^0^2}{m_2y^2}$$
 so that $\frac{8m_0y^0^2}{z^2m_2y} = 2K_2$,

we get,

and the same of th

$$f(i_{y},z) = \frac{1}{\kappa_{2}} \cdot i_{y} \cdot exp(\frac{-i_{y}^{2}}{2\kappa_{2}})$$
 . . . A.3

as the probability density distribution of bearing lengths $^{1}i_{y}$ along the direction of grinding.

Considering the bearing area to be elliptical given by

$$a_b = -\frac{\pi}{4} - ix \cdot iy , ... A.4$$

the distribution of 'ab' is now obtained by using the transformation given by equations A.4 on the distributions in equations A.2 and A.3. This is obtained by substituting =ly so that $1_{x} = 4a_{b}/\pi\omega$, therefore,

$$|J| = -\frac{4}{\pi\omega} \qquad . \qquad . \qquad . \qquad A.5$$

Now, after proper substitution, we get the distribution of bearing area as,

$$f(a_b) = \int_{\pi}^{\infty} \frac{16}{2\kappa_1 \kappa_2} \cdot a_b \cdot \exp\left(\frac{-16a_b^2}{2\pi^2 \omega^2 \kappa_1} - \frac{2}{2\kappa_2}\right) d\omega \cdot ... A.6$$

letting $y = \omega^2$ so that $dy = 2 \omega d\omega$ we get,

$$f(a_b) = \frac{16a_b}{2\pi^2 K_1 K_2} \int_0^{\infty} \frac{1}{y} \cdot \exp \frac{-16a_b^2}{2\pi^2 K_1} \frac{1}{y} \frac{y}{2K_2} dy \cdot \cdot \cdot A.7$$

considering the generalized inverse Gaussian distribution whose probability density function is

$$\mu_{\phi,\psi,T}$$
 (dx) = $\frac{(\psi/T)^{\phi-1}}{2 K_{\phi}(\sqrt{T\psi})}$ $x^{\phi-1}$ $e^{-1/2(T x^{-1} + \psi x)}$

which has the property of infinite divisibility, > 0, > 0.

For
$$\phi = 0$$
 (in this case) and $T = \begin{pmatrix} 16a_b \\ -\frac{1}{2}K_1 \end{pmatrix}$, $\psi = \begin{pmatrix} 1 \\ -\frac{1}{2}K_2 \end{pmatrix}$

$$f(a_b) = \frac{16a_b}{-\frac{7}{2}(K_1K_2)} K_0 \frac{4a_b}{\pi^{K_1K_2}}$$

ÇÀ.

· to · Pile · The control of the book of t

APPENDIX B

The distribution of heights '2' and curvatures R_{χ} and R_{γ} is given by Gaussian distribution. Therefore, the joint distribution of these two variables are given by:

$$f(z,R_{x}) = \frac{|R_{x}|}{(2\pi\Delta_{x}m_{4})^{1/2}} \exp \frac{1}{2\Delta_{x}} (m_{4x}z^{2} + 2m_{2x}zR_{x} + m_{0x}R^{2}_{x})$$

where
$$\Delta_x = m_{0x}m_{4x}-m_{2x}^2$$

The distribution of the curvatures of peaks in conbtact for different values of Z/ m_{0x} can be given by:

$$f(R_{X}/Z \leq H) = \int_{0}^{\infty} f(Z, R_{X}) dz$$

$$H$$

$$\int_{0}^{\infty} \int_{0}^{\infty} f(Z, R_{X}) dZ dR_{X}$$

where $z = z//m_{0x}$

expressing B.l as

$$f(Z, R_X) = c_1 |R_X| \exp - (c_2 Z + c_3 Z R_X + c_4 R_X)$$
 . . . B.4

equation B.3 can be written as,

$$f(R_{x} \quad Z \ge H) = c_{1} \quad |R_{x}| \quad x \quad \frac{1}{2} \quad \frac{\pi}{c_{2}} \quad e^{\frac{C_{2}}{c_{2}}} \frac{e^{\text{erfc}(C_{2}H-C_{3}R_{x})}}{\sqrt{c_{2}}}$$

$$erfc(H) \quad ... \quad B.5$$

Similarly we can get the distribution of curvature at any height along the direction of grinding from B.2.